AD-A256 970

8

STRENGTHENING OF NiAl MATRIX COMPOSITES

ANNUAL REPORT

OF

N00014-91-J-1353

DTIC
ELECTE
OCT 23 1992
S D

FROM

OFFICE OF NAVAL RESEARCH

PREPARED BY

R.J.ARSENAULT

METALLURGICAL MATERIALS LABORATORY

UNIVERSITY OF MARYLAND

COLLEGE PARK, MARYLAND

October, 1992

DISTRIBUTION STATEMENT A
Approved for public release;
Distribution Unlimited

SECURITY CLASSIFICATION OF THIS PAGE

REPORT DOCUMENTATION PAGE

1a. REPORT SECURITY CLASSIFICATION Unclassified	1b. RESTRICTIVE MARKINGS
2a. SECURITY CLASSIFICATION AUTHORITY	3. DISTRIBUTION/AVAILABILITY OF REPORT DISTRIBUTION STATEMENT A Approved for public release; Distribution Unlimited
2b. DECLASSIFICATION/DOWNGRADING SCHEDULE	
4. PERFORMING ORGANIZATION REPORT NUMBER(S) MML-1992-1	5. MONITORING ORGANIZATION REPORT NUMBER(S)
6a. NAME OF PERFORMING ORGANIZATION University of Maryland 6b. OFFICE SYMBOL (If applicable)	7a. NAME OF MONITORING ORGANIZATION
6c. ADDRESS (City, State and ZIP Code) Dept. of Mat.& Nuclear Engr. University of Maryland College Park, MD 20742	7b. ADDRESS (City, State and ZIP Code)
8a. NAME OF FUNDING/SPONSORING ORGANIZATION Office of Naval Research 8b. OFFICE SYMBOL (If applicable)	9. PROCUREMENT INSTRUMENT IDENTIFICATION NUMBER
8c. ADDRESS (City, State and ZIP Code) Office of Naval Research Code 1131N Arlington, VA	10. SOURCE OF FUNDING NOS. PROGRAM ELEMENT NO. / PROJECT NO. / TASK NO. / WORK UNIT NO. 4311 875
11. TITLE (Include Security Classification) Strengthening of NiAl Matrix Composites	
12. PERSONAL AUTHOR(S) Richard J.Arsenault	
13a. TYPE OF REPORT Annual 13b. TIME COVERED FROM Oct.1991 TO Sept.1992	14. DATE OF REPORT (Yr., Mo., Day) 1992 Oct. 15. PAGE COUNT
16. SUPPLEMENTARY NOTATION	

17 COSATI CODES			18. SUBJECT TERMS (Continue on reverse if necessary and identify by block number)
FIELD	GROUP	SUB GR.	Intermetallic Matrix Composites TiB_2/NiAl

19. ABSTRACT (Continue on reverse if necessary and identify by block number)

An investigation was undertaken to determine if by cryomilling NiAl and TiB_2 powders ultra fine subgrain or grain size material could be obtain. If this ultra fine grain size composite were produced then it was assumed there should be a significant increase in the strength. Cryomilling did decrease the grain or subgrain size but the strength of the 20 V% TiB_2/NiAl composite was the same as 20 V% TiB_2 made by the XD™ process. Also, a 0 V% TiB_2/NiAl composite produced from cryomilled NiAl was about the same strength as the 20 V% TiB_2/NiAl composites. The above mentioned composites were made by HIPPing and extrusion. If the 0 V% TiB_2/NiAl cryomilled composite is tested in the as HIPPed condition, the strength is much greater.

A TEM investigation has shown that in case of extruded cryomilled composites there is a dispersion of small 10-20 nm Al_2O_3 and AlN particles. In the case of the as HIPPed cryomilled composite, the Al_2O_3 and AlN formed a network at the grain boundaries.

20. DISTRIBUTION/AVAILABILITY OF ABSTRACT UNCLASSIFIED/UNLIMITED ☒ SAME AS RPT. ☐ DTIC USERS ☐	21. ABSTRACT SECURITY CLASSIFICATION	
22a. NAME OF RESPONSIBLE INDIVIDUAL Dr. S.G.Fishman	22b. TELEPHONE NUMBER (Include Area Code) 703-696-0285	22c. OFFICE SYMBOL ONR/1131N

DD FORM 1473, 83 APR EDITION OF 1 JAN 73 IS OBSOLETE

SECURITY CLASSIFICATION OF THIS PAGE

TABLE OF CONTENTS

I. Summary 1

II. List of Publication and Presentations 2

III. Publications (A selected few) 4

INTERFACES IN XD™ PROCESSED TiB_2/NiAl COMPOSITES
Metall. Trans. 22A, 1991, 3031

COMMENTS ON MILLER AND HUMPHREY'S PAPER
Scripta Metall. 25, 1991, 2617

THE EFFECT OF THERMAL RESIDUAL STRESSES ON THE ASYMMETRIC CONSTITUTIVE BEHAVIOR OF METAL MATRIX COMPOSITES
J.of Comp.Tech. & Res., Winter 1991, 211

FRACTURE TOUGHNESS OF DISCONTINUOUS METAL MATRIX COMPOSITE
Ed. by G.Z.Voyiadjis, ASCE, 1992

INFLUENCE OF THERMALLY INDUCED PLASTICITY AND RESIDUAL STRESS ON THE DEFORMATION OF SiC/Al COMPOSITES
6th Japan-U.S. Conference on Composite Materials.

Accession For
NTIS GRA&I ☒
DTIC TAB ☐
Unannounced ☐
Justification
By per ADA 242236
Distribution/
Availability Codes
Dist | Avail and/or Special
A-1

92-27689

Annual Report

on

Strengthening of NiAl Matrix Composites
N00014-91-J-1353

I. Summary

An investigation was undertaken to determine if by cryomilling NiAl and TiB_2 powders ultra fine subgrain or grain size material could be obtain. If this ultra fine grain size composite were produced then it was assumed there should be a significant increase in the strength. Cryomilling did decrease the grain or subgrain size but the strength of the 20 V% TiB_2/NiAl composite was the same as 20 V% TiB_2 made by the XD™ process. Also, a 0 V% TiB_2/NiAl composite produced from cryomilled NiAl was about the same strength as the 20 V% TiB_2/NiAl composites. The above mentioned composites were made by HIPPing and extrusion. If the 0 V% TiB_2/NiAl cryomilled composite is tested in the as HIPPed condition, the strength is much greater.

A TEM investigation has shown that in case of extruded cryomilled composites there is a dispersion of small 10-20 nm Al_2O_3 and AlN particles. In the case of the as HIPPed cryomilled composite, the Al_2O_3 and AlN formed a network at the grain boundaries.
It may be speculated that the greater strength of the as HIPPed composite could be due to the network of Al_2O_3 and AlN acting as a continuous filament.

The various theories that have been proposed to account for fracture toughness of discontinuous metal matrix composites, or the lack there of , were examined. It was observed that the fracture toughness is independent of particle size and the fracture proceeds through the matrix. A significant factor which has not been considered in the past is that the matrix is in a severely cold worked condition. The cold worked state is the major factor contributing to the low fracture toughness of discontinuous metal matrix composites.

The Finite Element Method (FEM) was employed to investigate the matrix plastic flow in a whisker reinforced SiC/Al composite under external tensile load. It was found that the plastic zone induced by the plastic relaxation of thermal stresses expands under the external tensile load. The overall matrix plastic flow was characterized by the expansion and interconnection of the plastic zones around whiskers. This process can be divided into several characteristic stages, and related to the global stress-strain relationship. It was also found that composite asymmetric constitutive response to external tensile and compressive loads as well as the composite asymmetric Bauschinger behavior was due to the thermally induced plasticity and residual stresses.

II. List of Publications and Presentations

1. Papers Published and Submitted, and Book Chapters

(1). INTERFACES IN XD™ PROCESSED TiB_2/NiAl COMPOSITES
L.Wang and R.J.Arsenault
Metall. Trans. 22A, 1991, 3031

(2). COMMENTS ON MILLER AND HUMPHREY'S PAPER
Scripta Metall. 25, 1991, 2617

(3). A FEM STUDY OF THE DEFORMATION PROCESS OF SiC/Al COMPOSITES
N.Shi, R.J.Arsenault and B.Wilner
Accepted for publication in Acta Metall.

(4). DEFORMATION INDUCED RESIDUAL STRESS CHANGES IN SiC WHISKER REINFORCED 6061 Al COMPOSITES
N.Shi, R.J.Arsenault, A.D. Krawitz and L.F.Smith
Accepted for publication in Metall.Trans.

(5). RESIDUAL STRESSES IN DISCONTINUOUS METAL MATRIX COMPOSITES
L.F.Smith, A.D.Krawitz, P.Clarke, S.Saimoto, N.Shi and R.J.Arsenault
Accepted for publication in Mat.Sci.& Eng.

(6). INFLUENCE OF THERMALLY INDUCED PLASTICITY ON THE DEFORMATION OF SIC/AL COMPOSITES UNDER TENSILE, COMPRESSIVE AND CYCLIC LOADING
N.Shi and R.J.Arsenault
Accepted for publication in Scripta Met.

(7). THERMO - MECHANICAL - MICRO-PLASTIC FLOW IN WHISKER REINFORCED SIC/AL COMPOSITES
N.Shi and R.J.Arsenault
Accepted for publication in Polish Academy of Materials Science

(8). MICROSTRUCTURAL CHANGES DURING CREEP OF A SiC/AL_20_3 COMPOSITE
J.C.Romero and R.J.Arsenault
Submitted for publication

(9). INTERFACIAL STRUCTURE OF A SiC/AL COMPOSITE
J.C.Romero and R.J.Arsenault
Submitted for publication

(10). ANOMALOUS PENETRATION AND DIFFUSION OF AL INTO SiC
J.C.Romero and R.J.Arsenault
Submitted for publication

(11). Strengthening and Deformation Mechanisms of Discontinuous Metal Matrix Composites
Egypt.

(12). Fracture Toughness of Discontinuous Metal Matrix Composite
Ed. by G.Z.Voyiadjis, ASCE, 1992

(13). Influence of the Thermally Induced Plasticity and Residual Stresses on the Deformation of SiC/Al Composites
6th Japan-U.S. Conference on Composite Materials.

2. Presentations

(1). University of Southern California, 1991, "Strengthening and Deformation Mechanism in Metal Matrix Composites"

(2). Westinghouse Science Center, 1991, "Strengthening and Deformation Mechanisms in Metal Matrix Composites

(3). University of Tennessee, 1992, "Strengthening and Deformation Mechanisms in Metal Matrix Composites"

(4). Ninth Engineering Mechanics Conference ASCE, 1992, "Fracture Toughness of Discontinuous Metal Matrix Composites"

(5). XIII Advanced Materials and Technologies Conference, Poland, 1992, "Thermo-Mechanical-Micro-Plastic Flow in Whisker Reinforced SiC/Al Composites"

(6). 13th Annual DMMC meeting, 1991, "Residual Stresses in SiC/Al Composites"
N. Shi and R.J. Arsenault

(7). Fall Meeting of ASM/AIME 1991, "Strengthening of NiAl by TiB_2"
L.Wang and R.J.Arsenault

(8). Fall Meeting of ASM/AIME 1991, "Segregation at Metal-Ceramic Interfaces"
R.J.Arsenault, L.Wang, and J.Romero

(9). Winter Meeting of ASME, 1991, "Plasticity of SiC/Al Composites"
N.Shi and R.J.Arsenault

(10). 14th Annual DMMC Meeting, 1992, "The Strengthening of NiAl by TiB_2",
L.Wang and R.J.Arsenault.

(11). 6th Japan-U.S. conference on Composite Materials, 1992, "An FEM Study on the Plastic Deformation Process of a Whisker Reinforced SiC-Al Composite", N.Shi and R.J.Arsenault.

Interfaces in XD Processed TiB_2/NiAl Composites

L. WANG and R.J. ARSENAULT

Interfaces of TiB_2-NiAl and α-Al_2O_3-NiAl in TiB_2/NiAl composites have been investigated by analytical electron microscopy. Although no consistent crystallographic orientation relationships have been found between NiAl and TiB_2 or Al_2O_3, semicoherent interfaces between α-Al_2O_3 and NiAl have been observed by high-resolution electron microscopy (HREM) in areas where the low indexed crystallographic planes of α-Al_2O_3 aligned with that of NiAl. No semicoherent interfaces between NiAl and TiB_2 have been observed. Silicon segregation was consistently detected by X-ray energy-dispersive spectroscopy (EDS) at the TiB_2/NiAl interface region. Segregation has not been detected in the α-Al_2O_3-NiAl interface region. The segregation layer observed at the TiB_2-NiAl interface is too thin to absorb any of the thermal residual stress.

I. INTRODUCTION

IT is generally accepted that excellent bonding between the metal matrix and the ceramic reinforcement can be achieved by the XD* (exothermic dispersion) process for several of the metal matrix composites reinforced with TiB_2 particles, such as TiB_2-NiAl,[1,2] TiB_2-TiAl,[3] and TiB_2-Al alloy.[4] During the XD process, the TiB_2 particles are formed *in situ* in the molten metal matrix, so they have clean, nonoxidized interfaces and typically are single crystals of high purity. Usually, the crystal structures of the metal matrix and the ceramic particles are so different that no simple topotaxial relationship exists[3] in XD-processed metal-matrix composites. Recently, it was found that during high-temperature deformation, dislocations can be generated from a matrix-particle interface into both the matrix and the particles in XD processed TiB_2/NiAl composite.[5,6] Therefore, interface structures might be very important in controlling the mechanical properties at these composites. However, another intriguing observation concerning the TiB_2/NiAl composites is the lack of dislocation generation due to cooling from the high-temperature (1673 K) annealing.[5,6] The predicted thermal residual stress should be very large, and this stress should be relieved by dislocation generation.[7] It is possible that an interface layer exists between the TiB_2 and the NiAl which can act as a stress absorber.[7]

The purpose of the current investigation was to determine if an interface layer exists and then determine if it is of sufficient thickness and also to determine if any consistent crystallographic relationships could be found between the matrix and the reinforcement.

*XD is a trademark of Martin Marietta Corporation, Bethesda, MD.

II. EXPERIMENTAL PROCEDURE

Composites of 0, 10, and 20 vol pct TiB_2/NiAl were purchased from the Martin Marietta Corporation (Bethesda, MD). A series of compression tests at 1033, 1143, and 1273 K were performed in the strain-rate range from 10^{-6} to 10^{-2} s^{-1}. The transmission electron microscopy (TEM) foils were obtained from the compressive-tested sample by electric discharge machining disks with a thickness of 0.5 mm and then dimple grounding to a thickness of 0.07 to 0.1 mm at the center. Foils for conventional TEM were prepared by twin-jet electrolytic polishing in a 5 pct perchloric acid-ethanol solution, whereas samples for high-resolution electron microscopy (HREM) were prepared in the same way as for conventional TEM except they were ion milled from 10 minutes to 1 hour to clean the surface as the final procedure. Most of the conventional TEM work was carried out on the 1 MeV high-voltage electron microscope (HVEM) at the Argonne National Laboratory (Argonne, IL). High-resolution electron microscopy and X-ray energy-dispersive spectroscopy (EDS) analyses were performed on a JEOL 2000 FX analytical microscope. The X-ray wavelength dispersive spectroscopy (WDS) analyses were carried out on a JEOL 840A scanning electron microscope.

It is necessary to tilt the sample to such an orientation that strong low-index reflections exist on both sides of the interface and, for best results, the electron beam is parallel to the interface when performing HREM investigations of these composites. Although there is a very small chance of obtaining two-dimensional (2-D) lattice fringes on both sides of the interface, when the orientation relationship between the particles and the matrix is random, it is usually not difficult to get one-dimensional (1-D) lattice fringes in both the matrix and the particles.

III. EXPERIMENTAL RESULTS AND DISCUSSION

Figures 1 and 2 are TEM micrographs of 0 and 20 vol pct TiB_2/NiAl composites, respectively, which were taken on the 1 MeV HVEM at a low magnification, representing the general view of the microstructures of the composites. Particles which appeared in the 0 vol pct sample are α-Al_2O_3. There may be as much as 5 to 10 vol pct of these particles in all of the 0, 10, and 20 vol pct TiB_2/NiAl composites. Therefore, in Figure 2, which is a micrograph of a 20 vol pct TiB_2/NiAl composite,

L. WANG, Graduate Student, and R.J. ARSENAULT, Professor, are with the Metallurgical Materials Laboratory, Department of Materials and Nuclear Engineering, University of Maryland, College Park, MD 20742-2115.

Manuscript submitted January 30, 1991.

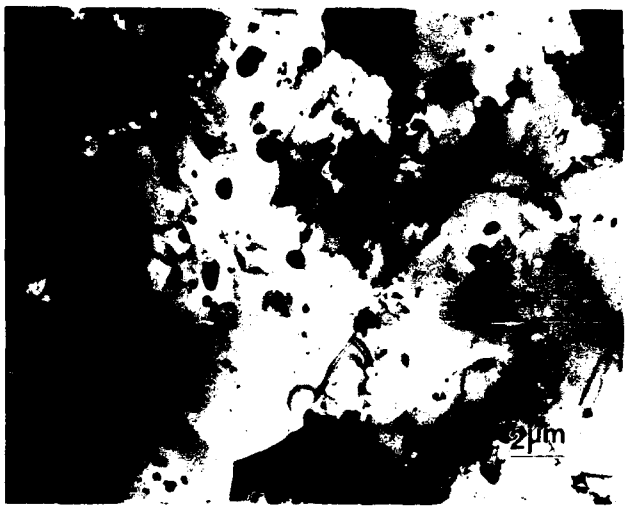

Fig. 1—TEM micrograph of 0 vol pct TiB_2/NiAl composite. Low magnification.

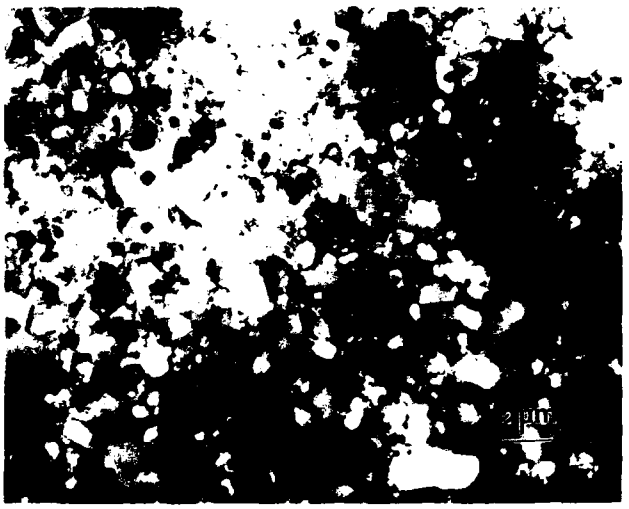

Fig. 2—TEM micrograph of 20 vol pct TiB_2/NiAl composite. Low magnification.

there are particles of both TiB_2 and α-Al_2O_3. Most of the larger ones are TiB_2 particles, since the average particle size of α-Al_2O_3 is smaller than that of TiB_2 particles. The grain size and particle size, including that of α-Al_2O_3, remain constant throughout the whole deformation process, independent of the testing temperature and strain rate.

It has been found that the matrix composition deviated from the stoichiometric composition by quantitative X-ray WDS investigations, *i.e.*, the matrix contains ~52 at. pct nickel. Apparently, this is partly due to the formation of the α-Al_2O_3 particles during the processing which consumed a certain amount of aluminum.

An investigation was undertaken to determine if any crystallographic orientation relationships existed between the reinforcement (including α-Al_2O_3) and matrix materials. Although, in some cases, one or two lower indexed crystal planes of α-Al_2O_3 or TiB_2 phases can be aligned with that of the matrix phase, no consistent crystallographic orientation relationships were found between the reinforcements and the matrix phase. In other words, there was a random crystallographic orientation relationship between the particles and the matrix.

However, despite the differences between their crystal structures and their random crystallographic orientation relationships, there are some interesting aspects of interfaces between Al_2O_3 and NiAl. In some cases, it seems that one or two disordered atomic layers on the α-Al_2O_3 side exist, as shown in Figure 3. It is possible that this observation is an image effect. However, it has been proposed that a disordered region occurs to obtain atomically well-matched interfaces where, crystallographically, there is a large level of atomic mismatch.[8] Unfortunately, there are at least two difficulties preventing us from carrying out computer image simulations to interpret the observations. The first difficulty is that the crystal orientations between NiAl and α-Al_2O_3 are random. As a consequence of this, there is a second difficulty; *i.e.*, there is a lack of theoretical models for interface structures. There are too many possible ways to construct the interface. Since the observed disordered layer is apparently in α-Al_2O_3 which has a higher elastic modulus than NiAl,[12,9,10] it makes the interpretation even

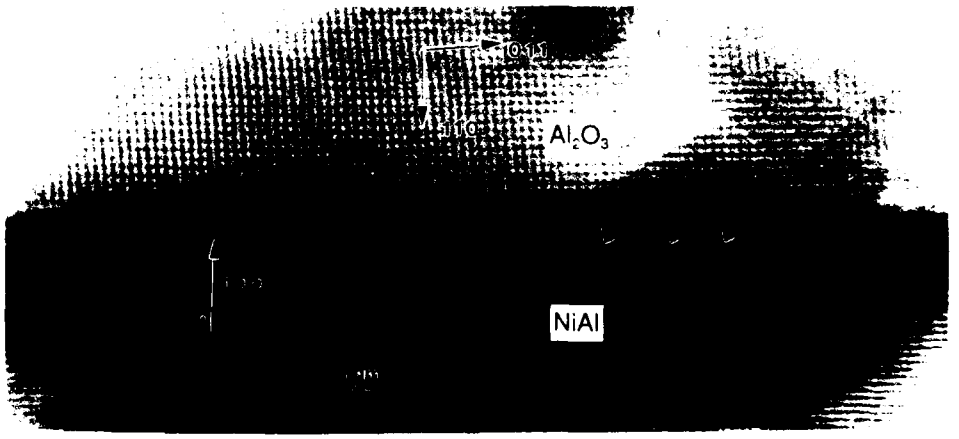

Fig. 3—HREM micrograph of α-Al_2O_3-NiAl interface. Arrows indicate the disturbed interface.

more difficult, except we believe that elastic anomalies[11,12] of α-Al_2O_3 occur at the interface region.

In the case of the lower indexed planes of α-Al_2O_3 aligned with that of the matrix, semicoherent interfaces were observed. For instance, Figure 4 showed a semicoherent interface when the {100} planes of NiAl aligned with {110} (in a rhombohedral coordinate system) planes of α-Al_2O_3. By using a hard sphere model of the interfaces structure, the distance between misfit dislocations is $D = d_1d_2/(d_1 - d_2)$,[13] where d_1 and d_2 are the interplanar distances for reinforcements and the matrix, respectively. The interplanar distances of (100) plane in NiAl and (110) planes in α-Al_2O_3 are 0.288 and 0.3479 nm, respectively. Calculated, D = 1.673 nm, which is just about six times as large as the interplanar distance of (100) planes in NiAl. In Figure 4, six of the (100) planes in NiAl planes aligned with five of the (110) planes in α-Al_2O_3 planes, with one misfit dislocation on the matrix side. This agrees with the calculated value very well. Coherent or semicoherent interfaces between TiB_2 and NiAl were not observed *via* HREM. At the TiB_2-NiAl interface, there exists a very thin layer (maybe a different crystal structure but one which is too thin to obtain a microdiffraction pattern) of atoms which had a different lattice spacing, as shown in Figure 5. The thickness of this layer was about 0.6 nm when the observation was made along the basal plane of TiB_2.

The results discussed above indicate that the interface layer at the TiB_2-NiAl interface is very thin (0.6 nm); therefore, it is not thick enough to absorb the thermal residual stress, but there is a possibility that the thermal residual stress is relaxed by diffusion of atoms which have a larger atomic radius than the matrix atoms in the interface region. This relaxation would occur because the matrix is in hydrostatic tension[7] and the oversized atoms would reduce the stress. The possibility of segregation was investigated by X-ray EDS analysis. In Figures 6 and 7, which are TEM images of α-Al_2O_3 and TiB_2 particles, respectively, locations A through C are the areas at which the EDS micrographs were taken, which represent within the particles, the interface region, and the matrix, respectively. A beam size of ~20 nm was employed for the interface region and a slightly larger size for the particle and matrix regions. In the EDS profiles, there is a small carbon peak which is due to contamination.

Figure 5(a) is the EDS profile taken inside an α-Al_2O_3 particle. Apparently, there are no impurities inside the α-Al_2O_3 particles except for a trivial amount of nickel

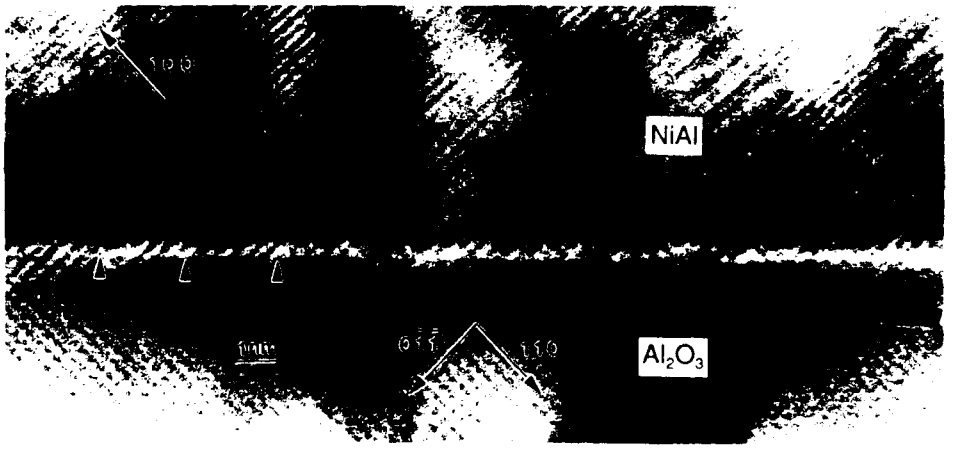

Fig. 4 — HREM micrograph of α-Al_2O_3-NiAl interface. Arrows indicate the misfit dislocations in the NiAl.

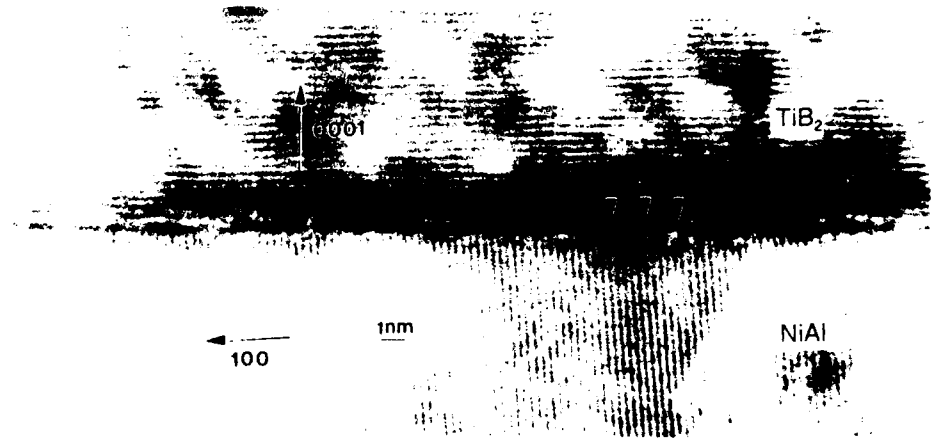

Fig. 5 — HREM micrograph of TiB_2-NiAl interface. Arrows indicate the silicon segregated layer

Fig. 6—TEM micrograph of α-Al_2O_3 particles of 0 vol pct TiB_2/NiAl composite.

which is not much more than background. Profiles taken in the Al_2O_3-NiAl interface region and the NiAl matrix close to the interface are also shown in Figures 8(b) and (c). A small amount of sulfur was detected both at the interface region and in the matrix. In comparing the counts obtained from the interface region and matrix, it is suggested that there is no preferential segment for sulfur atoms. Figure 9(a) presents the profile obtained inside a TiB_2 particle. TiB_2 particles are as pure as the α-Al_2O_3 particles. Figures 9(b) and (c) are profiles taken of the TiB_2-NiAl interface region and of the NiAl matrix close to the interface. A remarkable silicon peak was found at the interface region when comparing the profile obtained at the TiB_2-NiAl interface with those obtained from the NiAl matrix or TiB_2 particles. Since a silicon peak was only detected at the TiB_2-NiAl interface region by EDS, it might be speculated that this thin layer, as observed in the HREM investigation, might be mainly composed

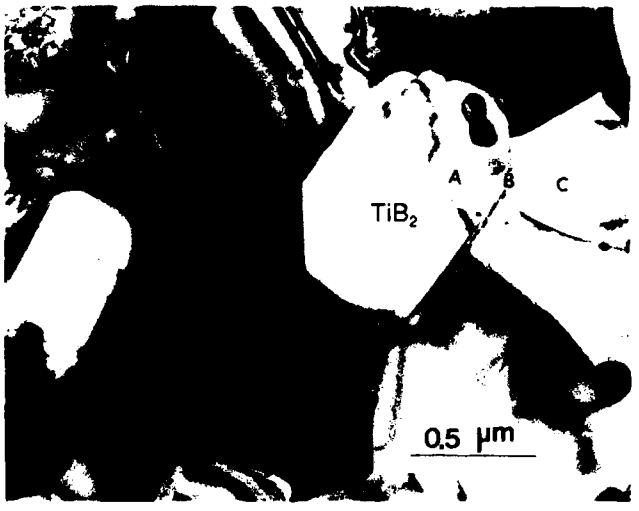

Fig. 7—TEM micrograph of TiB_2 particles of 20 vol pct TiB_2/NiAl composite.

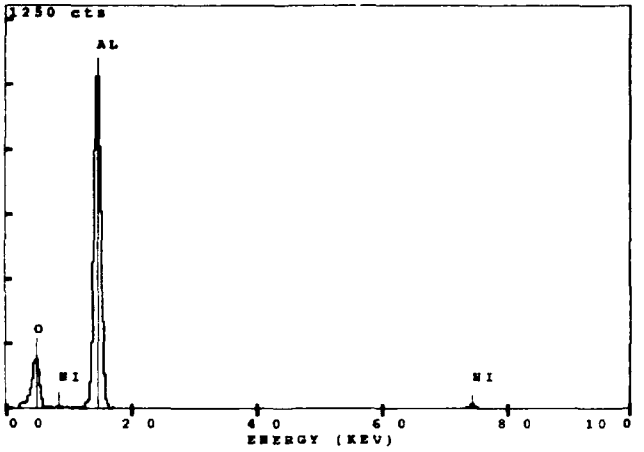

(*a*)

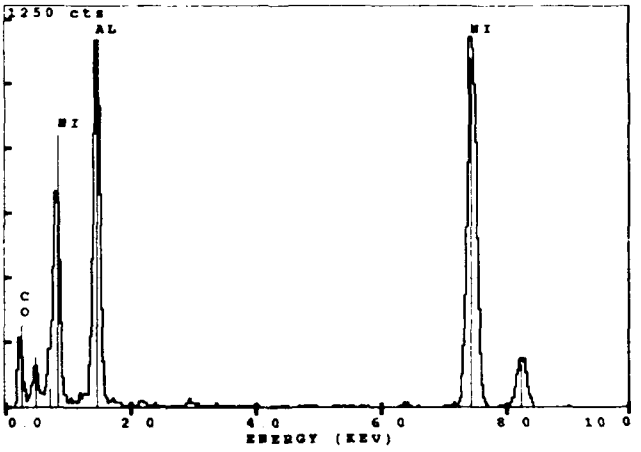

(*b*)

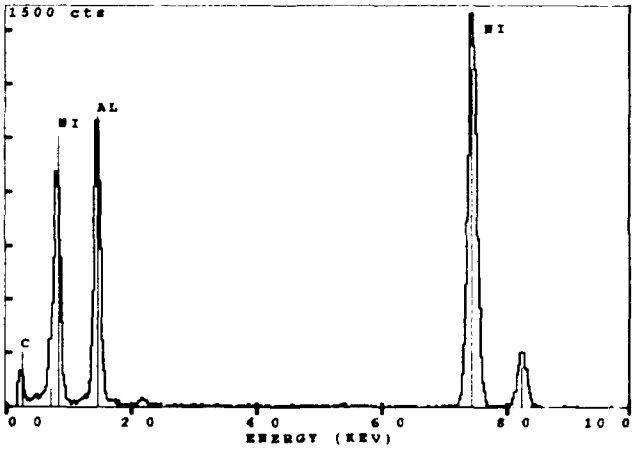

(*c*)

Fig. 8—EDS profiles of α-Al_2O_3 particles and close-by regions: (*a*) inside the α-Al_2O_3 particle, (*b*) interface region of α-Al_2O_3 and NiAl, and (*c*) NiAl matrix close to the α-Al_2O_3 particle.

of silicon atoms. The exact structure and composition of this segregation layer are unknown, and we encountered the same difficulties in attempting to carry out a computer image simulation as in the case of the α-Al_2O_3-NiAl interface. However, the consistency of the observation

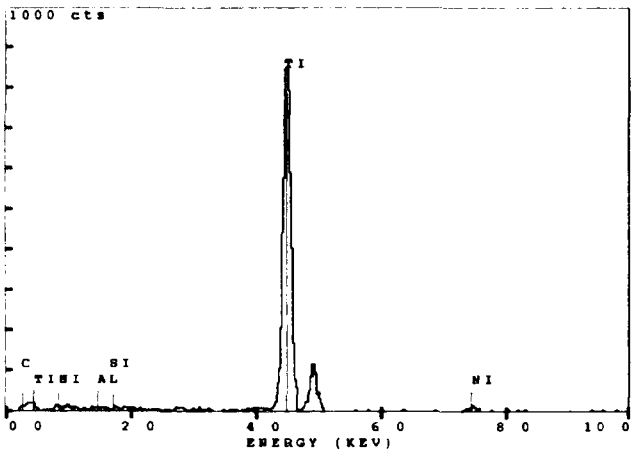

(*a*)

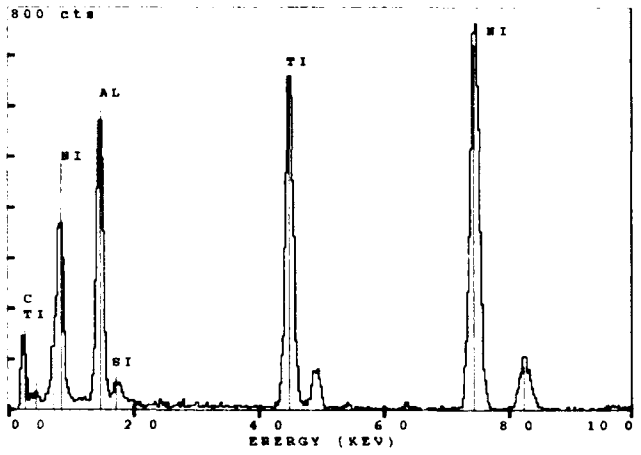

(*b*)

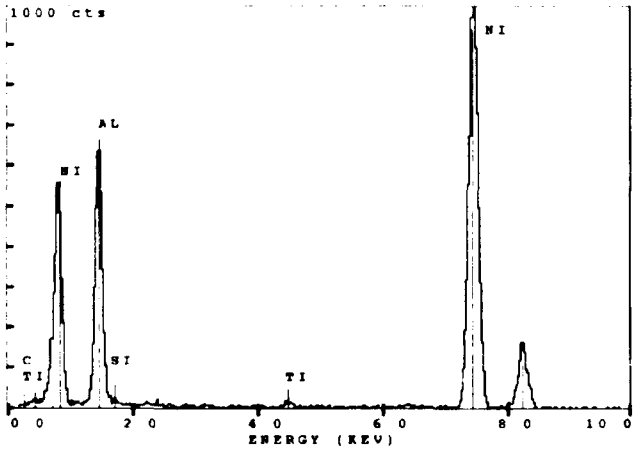

(*c*)

Fig. 9—EDS profiles of TiB_2 particles and close-by regions: (*a*) inside the TiB_2 particles, (*b*) interface region of TiB_2 and NiAl (silicon K_α peaks are visible), and (*c*) NiAl matrix close to the TiB_2 particles.

of the interface layer and Si segregation in all of the samples investigated confirmed the existence of a Si-rich interface layer at the TiB_2-NiAl interface. Because silicon is one of the most common impurities in commercial aluminum metal, the silicon atoms segregated at TiB_2-NiAl interfaces would probably come from impurities within the aluminum powders which are used in the processing of the composites. Silicon was not found at the NiAl subgrain or grain boundaries. Obviously, the TiB_2-NiAl interfaces are energetically preferential sites for silicon atoms. Experimentally, coherent or semicoherent interfaces between NiAl and TiB_2 have not been observed *via* HREM. Generally, interfaces in *in situ* composites have low energies and are usually semicoherent.[14] However, the tendency for forming semicoherent interfaces might be reduced by introducing silicon atoms to the TiB_2-NiAl interface region.

It is obvious from a consideration of the above data that an interface layer does not exist at the Al_2O_3-NiAl interface. The Si segregation layer at the TiB_2-NiAl interface is too thin to act as a shock absorber of the thermal residual stress.

The bond strength of a metal/ceramic interface is mainly determined by both the imperfections, such as voids and microcracks, at or close to the interface and the work of adhesion.[15,16] This is defined as $W_{ad} = \gamma_m + \gamma_c - \gamma_{m_c}$, where γ_m and γ_c are surface energies of free surfaces of metal and ceramic, respectively, and γ_{m_c} is the energy of a relaxed metal/ceramic interface. There is no direct correlation between bond strength and work adhesion in a number of metal/ceramic interface systems. The bond strength seems to depend mostly on the interface imperfections and local stresses.[15] For the TiB_2/NiAl composite samples which were deformed 30 pct at a temperature range of 760 °C to 1000 °C, no voids, cracks or any other debonding evidence has been observed at the interface region, and the HREM investigations have shown that both α-Al_2O_3 and TiB_2 formed a perfect atomic level match with the matrix materials (NiAl) after deformation. Therefore, both α-Al_2O_3 and TiB_2 formed an excellent bond with the matrix (NiAl).

IV. CONCLUSIONS

Based on the above observations, the following conclusions can be reached:

1. In XD-processed TiB_2/NiAl composites, NiAl formed an excellent bond with the reinforcement TiB_2 particles, as well as with the α-Al_2O_3 particles.
2. No consistent crystallographic orientation relationships have been found between the NiAl matrix and TiB_2 or α-Al_2O_3 particles, although in some cases, one or two low-indexed crystallographic planes of TiB_2 or α-Al_2O_3 might be aligned with those of NiAl.
3. Silicon segregation has been found in the TiB_2-NiAl interface region. No coherent or semicoherent interfaces have been observed between the TiB_2 and the NiAl, and the Si layer is too thin to absorb any of the thermal residual stress.
4. There is a strong tendency for the formation of semicoherent interfaces between α-Al_2O_3 and NiAl. No segregation has been found at these interfaces.

ACKNOWLEDGMENTS

This research was supported by the Office of Naval Research under Contract No. N00014-91-J-1353. We

would also like to acknowledge the support of the Argonne National Laboratory HVEM facility.

REFERENCES

1. R.K. Viswanadham, S.K. Mannan, and B. Sprissler: MML TR 87-66C, Martin Marietta Laboratories Annual Report, Bethesda, MD, 1987.
2. K. Sharvan Kumar and S.K. Mannan: MML TR 88-66C, Martin Marietta Laboratories Progress Report, Bethesda, MD, 1988.
3. O. Popoola, C. Cordier, P. Pirous, and A.H. Heuer: in *Interfaces in Metal-Ceramics Composite*, R.Y. Lin, R.J. Arsenault, G.P. Martins, and S.G. Fishman, eds., TMS, Warrendale, PA, 1990, p. 465.
4. R.M. Aikin, Jr.: NASA Contractor Report 4276, Feb. 1990.
5. L. Wang and R.J. Arsenault: *Mater. Sci. Eng.*, 1990, vol. A127, pp. 91-98.
6. L. Wang and R.J. Arsenault: *Phil. Mag. A*, 1991, vol. 63, pp. 121-30.
7. M. Taya and R.J. Arsenault: *Metal Matrix Composites, Thermomechanical Behavior*, Pergamon Press, Oxford, United Kingdom, 1989.
8. K.L. Merkle: in *Interfaces Between Polymers, Metals and Ceramics, MRS Symp. Proc., vol. 153*, B.M. Dekoven, A.J. Gellman, and R. Rosenberg, eds., Pittsburgh, PA, 1989, p. 83.
9. L.J. Wasilewski: *Trans. AIME*, 1966, vol. 236, p. 455.
10. *Handbook of Materials Science, Vol. 2*, C.T. Lynch, ed., CRC Press, Boca Raton, FL, 1974, p. 358.
11. I.K. Schuller, A. Fartash, and M. Grimsditch: *MRS Bull.*, 1990, vol. XV (10), pp. 33-37.
12. S.R. Phillpot, D. Wolf, and S. Yip: *MRS Bull.*, 1990, vol. XV (10), pp. 38-45.
13. W. Mader: *Characterization of Defects in Materials, MRS Symp. Proc., vol. 82*, R.W. Siegel, J.R. Weertman, and R. Sinclair, ed., Pittsburgh, PA, 1987, p. 403.
14. K.K. Chawla: *Composite Materials Sciences and Engineering*, MRE Series, Springer-Verlag, Germany, 1987, p. 79.
15. M. Nicholas: *J. Mater. Sci.*, 1986, vol. 3, p. 571.
16. A.G. Evans and M. Rühle: *MRS Bull.*, 1990, vol. XV (10), pp. 46-50.

Scripta METALLURGICA et MATERIALIA
Vol. 25, pp. 2617-2621, 1991
Printed in the U.S.A.
Pergamon Press plc
All rights reserved

STRENGTHENING MECHANISMS IN PARTICULATE MMC: Remarks on a Paper by Miller and Humphreys

R.J. Arsenault
Metallurgical Materials Laboratory, Department of Materials and Nuclear Engineering, University of Maryland, College Park, Maryland 20742-2115

(Received May 14, 1991)
(Revised July 16, 1991)

In a recent paper, Miller and Humphreys (MH)[1] make several statements which should be examined in further detail, and this examination will follow. However, there is one point that MH make which should be emphasized; "However as the ratio of fibre length to diameter decreases, the approximations made in the modified shear lag approach become questionable."

First, let us begin with the general concept of strengthening of aluminum and aluminum alloys by the addition of whisker or particulate SiC. MH state that several factors should be included when considering the strengthening of SiC/Al composites. Arsenault et al. have produced numerous publications of the list of the factors which can contribute to strengthening and have examined the contribution to strengthening of each one of them in detail [2-31], and have concluded that the strengthening was due to the work hardening of the matrix. For example, in one of the reference books cited by MH, there is such a list given by Arsenault [19].

Second, let us now consider some specific points raised by MH.

One: They state that the equation derived for the strengthening due to an increase in dislocation density generated by the difference in the coefficients of thermal expansion should indicate that the strengthening is directly related to volume fraction of reinforcement and inversely related to particle size to the 1/2 power. Let us consider the equation generated by Arsenault and Shi [8] to predict the increase in strength due to dislocation generation by the relaxation of the thermal residual stress which is caused by the difference in thermal coefficients of expansion between the particulate SiC and the matrix. This particular equation predicts (as stated when first derived) the most efficient method of stress relaxation due to dislocation generation. In other words, this equation predicts the increase in minimum dislocation density. However, more realistic attempts to obtain the upper limit of the dislocation density due to thermal residual stress relaxation have resulted in an unrealistically high dislocation density.

Further, in regard to the simple equation derived by Arsenault and Shi [8], it does show that the strength change due to dislocation generation is a function of the volume fraction of the particulate divided by the diameter of the particulate to the ½ power, i.e.,

$$\Delta\sigma \sim \frac{V_f}{d^{1/2}} \qquad (1)$$

Two: MH presume that dislocation generation will only occur during the

0036-9748/91 $3.00 + .00
Copyright (c) 1991 Pergamon Press plc

quenching of the sample. In other words, if the sample is furnace-cooled (cooled slower than 1°C/min), then there will be no dislocation generation. In Fig. 1 (dislocation density vs. volume fraction) and Fig. 2 (dislocation density vs. particle size) the data was obtained from samples which were **FURNACE-COOLED.**

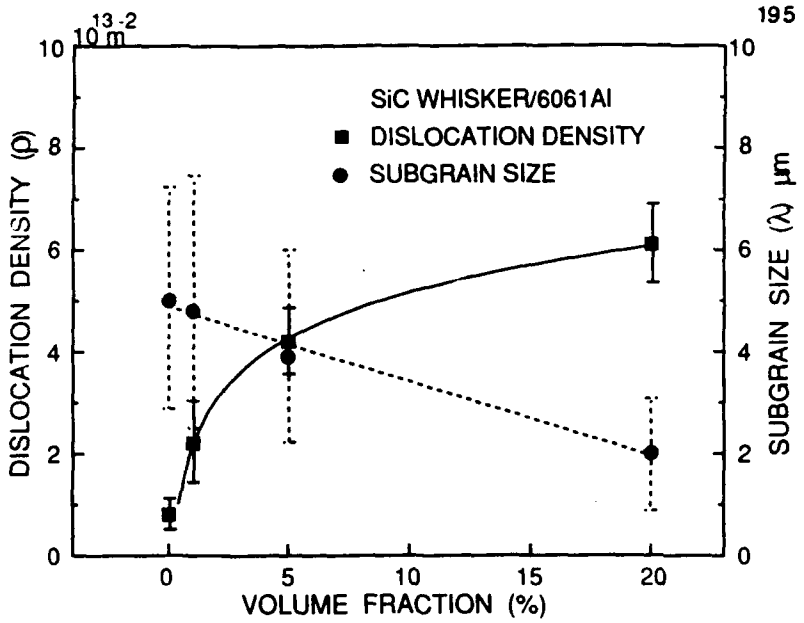

Fig. 1 The change in dislocation density as a function of volume fraction of SiC (SiC whiskers have a length to diameter ratio on average of ~ 2 and the dia ~ 0.5 μm). (Ref. 27).

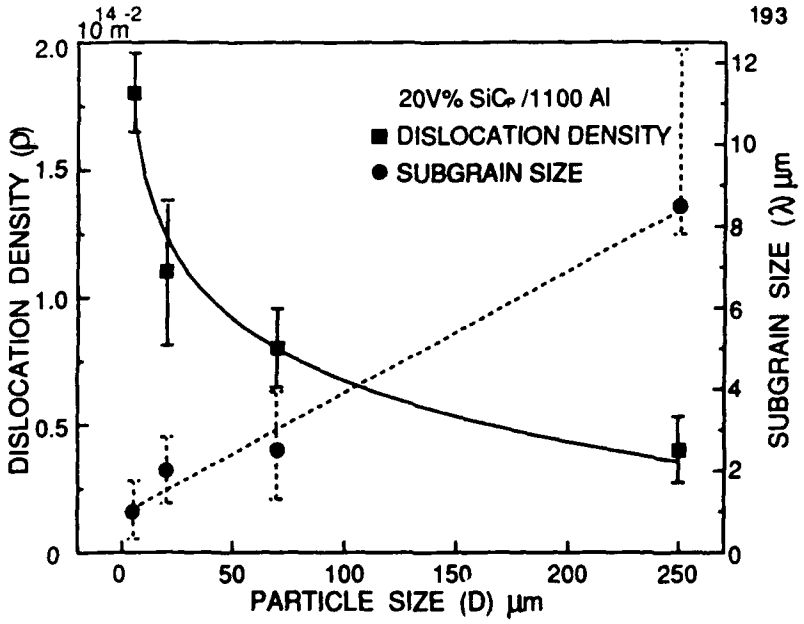

Fig. 2 The change in dislocation density as a function of particulate size. (Ref. 27.)

If we consider the data in Figs. 1 and 2 and make the assumption that the dislocation density is uniform (which it is not) and use the following equation

$$\Delta\sigma = \alpha\mu b\Delta\rho^{1/2} \quad (2)$$

where α is a constant ranging from 0.5 to 1.25, μ is the shear modulus, b is the Burgers vector, and $\Delta\rho$ is the change in dislocation density due to the ΔCTE effect, then it is possible the predicted increase in strength is due to the increase in dislocation density. The predicted increases in strength are given in Tables I and II.

Three: MH state that the change in subgrain size due SiC addition to Al is inconsequential. Figures 1 and 2 are experimental measurements of the decrease in subgrain size with increasing volume fraction and an increase in subgrain size with increasing particle size. Employing this experimental data with the experimental data of McQueen et al. [32] who measured the change in strength of Al as a function of subgrain size, it is possible to determine the strength increase due to the decrease in subgrain size. As can be seen in Tables I and II, there can be a considerable increase in the strength, for a particle size of 0.5 μm, $\Delta\sigma_{sg}$ = 131 MPa.

Four: MH state that the increase stress i.e. work hardening between the proportional limit and the yield stress defined at 0.2% offset strain is due to the formation of Orowon loops about the SiC whiskers or particles. It has been shown by a detailed FEM analysis that the plastic zones around the reinforcement expand upon loading[33]. There is no indication of deformation beginning in the matrix and expanding towards the reinforcement.

Fifth: Let us now consider the following statement of MH, "The *strength of particulate MMCs* is consistent with the estimates based on micromechanical models developed by conventional 2-phase alloys." The question that follows: Which conventional model has taken into account the strengthening due to dislocation generation and the reduction in subgrain size due to the ΔCTE effect? As far as we know, the models put forward by Arsenault et al. were the first to take into account the strengthening due to an increase in dislocation density **CAUSED BY THE ΔCTE EFFECT** and the reduction in subgrain size **DUE TO THE ΔCTE EFFECT**.

In conclusion, several points need to be made:

- The strength increase due to the addition of SiC whiskers or particulate to aluminum or aluminum alloys can more than adequately be accounted for by the increase in dislocation density and the reduction of the subgrain size due to ΔCTE effect.

- Arsenault et al. have considered several other possible contributing factors and have shown that they are inconsequential. In the past, Arsenault et al. have proposed that the strength of SiC/Al composites is due to a *nonconventional phenomenon*, i.e., the increase in dislocation density and the decrease in the subgrain size due to the ΔCTE effect.

Acknowledgement

The author wishes to acknowledge to continued support of Dr. Steven Fishman of the ONR. This research was supported by a contract from ONR N00014-91-J-1353.

Table I
Predicted Increase in Yield Strength of 20 V% SiC 1100 Matrix and Experimentally Measured Values

Particle Size D (μm)	$\Delta\sigma_\rho$ (MPa)	$\Delta\sigma_{SG}$ (MPa)	$\Delta\sigma_{res}$ (MPa)	$\Delta\sigma_{y_{pred}}$ (MPa)	$\Delta\sigma_{y_{exp}}$ (MPa)
0.5	126.6	131	0	257.6	153
9	99	69	17	151	88
70	79	20	17	82	69
250	59.7	0-13.8	17	42.7-56.5	26

$\Delta\sigma_\rho$ The predicted increase due to the increased dislocation density
$\Delta\sigma_{SG}$ The predicted increase due to the reduced subgrain size
$\Delta\sigma_{res}$ The predicted average tensile residual stress
$\Delta\sigma_{y_{pred}}$ The sum of $\Delta\sigma_\rho + \Delta\sigma_{SG} - \Delta\sigma_{res}$
$\Delta\sigma_{y_{exp}}$ The yield stress defined at 0.2% plastic strain minus the 0.2% yield stress of the 0 V% 1100 matrix

[Ref. 27]

Table II
Predicted Increase in Yield Stress of 6061/Al Alloy as a Function of Volume Fraction of SiC Whisker

Volume V%	$\Delta\sigma_\rho$ MPa	$\Delta\sigma_{SG}$ MPa	$\Delta\sigma_{res}$ MPa	$\Delta\sigma_{y_{pred}}$ MPa	$\Delta\sigma_{y_{exp}}$ MPa
1	37.7	0	1.7	36.0	6.9
5	56.6	7.0	8.6	55.0	52
20	70	48.3	34.5	83.8	100

$\Delta\sigma_\rho$ The predicted increase due to the increased dislocation density
$\Delta\sigma_{SG}$ The predicted increase due to the reduced subgrain size
$\Delta\sigma_{res}$ The predicted average tensile residual stress
$\Delta\sigma_{y_{pred}}$ The sum of $\Delta\sigma_\rho + \Delta\sigma_{SG} - \Delta\sigma_{res}$
$\Delta\sigma_{y_{exp}}$ The yield stress defined at 0.2% plastic strain minus the 0.2% yield stress of the 0 V% 1100 matrix

[Ref. 27]

REFERENCES

1. W.S. Miller and F.J. Humphreys, Scripta Metall. 25, (1991) 33.
2. R.J. Arsenault and R.M. Fisher, Scripta Metal. 17, 1983, 67.
3. R.J. Arsenault, Mater. Sci. Eng. 64, 1984, 171.
4. R.J. Arsenault and M. Taya, Acta Metal. 35, 1987, 651.
5. M. Vogelsang, R.J. Arsenault and R.M. Fisher, Metal. Trans. 17A, 1986, 379.
6. Y. Flom and R.J. Arsenault, Mater. Sci. Eng. 75, 1985, 151.
7. Y. Flom and R.J. Arsenault, Mater. Sci. Eng. 77, 1986, 191.
8. R.J. Arsenault and N. Shi, Mater. Sci. Eng. 81, 1986, 175.
9. Y. Flom and R.J. Arsenault, J. of Metals 38, 1986, 31.
10. R.J. Arsenault and B. Wu, Mater. Sci. Eng. 96, 1987, 77.
11. "Composites '86: Recent Advances in Japan and the United States, Proc. Japan-U.S. CCM III-," ed. by K. Kawata et al., 1986, Tokyo, 521.
12. M. Taya and R.J. Arsenault, Scripta Metal. 21, 1987, 349.
13. "Mechanical Behavior of Materials," Ed. by M.G. Yan, S.H. Zhang and Z.M. Zhang, p. 1253, 1987.
14. Y. Flom and R.J. Arsenault, Sixth Int. Conf. on Composite Material, Ed, by F.L. Mathews et al., p. 189, Elsevier Appl. Sci., Vol. 2, 1987.
15. R.J. Arsenault, "Composite Structures," ed. by I.H. Marshall, p. 70, Elsevier Appl. Sci. 1987.
16. R.J. Arsenault and S.B. Wu, Scripta Metal. 22, 1988, 762.
17. R.J. Arsenault and S.B. Wu, Proc. Advances in Cast Reinforced Composites, Ed. S. Fishman and A. Dhingra, p. 31, ASM, 1988.
18. R.J. Arsenault and M. Taya, Mater. Sci. Eng. A 108, 1989, 285.
19. Proc. 9th Riso Int. Symposium on Metallurgy and Materials Science, 1988, Ed. S.I. Anderson, H. Lilholt and O.B. Pederson, 279.
20. R.J. Arsenault, Scripta Metal. 23, 1989, 293.
21. R.J. Arsenault, C.R. Feng and N. Shi, U.S.-Japan Proc. on Composite Materials, to be published.
22. R. J. Arsenault, Composite Tech. Research, 10, 1988, 140.
23. Y. Flom and R.J. Arsenault, Acta Metal. 37, 1989, 2413.
24. N. Shi and R.J. Arsenault, Accepted for publication in "The 7th Int. Conf. on Composite Materials," China.
25. Y. Flom, S.B. Wu and R.J. Arsenault, SAMPE Proc, to be published.
26. R.J. Arsenault, N. Shi, C.R. Feng and L. Wang, Mater. Sci. Eng. A, 131 (1991) 55.
27. R.J. Arsenault, L. Wang and C.R. Feng, Acta Metall. 39 (1991) 47.
28. R.J. Arsenault and Y. Flom, In "Structure and Deformation of Boundaries," ed. by K.N. Subramanian and M.A. Iman, AIME 1986, 261.
29. N.Shi, and R.J.Arsenault, accepted for publication, Comp.Sci. and Technology. 1991.
30. R.J. Arsenault, "Metal Matrix Composites," ed. R. Everrett and R.J. Arsenault, Academic Press, NY, 1990, p. 133.
31. Ibid., p. 79.
32. H.McQueen and J.E. Hackett, Metall. Trans. 1 (1970) 2997.
33. N. Shi and R.J. Arsenault, to be submitted for publication.

Ning Shi[1] *and Richard J. Arsenault*[1]

The Effect of Thermal Residual Stresses on the Asymmetric Constitutive Behavior of Metal-Matrix Composites

Authorized Reprint 1992 from Journal of Composites Technology & Research, Winter 1991
Copyright American Society for Testing and Materials, 1916 Race Street, Philadelphia, PA 19103

REFERENCE: Shi, N. and Arsenault, R. J., "**The Effect of Thermal Residual Stresses on the Asymmetric Constitutive Behavior of Metal-Matrix Composites,**" *Journal of Composites Technology & Research*, Vol. 13, No. 4, Winter 1991, pp. 211–226.

ABSTRACT: An analytical investigation of the difference in the constitutive behavior of silicon carbide-aluminum (SiC-Al) composites under uniaxial compressive and tensile loading was carried out, and the associated changes of the residual stresses were studied. It is suggested that the observed asymmetric response of the constitutive behavior is primarily due to the existence of residual stresses in the composite. These residual stresses are initially introduced because of the differences in the coefficients of thermal expansion (ΔCTE) during the cooling process and subsequently changed after the external load is applied. A two-dimensional (2-D) finite element analysis of a hexagonal array of SiC whiskers in an Al matrix was performed, the result of which testifies to the appropriateness of the proposed explanation. It is concluded that the 2-D finite element analysis is an economical way of adequately reproducing the most prominent features of the material's constitutive behavior. Based upon the theory of mechanics of composite material, simplified analytical models were developed which can be used to investigate the influences of the whisker-matrix interface shear load transfer and the volume mismatch on the residual stresses. It is concluded that the mechanism of load transfer in terms of normal stress at the whisker tip, which is governed by the volume (bulk) mismatch between the matrix and the whisker, is predominantly responsible for altering the specific pattern of the residual stresses under the applied load. In contrast, the effect of shear load transfer at the longitudinal whisker-matrix interface is only restricted to a very small region in the vicinity of the whisker and does not influence the overall symmetry of the constitutive behavior.

KEY WORDS: thermal residual stress, deformation induced residual stress, asymmetric constitutive behavior, whisker-reinforced metal-matrix composites, FEM, volume mismatch, interface load transfer (shear lag)

Nomenclature

σ_{ij}	Stress
$\langle\sigma_{ij}\rangle$	Average stress
A_k	Area of element K
$\bar{\sigma}_{ij}$	Effective average stress
q	Applied load intensity
σ'_w	Thermal residual stress in the whisker
$\Delta\alpha$	Difference in the coefficients of thermal expansion
ΔT	Magnitude of temperature change
Δw	Difference of displacement at the whisker matrix interface and longitudinal displacement away from the interface
τ_{rz}	Interfacial shear stress
Δw_y	Δw when matrix approaches yielding (σ_{zz})
D and d	Diameters of the unit cell and whisker
V_w	Whisker volume fraction
E_m	Young's modulus of the matrix
E_w	Young's modulus of the whiskers
E_{mt}	Work-hardening rate of the matrix
σ_{my}	Matrix yield stress
l	Total length of the whisker
G_{mt}	Tangential shear modulus of the matrix
σ_{zz}	Applied stress
ε_{zz}	Total applied strain
$\langle\sigma'_m\rangle$	Average longitudinal matrix residual stress as a result of external applied stress σ_{zz}
E_c	Young's modulus of the composites
C^m_{ijkl} and C^{mt}_{ijkl}	Stiffness and tangential stiffness of the matrix
ε_y and σ'_y	Average strain and stress on the yield surfaces in the strain and stress space
ν_c	Poisson's ratio of the constituent in the composites
$\langle\sigma'_m\rangle$	Average longitudinal thermal residual stress in the matrix
V_{mi}	Volume fraction of the initial tension zone in the matrix
$\langle\sigma'_{mi}\rangle$	Average longitudinal matrix thermal residual stress in the initial tensile zone
$\langle\sigma'_{mc}\rangle$	Average thermal residual stress in the compressive zone
ΔT_c	Magnitude of the temperature change that will induce plastic deformation at the top of the whisker
ΔT_y	Magnitude of the temperature change by which the entire matrix is plastically deformed
$\langle\sigma'_{mi}\rangle$, $\langle\sigma''_{mi}\rangle$	Average longitudinal internal stress in the initial tensile and compressive zone, respectively, when a uniaxial external applied stress is applied
$\langle\sigma'''_{mi}\rangle$, $\langle\sigma'''_{mc}\rangle$	Average longitudinal residual stress in the initial tensile and compressive zone after the uniaxial applied external load is released
ε_{zzp}	Applied plastic strain

[1]Graduate student and professor, respectively, Metallurgical Materials Laboratory, Department of Materials and Nuclear Engineering, University of Maryland at College Park, MD 20742–2115.

© 1991 by the American Society for Testing and Materials

Introduction

A previous investigation of the deformation behavior of short whisker-reinforced silicon carbide-aluminum (SiC-Al) composites [*1*] has indicated that the constitute behavior of these composites is distinctly different under uniaxial compressive deformation as compared to tensile deformation. It was generally found that the compressive yield strength of these composites

was larger than that of the tensile yield strength, while the apparent Young's modulus for compression was smaller than that in tension. If monolithic aluminum is initially deformed plastically in tension, then reverse deformed in compression, a difference in stress is required to initiate plastic deformation in the reverse cycle. Usually, the magnitude of the yield stress in the reverse cycle is less than the flow stress in the forward cycle. This reduction in stress (or the strain necessary to reach the previous level of flow stress) is defined as the Bauschinger effect. In the case of monolithic aluminum, the direction of initial deformation (that is, tensile or compressive) does not have any influence on the Bauschinger effect. The SiC-Al composites, however, exhibit a remarkable characteristic, that is, the flow stress drop (or alternatively, the Bauschinger strain) is larger when the composite is first precompressed plastically and subsequently deformed in tension than when the composite is first deformed in tension and then in compression [*1*].

It is the opinion of the authors that the aforementioned differences in the constitutive behavior under tensile and compressive loading as well as the asymmetric Bauschinger phenomenon are primarily due to the influence of the residual stresses. It has been shown that thermal residual stresses affect not only the elasto-plastic deformation behavior of the composites [*1*], but also the fracture behavior [*2*]. Therefore, it becomes increasingly important to investigate the influence of residual stress on the deformation process.

The material to be simulated in this investigation consists of an annealed 6061 aluminum alloy matrix reinforced by silicon carbide whiskers. The primary goal of this paper is to, first, investigate analytically the generation, arrangement, and magnitude of the residual stresses caused by the difference in coefficients of thermal expansion (ΔCTE) between the reinforcement and the matrix during the cooling process; second, study the changes in the residual stress as a result of external deformation either in tension or compression; and finally, investigate the differences in the constitutive behavior under different external loading, that is, deformation conditions.

In an experimental procedure described elsewhere [*1,3*], the materials is annealed at 723K and then tested either in uniaxial tension or compression at room temperature. Our commitment in this investigation is to adhere to this physical process and, thereby, to simulate the constitutive behavior of the composites and monitor the change of the residual stresses. These residual stresses were induced during the cooling process and subsequently altered by external load.

While several investigators have concentrated their efforts on the thermal residual stresses [*4-8*], others [*9-18*] have worked on the elasto-plastic behavior of the short whisker-reinforced composites with emphasis on the stress-strain relationship of the composites, that is, the constitutive behavior. Their research includes numerical treatments that use finite element procedures [*9-13*]. Some of them paid special attention to the microstructural change in the matrix [*10,13*], while others were based on various theoretical bases with different assumptions [*14-18*].

Recently, Arsenault and Taya [*19*] and Withers et al. [*20*] used the Eshelby method [*21,22*] to explain the yielding behavior of the short whisker-reinforced metal-matrix composites (MMC) under the influence of the thermal residual stresses. They found that the residual stresses are totally responsible for the difference in the yield strength of the whisker-reinforced MMC between tensile and compressive uniaxial loading. However, despite the effort by the previous investigators [*19,20*], the role residual stresses played in the constitutive behavior of the composites or the effect of the external loading on the formation of the residual stresses has never been systematically investigated. Nevertheless, these experimental and theoretical results [*19,20*] have provided us with a clear indication that the residual stresses may be a dominating factor that accounts for the differences of the constitutive behavior of the composites under a uniaxial tensile or compressive load.

The analytical investigation in this study is carried out by two distinct methods: a finite element analysis and a phenomenological modelling scheme involving two models. The main objective of the finite element analysis is to monitor the stress-strain relationship and the changes that occur in the value of the residual stresses as a result of the external deformation. The purpose of the phenomenological models, on the other hand, is to obtain some physical insight into the various factors that control the processes of residual stress generation and alteration and the role these play in influencing the constitutive behavior of the composites.

The Finite Element Model

To determine the response of the composite material under the influence of residual stresses, a simplified two-dimensional (2-D) plane strain finite-element analysis was carried out using the ADINA code. In this analysis, the reinforcement is assumed to be perfectly elastic, the matrix is assumed to follow bilinear stress-strain relationship, and the isotropic hardening rule is used. Particular interest was paid to determining the macroscopic stress-strain behavior of the composite and performing a microscopic analysis of the subsequent changes that occur in the values of the matrix longitudinal residual stresses after the external load was removed. The modelling of the change of the residual stress as a function of applied load was also performed through three-dimensional (3-D) finite element method (FEM) analysis with the same boundary condition consideration. The results are compared with those obtained from the 2-D plane strain model.

A recent study by Takao and Taya [*23*] showed that the use of the volume-average aspect ratio will provide an accurate account for the overall properties of the composites, and the employment of the perfect alignment assumption will give rise to satisfactory results. Therefore, in the analyses, the value of the volume fraction of the whiskers as well as the whisker aspect ratio were held constant ($V_w = 20\%$ and $l/d = 4$). A value of $l/d = 4$ is a typical representation of the average value observed experimentally [*24,25*]. Furthermore, it was assumed that the composite consists of an array of hexagonally distributed parallelepiped SiC whiskers embedded in a 6061 aluminum alloy matrix (Fig. 1). A unit cell can be constructed because of periodic reinforcement arrangement. Previous investigations [*9,11*] and our current analysis have indicated that within a particular region, a small variation in the values of interparticle spacing does not significantly affect the material behavior (for example, for yield stress, see Fig. 2). The value of V/H in Fig. 1, therefore, was not selected as a critical parameter in the analysis and was kept as a constant (0.29) throughout the analyses. Note that although from Fig. 1 it appears that the effect of the variation of V/H is slightly smaller when a larger V/H value is selected, the rate of convergency is better when the current value was

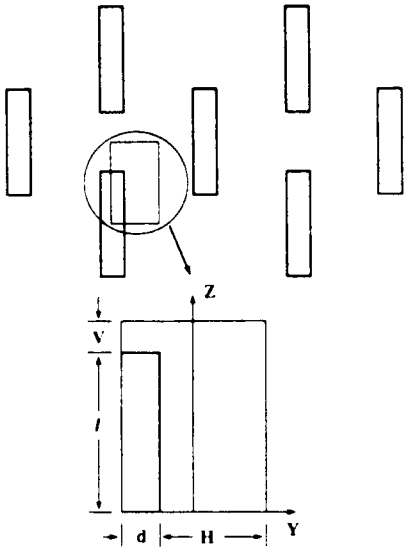

FIG. 1—*The whiskers are distributed as a periodic hexagonal infinite array in the matrix. By considering symmetry, a unit cell that contains only a quadrant of the particle is needed, as indicated in the figure.*

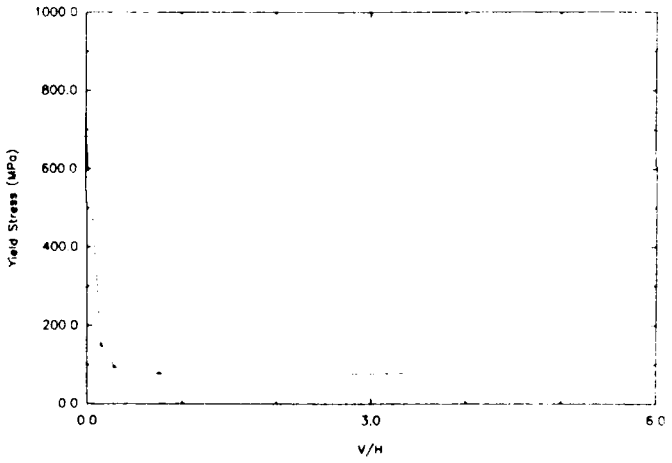

FIG. 2—*FEM results indicate that the yield stress of the composites is not sensitive to the ratio of V/H defined in Fig. 1.*

selected, that is, it will result in a more efficient usage of computer time.

Figure 3 indicates the exact details of the finite-element mesh. Only a quadrant of the composite material which contains the SiC whisker was selected to represent the whole infinite array of fibers in the matrix. A multi-constraint boundary condition was used in the analysis to consider the geometrical symmetry and the condition of the internal stress indicated as the following:

$$\int_{l_k} \sigma_{ij} n_j dl = \sigma_{ij}^{\infty}$$

where σ_{ij} is the stresses at the boundary, σ_{ij}^{∞} is the applied stress, n_j is the unit outward normal, and l_k represents four different sides of the boundary of the unit cell.

Since the constitutive behavior of the SiC/Al whisker composites has been extensively investigated experimentally [1,25,26],

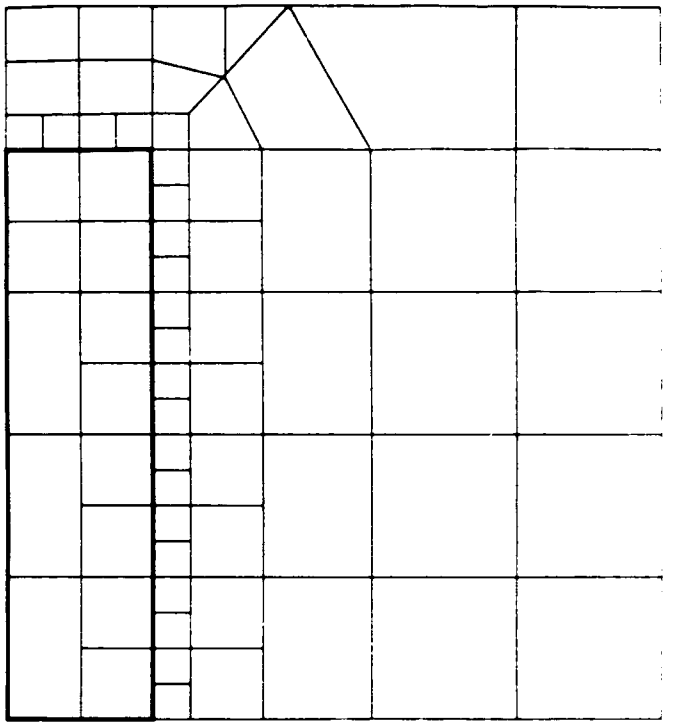

FIG. 3—*FEM mesh where six- to eight-node elements were used.*

it is appropriate to compare our FEM results with the experimental results. The experimental evidence [1] indicated that the apparent Young's modulus and the yield strength of the composites were different when a uniaxial tensile and compressive load was applied. The apparent Young's modulus is larger under tensile uniaxial applied load, whereas the yield strength is higher under compressive load. It is a hypothesis at this stage that the differences in the constitutive behavior of the composites are due mainly to the presence of the thermal residual stresses. Therefore, by considering the initial thermal residual stresses which are generated during the cooling process, such differences should be reproduced by the FEM simulation. Consequently, if such differences are predicted, then the residual stresses that are responsible for producing such differences should be reasonably well predicted. Figure 4 shows the uniaxial stress-strain curves produced by the FEM analysis where the global stress and strain are defined as:

$$\varepsilon = \frac{u_i}{V + l}; \qquad \sigma = \langle \sigma_{ij} \rangle$$

where u_i and $\langle \sigma_{ij} \rangle$ are the average displacement and normal stress along the boundary whose normal is parallel to the direction of the uniaxial loading. The value $\langle \sigma \rangle$ can also be defined as the applied load intensity (q) and V/l are defined in Fig. 1.

Comparing the stress-strain relationship under tension and compression, it can be seen that the differences in Young's modulus and yield strength of the composites have been reproduced in a correct way.

A Bauschinger test can also be carried out by FEM. The direction of initial loading has an effect on the magnitude of the Bauschinger strain (ε_B), as defined in Fig. 5. If initially tested in

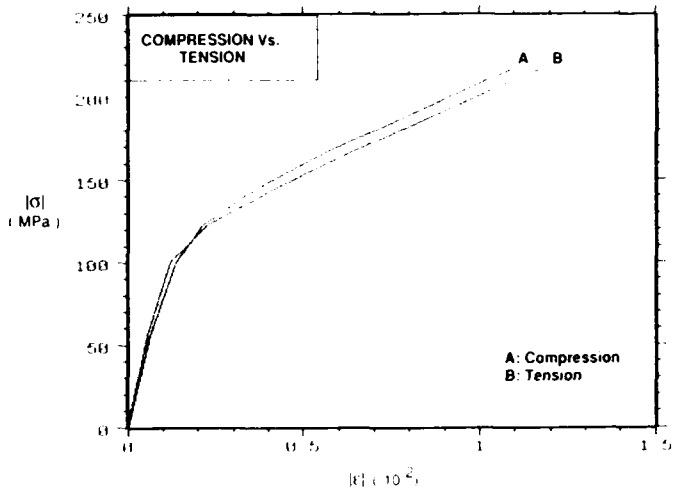

FIG. 4—*Stress-strain curves predicted by FEM where the apparent Young's modulus of the composite is higher when it is in tensile load, whereas the yield stress is greater when the sample is under compressive load.*

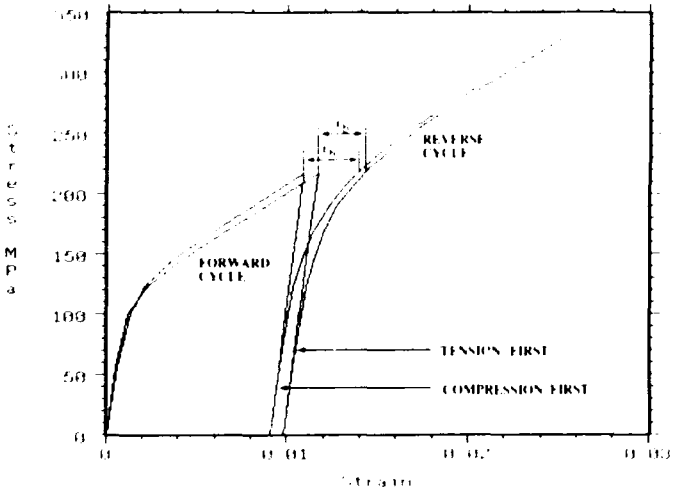

FIG. 5—*FEM prediction of Bauschinger strain (ϵ_B) where ϵ_B is larger if the sample is under the compression-first loading scheme.*

tension and then reverse loaded into compression, the Bauschinger strain is smaller compared to the case in which initial loading is in compression followed by tension (Fig. 5). This has been observed experimentally [*1*].

In the study of the internal stresses in composite materials, it is a common practice to use the concept of volume average both experimentally [*27,28*] and theoretically [*19,20,29*]. In this research, the same method is employed. Because the longitudinal thermal residual stress is much larger than the transverse residual stress [*19*], it is believed that the observed differences in constitutive behavior are due mainly to the longitudinal thermal residual stress. The longitudinal thermal residual stress in the composite was therefore determined by first evaluating the residual stress in finite-element mesh and then averaging these values over the whole specimen. The overall average residual stress in the matrix was calculated through a simple averaging scheme given by the following equation:

$$\langle \sigma_{ij} \rangle = \frac{\sum_k (\sigma_{ij})_k A_k}{\sum_k A_k} \qquad (i = j = 3) \tag{3}$$

where $(\sigma_{ij})_k$ is the stress in element k, and A_k is the area of that element.

Using such a simplified averaging scheme, it was found that upon application of 1% plastic strain, if the applied loading is tensile, the average matrix residual stress changes from its initial tensile state of 47.5 MPa to the compressive state of −10.8 MPa, while if the applied loading is compressive, the average matrix longitudinal (tensile) residual stress drops 20.1 MPa and then increases back up to 29.3 MPa when it reaches 1% plastic strain.

The overall change in residual stress as a function of applied strain is shown in Fig. 6. It is clear that the primary effect on the longitudinal residual stress from compressive loading is that the magnitude of the residual stress in the matrix reduces and then increases upon further loading while tensile deformation produces an overall reduction in the tensile residual stress and eventually changes the residual stress from tensile to compressive. That is, the change in residual stress does not occur monotonically with increasing deformation.

It is also interesting to see that, in the case of compressive deformation, the initial tensile residual stress reduces until the total applied strain reaches about 0.3% which is within close proximity of 0.2% strain of yielding. At this point, the tensile residual stress reaches a minimum. Upon further deformation, there is an increase in the tensile residual stress. In the case of tensile deformation, the tensile residual stress initially decreases at a more rapid rate to ~0.3% total strain, then the rate of decrease becomes less. At a total strain of ~0.8%, the residual stress becomes compressive. The longitudinal residual stress contour after different levels of the total applied strain is shown in Figs. 7 through 11.

Despite the fact that the total average longitudinal thermal residual stress is in tension, previous FEM results [*13*] have in-

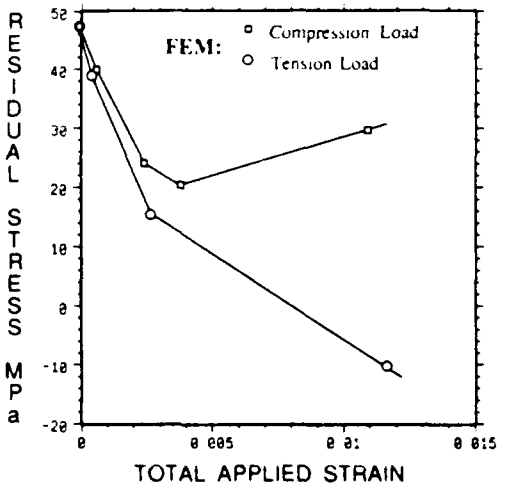

FIG. 6—*Average longitudinal residual stress as a function of the total applied strain predicted by FEM.*

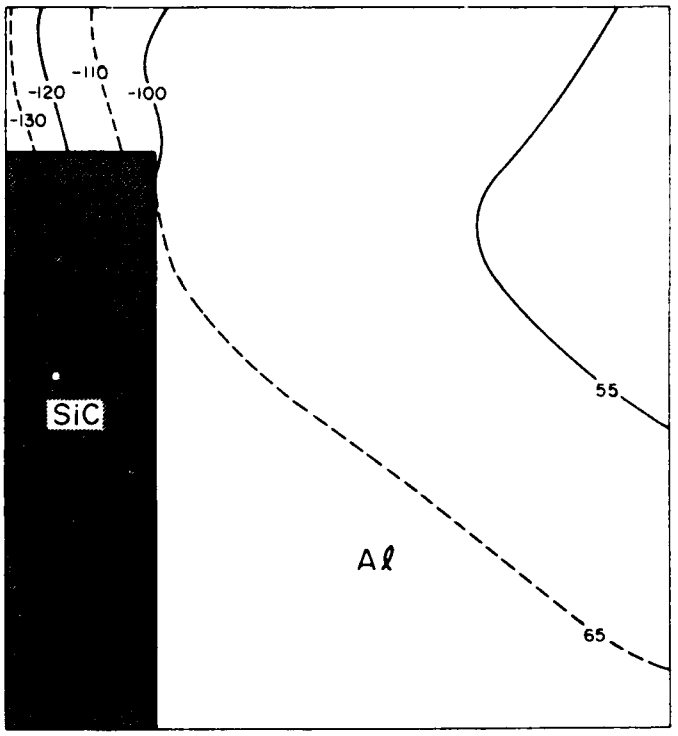

FIG. 7—*Longitudinal residual stress contour at a total applied strain of* $\varepsilon_{total} = 0$ *(thermal residual stress)*

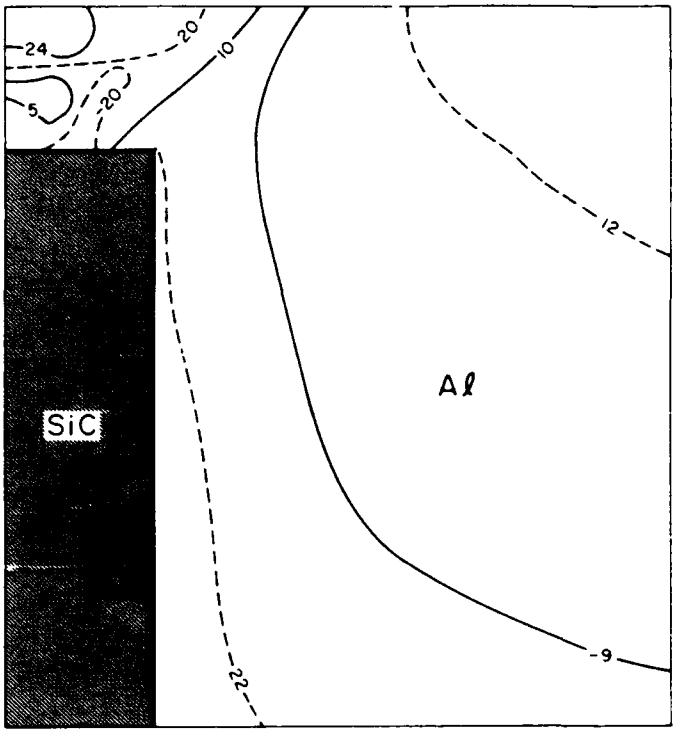

FIG. 9—*Longitudinal residual stress contour at a total applied strain of* $\varepsilon_{total} = 0.47\%$.

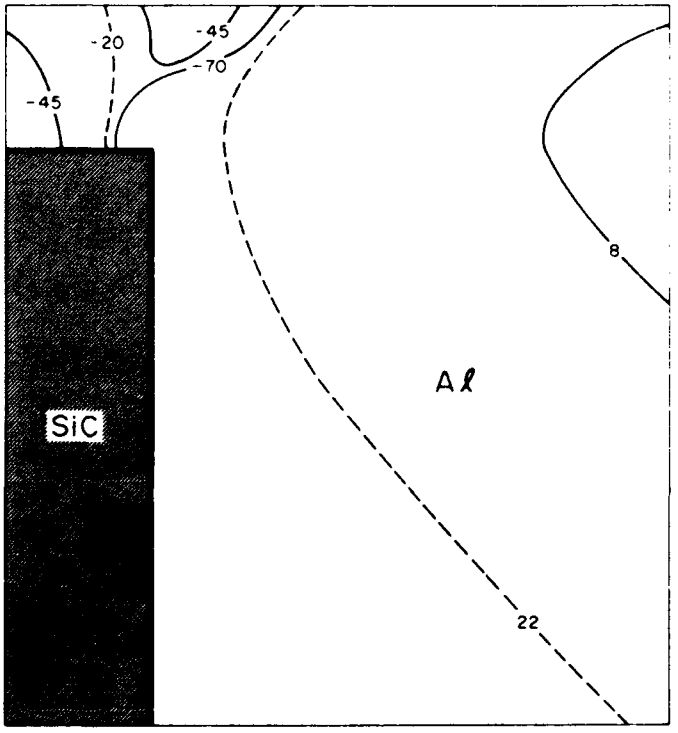

FIG. 8—*Longitudinal residual stress contour at a total applied strain of* $\varepsilon_{total} = 0.4\%$.

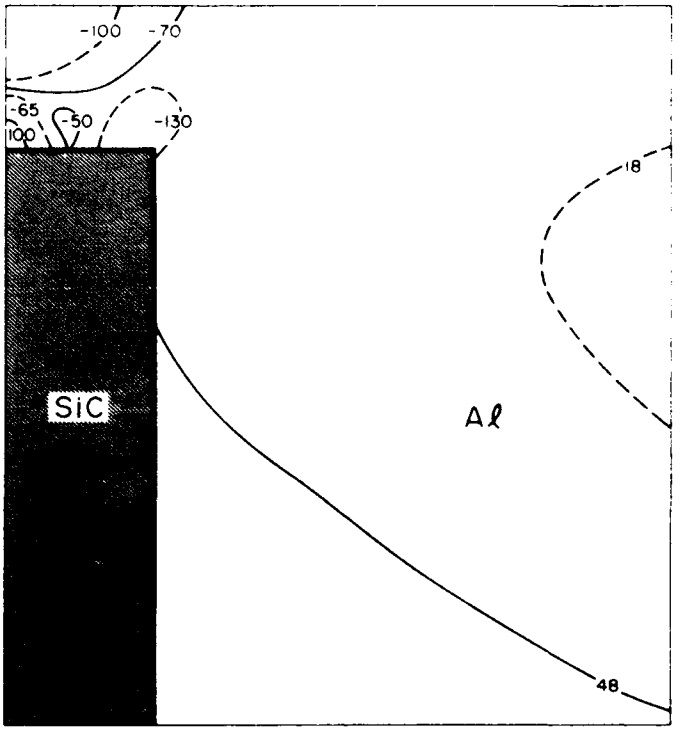

FIG. 10—*Longitudinal residual stress contour at a total applied strain of* $\varepsilon_{total} = 0.94\%$.

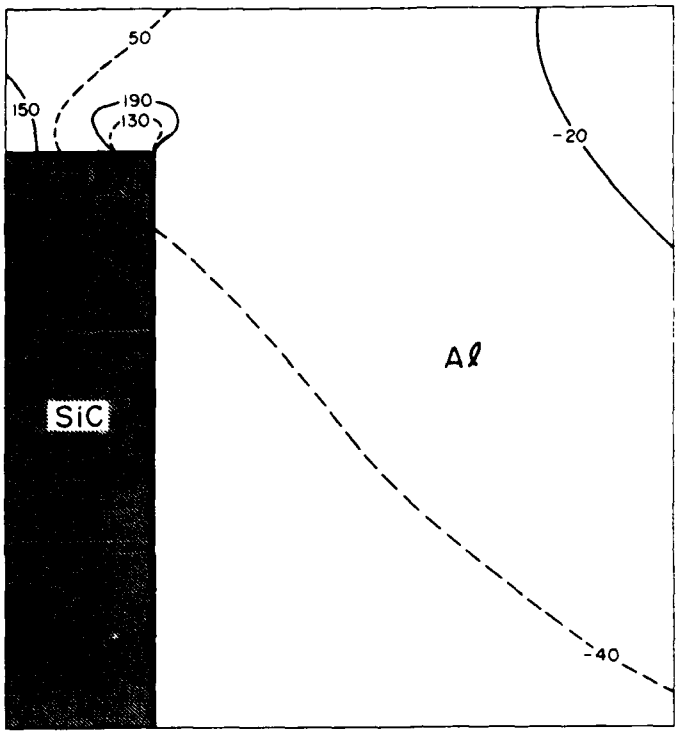

FIG. 11—*Longitudinal residual stress contour at a total applied strain of* $\varepsilon_{total} = 1.03\%$.

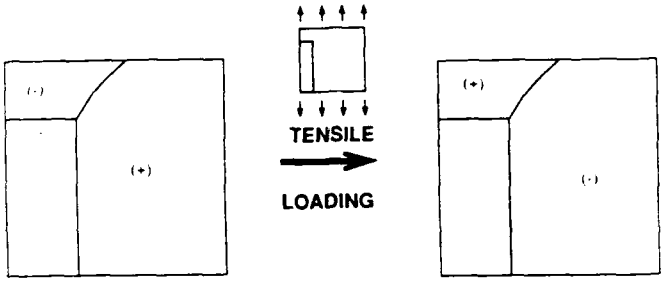

FIG. 12—*As a result of tensile loading, the arrangement of residual stress alters so that, at the whisker tip, the sign of the residual stress changes from tension to compression.*

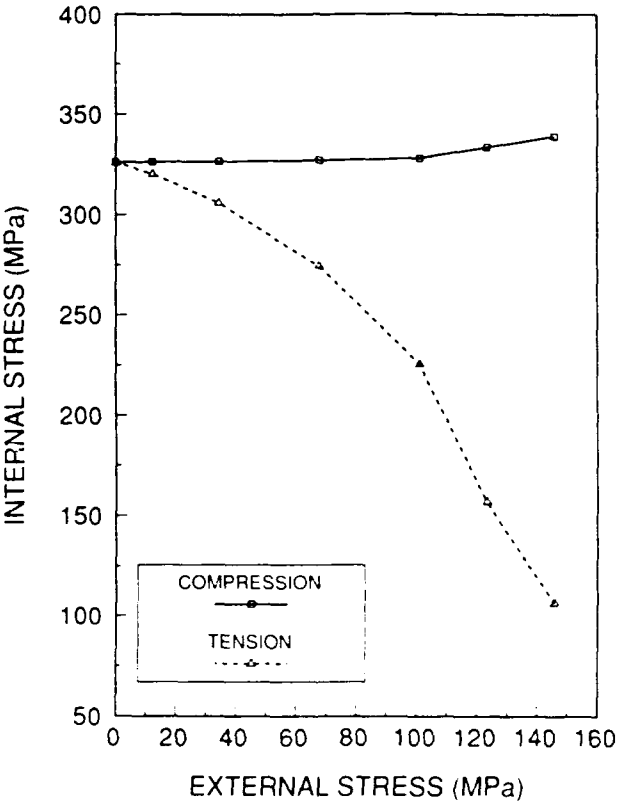

FIG. 13—*Average residual stress near the longitudinal matrix whisker interface as a function of applied stress. The residual stress is taken from an area of 0.3l × 0.2d around the transverse centerline of the whisker near the interface.*

dicated that in whisker-reinforced composite materials, the residual stress distribution is such that near the tip of the whisker, the matrix is under compression while the rest of the matrix is in tension, thus giving rise to an overall tensile average residual stress in the matrix. Interestingly enough, our finite element analysis indicated that under applied tensile load, the compressive and tensile zones exchanged their signs within a reasonable range of strain (Figs. 7–11), while compressive loading led to a residual stress increase in both regions. Figure 12 is a schematic diagram of the tensile deformation-induced redistribution of the longitudinal thermal residual stress.

Another persuasive fact to be noted is that while the global average residual stress exhibited a non-monotonic behavior, the residual stress near the whisker matrix interface never showed an initial drop after loading as it did in the case of global average residual stress. The response of the residual stress to the external load in the interface was such that the longitudinal residual stress increased upon an initial compressive plastic prestrain and decreased with an initial tensile plastic prestrain, as can be seen in Fig. 13.

Although the simplified averaging scheme discussed above is easy to use, it reflects the nature of the stress distribution of a uniform field. It is evident that this scheme does not reflect the fact that the deformation upon loading is inhomogeneous in the matrix. Because of this deformation inhomogeneity, for the same applied load increment, the importance of the residual stress will vary depending on the local stress concentration. The higher the load deformation rate, the higher the stress concentration. Furthermore, the difference in the value of the local deformation rate at different locations in the matrix constitutes the deformation gradient in the matrix. It is well known that a gradient in plastic deformation is responsible for the deformation generated residual stress.

In the previous investigations, it was a common practice to assume that residual stress was generated due only to the deformation gradient between the reinforcement and the matrix [*20*]. Therefore, to evaluate best the effect of the thermal residual stress on the subsequent loading and the degree of matrix deformation inhomogeneity, a new averaging rule should be developed. The authors believe that application of a weighted-averaging scheme is more appropriate and will lead to a more accurate account of the actual physical process. That is, to in-

corporate the local loading rate $(\partial\sigma_{ij}/\partial q)$, as a measure of deformation gradient, directly into the average stress formula. An averaging formula of the type

$$\bar{\sigma}_{ij} = \frac{\sum_k \left(\frac{\Delta\sigma_{ij}}{\Delta q}\right)_k^2 (\sigma_{ij})_k A_k}{\sum_k \left(\frac{\Delta\sigma_{ij}}{\Delta q}\right)_k^2 A_k} \tag{4a}$$

where

$$(\Delta\sigma_{ij}) = (\sigma_{ij})_k|_{t+\Delta t} - (\sigma_{ij})_k|_t \tag{4b}$$

and

$$\Delta q = q|_{t+\Delta t} - q|_t \tag{4c}$$

was then used, where q is the applied load intensity and $\bar{\sigma}_{ij}$ now denotes the new average residual stress. From Eq 4*a* it can be seen that for homogeneous matrix deformation, the stress rate $(\Delta\sigma_{ij}/\Delta q)_k$ is a constant over the entire matrix. Therefore, the average residual stress predicted by Eq 4*a* is the same as the prediction made through Eq 3. Evaluating the average matrix residual stress using Eq 4*a*, it was found that upon an initial load, the ratio between the two averages is:

$$\frac{\langle\sigma_{ij}\rangle}{\bar{\sigma}_{ij}} = 1.55 \qquad (i = j = 3) \tag{5}$$

The factor 1.55 is an indication of the degree of deformation heterogeneity of the composite material. Equation 5 indicates that the simplified average thermal residual stress is greater than the one produced from the weighted scheme, which means that the weighting factor is larger in the region where the residual stress has a negative value. This simply means that deformation in the compressive zone (tip of whiskers) is more severe with a uniaxial applied external load.

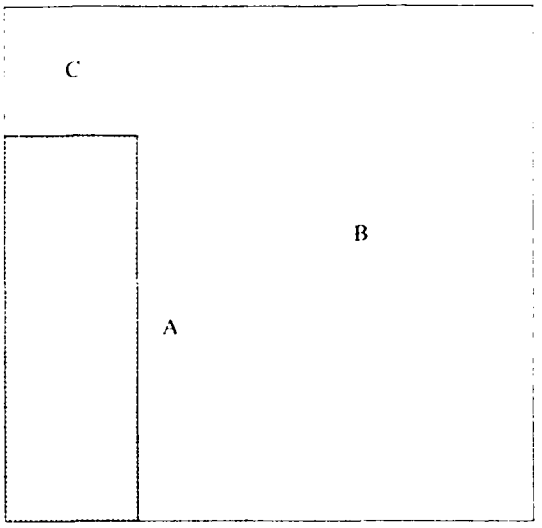

FIG. 14—*FEM results indicated that the residual stress field can be characterized into three regions in terms of stress rate, where at the whisker tip, the stress rate is highest.*

To understand better the heterogeneous deformation field in the matrix as a result of the existence of the whiskers, an average stress rate $(\partial\sigma/\partial q)$ diagram was constructed for the composite at different points of the matrix when the composite is initially loaded in tension, as shown in Fig. 14. In particular, three regions within the matrix were of interest. The analysis indicated that the average stress rate within the Regions A, B, and C were, respectively, 6×10^{-2}, 9×10^{-2}, and 13×10^{-2} (MPa/MPa). These results support the notion that the compressive zone at the tip of the whisker responds faster to external loading than any other region in the matrix. On the other hand, in the vicinity of the longitudinal whisker-matrix interface, the response of the internal stress to applied loading is the slowest. Finally, in Region b, where some interaction with the whisker tip is expected, the response to applied loading falls within an intermediate state.

The finding that there is a stress concentration at the whiskers tips is consistent with what was observed experimentally. Sato et al. [*30*] have reported extensive damages at short fiber tips as a result of excess plastic deformation. Note that the low deformation rate in Region A is due mainly to the interfacial load transfer, whereas, the disparity of deformation rate between Regions B and C is a result of the volume mismatch between the reinforcement and the matrix.

In consideration of the deformation process in the matrix, it is believed that the differences of microstrain rate in different parts of the matrix, that is, inhomogeneous matrix deformation, are solely due to the presence of the whisker. That is, near the longitudinal whisker-matrix interface, deformation is restricted because of the high stiffness of the SiC whisker, and at the same time, the matrix material at the whisker tip deforms more to accommodate the global strain. Therefore, the nature of the deformation gradient is not expected to exhibit a large change during the entire course of deformation.

The finite-element analysis presented in this paper has been performed with the sole intention of obtaining a better understanding of the effect of the residual stresses on the constitutive behavior of discontinuously reinforced metal-matrix composites. It is evident that the most prominent characteristics of the constitutive behavior of the composites have been adequately predicted using 2-D FEM. The physical reason for the effectiveness of the current 2-D analysis is, as shall be seen in the later discussion, that the 2-D composite does not destroy the inherent mechanism of residual stress generation. However, note that although the 2-D FEM model provides a good economical tool for understanding how the system operates, it was not the intention of the authors in the present investigation to compare quantitatively the analytical results with those obtained experimentally. It is evident that the plane-strain representation of an otherwise much more complex 3-D array of whiskers in a matrix is an oversimplification for quantitative analysis. Figure 15 shows a comparison of residual stress as a function of applied strain predicted by the plane strain model and the actual 3-D FEM with the same volume fraction. Note that there is no fundamental difference in the pattern of the change in residual stress as a result of external deformation. The only feature noticeable is the steeper overall slope predicted by the 3-D FEM.

Phenomenological Modelling

The results of the finite-element analysis discussed in the previous section indicate that the magnitude of the residual stress

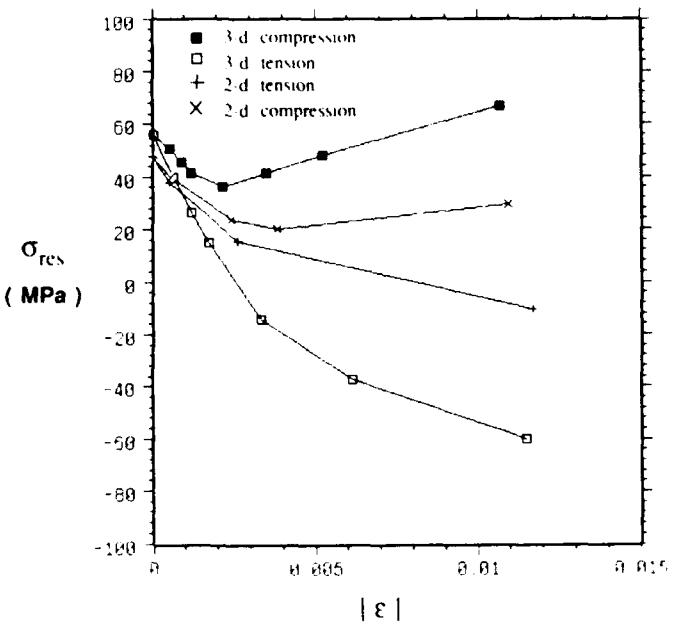

FIG. 15—*Comparison of average residual stress predicted by 2-D and 3-D FEM.*

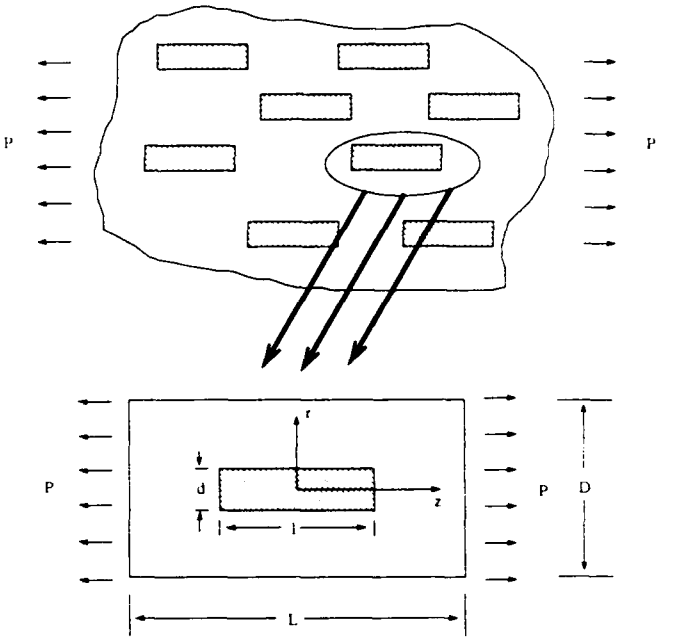

FIG. 16—*Schematic diagram for the interface model*

as a result of ΔCTE and its subsequent change under the influence of mechanical deformation are primarily governed by the deformation gradient in the matrix. It is our belief that the existence of the initial compressive zone is a direct consequence of volume mismatch between the whisker and the matrix, which occurs as a result of ΔCTE in the composite. On the other hand, the fact that the average matrix residual stress is in tension can also be obtained through interface shear load transfer. It is, therefore, clear that the process of residual stress generation and residual stress change are basically controlled by two factors: the nature of the interfacial shear load transfer between the SiC whiskers and the Al matrix and the volume mismatch between the two constituents. The mismatch of the volume is introduced by either the CTE mismatch when under thermal loading or the differences in Young's modulus and Poisson's ratio when under external loading.

To maintain overall compatibility, the two factors must work together. The volume difference is matched through interfacial normal stress, and the interfacial compatibility is satisfied by means of interfacial shear stress. To comprehend the separate roles of "interface effect" and "volume mismatch" on the residual stress response after the mechanical loading, two distinct analytical models were developed. The first model, subsequently referred to as the "interface model," is shown in Fig. 16, which assumes that the material consists of a discontinuous filament embedded in the matrix. It is essentially the same as the shear lag model with a consideration of thermal stress and average plastic deformation. It is also assumed that there is full elastic continuity across the whisker-matrix interface. The whiskers, therefore, remain fully bonded to the matrix, causing complete load transfer between the two constituents. The primary purpose of this type of modelling is to understand the effect of load transfer at the interface on the residual stress as a result of the applied loading.

In the second model, it is assumed that a discontinuous whisker is embedded in the matrix. To discount the effect of interfacial shear load transfer, interfacial sliding is allowed across the whisker-matrix interface along the direction of the whisker axis, but there is full continuity of the interfacial normal stress and displacement at the tip of the whisker between the whisker and the surrounding matrix. It is further assumed that a boundary is made along the extension of the longitudinal SiC/Al interface, as shown in Fig. 17. This model, which is referred to as the "volume mismatch model," is shown in Fig. 17. The main purpose of this model is to explain how the volume mismatch affects the residual stress arrangement as a result of a temperature change and external loading.

In both of these analyses, the matrix material is assumed to follow a bilinear stress-strain relationship, and the reinforcement is assumed to be perfectly elastic. The two analytical models are discussed in more detail below.

The Shear Lag Model

The simplest and yet most effective approach to account for the mechanism of shear load transfer at the matrix-reinforcement interface is the "shear lag" theory introduced by Cox [*31*]. Ever since the advent of this theory, it has been widely used because of its simplicity. Some investigators [*32,33*] have claimed it to be quite accurate in predicting mechanical properties of composites; others [*25,34*] have found it less attractive. In this section a modified "shear lag" method is used to try to account for the generation of the residual stresses. It is assumed that the overall constitutive response of the matrix remains elastic until the average matrix stress state becomes plastic.

When the composite is cooled down from the annealing temperature, longitudinal thermal residual stresses are developed in the matrix and the whisker. These will be denoted as $\langle\sigma'_m\rangle$ and $\langle\sigma'_w\rangle$, respectively. Using a modified shear lag model that incorporates temperature effect and plasticity, appropriate expressions may be readily derived for $\langle\sigma'_m\rangle$ and $\langle\sigma'_w\rangle$. The governing equation for the modified shear lag model is (further

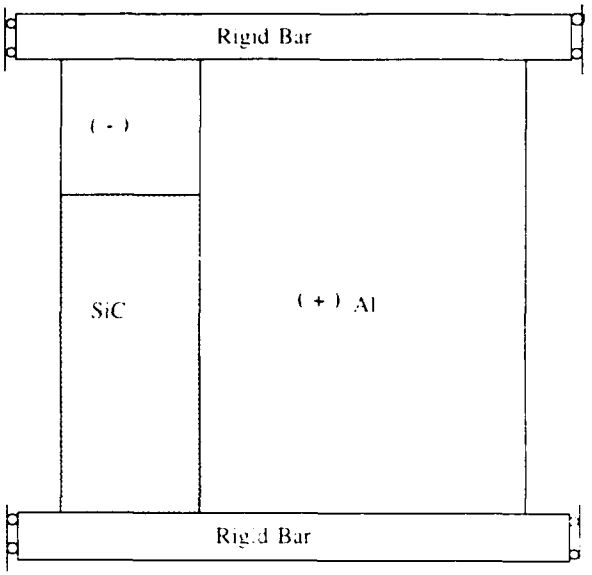

FIG. 17—*Schematic diagram for the volume mismatch model, where interfacial bonding is ignored.*

details are given in Appendix A and elsewhere [35]):

$$\frac{d\sigma_w}{dz} = h(\Delta\alpha\,\Delta T z + \Delta w - \Delta w_y) - \frac{2D}{d^2}\sigma_{y_m} - \frac{4\tau_y}{d} \tag{6}$$

where $\Delta\alpha$ is ΔCTE; ΔT is the magnitude of temperature change, $\Delta w = u - v$ where u and v are the displacements along whisker axes at and away from the interface in the matrix, Δw_y represents Δw when the matrix becomes plastically deformed, σ_{y_m} is the matrix yield stress, σ_w is the whisker stress, h is a constant to be determined, and D and d are the diameters of the unit cell and the whisker, respectively. If the temperature differential (ΔT) is such that the strains in both the matrix and the whisker remain elastic, then Δw_y and σ_{y_m} may be taken away from Eq 6, and Eq 6 will reduce to the form given by Cox [31] with a new thermal mismatch term ($h_c\Delta\alpha\,\Delta T$). For a 20% SiC/Al composite, it is likely that the matrix will be plastically deformed as a result of the cooling process. Following the procedure summarized by Kelly [36], the general form of the solution is obtained as follows (See Appendix A):

$$\langle\sigma'_m\rangle = -\frac{E_m\left[1 - \frac{\tanh(\beta l/2)}{(\beta l/2)}\right]\left[\sigma_{y_m}\left(\frac{1}{E_{m_p}} - \frac{1}{E_m}\right) + \Delta\alpha\,\Delta T\right]}{1 + \frac{V_w}{1-V_w}\frac{E_m}{E_{m_p}}\left[1 - \frac{\tanh(\beta l/2)}{(\beta l/2)}\right]} \tag{7a}$$

$$\langle\sigma'_w\rangle V_w + \langle\sigma'_m\rangle(1 - V_w) = 0 \tag{7b}$$

$$\beta = \sqrt{\frac{h}{E_w}} \tag{7c}$$

where V_w is the volume fraction of the whiskers, E_m and E_w represent the Young's moduli of the matrix and whisker, E_{m_p} is the work-hardening rate of the matrix, σ_{y_m} is the matrix yield stress, l is the total length of the whisker, and h and β can be determined as follows:

$$h = \frac{8G_{m_p}}{d^2\ln(D/d)} \tag{8a}$$

$$\beta = \frac{2\sqrt{2}}{d}\sqrt{\frac{\overline{G_{m_p}}\,\overline{E_m}}{\ln(D/d)}} \tag{8b}$$

where G_{m_p} is the tangential shear modulus of the matrix.

When a uniaxial loading (σ_{ap}) corresponding to the total strain (ε_{tot}) is applied along the whisker's direction in either tension or compression, and the composite is then unloaded, it may be shown that the matrix residual stress ($\langle\sigma'^{ap}_m\rangle$) as a result of applied loading now becomes:

$$\langle\sigma'^{ap}_m\rangle - \langle\sigma'_m\rangle = \frac{V_w E_m(E_m - E_{m_p})}{E_c}\varepsilon_{ap}\left[1 - \frac{\tanh\left(\frac{\beta l}{2}\right)}{\left(\frac{\beta l}{2}\right)}\right] \tag{10a}$$

$$\langle\sigma'^{ap}_w\rangle = -\frac{V_m}{V_w}\langle\sigma'^{ap}_m\rangle \tag{10b}$$

$$\beta = \frac{2\sqrt{2}}{d}\sqrt{\frac{G_{m_p}E_c}{\ln(D/d)}} \tag{10c}$$

where ε_{ap} represents the applied plastic strain and E_c is the Young's modulus of the composites. Here, as in the original references 31 and 36, the Young's modulus of the composites is assumed to follow the rule of mixture [$E_c = E_m(1 - V_w) + E_w V_w$]. Since $E_{m_p} < E_m$, clearly, the matrix residual stress decreases upon tensile loading ($\varepsilon_{ap} > 0$) and increases on compressive loading ($\varepsilon_{ap} < 0$). The overall changes in the residual stress remain monotonic.

The set of equations state above apply equally to both cases of compressive and tensile loading provided we consider the transformation:

$$\varepsilon_{ap} \rightarrow -\varepsilon_{ap}$$

This means that $\langle\sigma'^{ap}_m\rangle$ is symmetric about $\langle\sigma'_m\rangle$ when plastic deformation is considered. It also can be seen that Eq 10 is only a function of applied plastic strain, which means that elastic strain will not alter the value of the residual stress which contradicts the fact that there is an initial residual stress drop regardless of the loading directions predicted by FEM. It is, therefore, clear that the modified shear lag model cannot adequately predict the effect of the loading directions on the asymmetric behavior of the average residual stress. In other words, the mechanism of load transfer through the matrix-whisker interface cannot have a predominant effect on the average value of the residual stress and the residual stress change and, consequently, on the constitutive behavior. In fact, the outcome of this model matches the results of the finite-element analysis given earlier that within the immediate proximity of the longitudinal matrix reinforcement interface, the residual stress changes is monotonic (Fig. 13). This signifies that the matrix influenced solely by the inter-

face effect is primarily restricted to a very small region in the close vicinity of the whisker-matrix interface.

The Volume Mismatch Model

The term volume mismatch is derived from the difference in volume of the matrix as a result of the ΔCTE effect between the reinforcement and the matrix. Considering that the thermal residual stress is in compression at the tip of the whisker, the material, therefore, may be regarded as being composed of three distinct zones: the region of matrix which is under tension (denoted by subscripts *mt*), the region of the matrix which is under compression (denoted as *mc*), and the whisker zone (denoted by *w*). The combination of the two regions in the matrix (*mt* + *mc*) makes up the entire matrix region in the unit cell.

Although the local field in each zone is not uniform, since our interest is the average residual stress, it is often convenient to work with volume averages of the non-uniformed field in each zone defined by Eq 11, which is equivalent to Eq 3 defined in a previous section:

$$\langle \cdot \rangle_{A_n} = \frac{1}{A_n} \int A_n(\cdot) dv \tag{11}$$

where A_n is the area of each zone, that is, $n = mt$, mc, and w.

Considering virtual work and Gauss' theorem, it can be shown that the following relationship exists:

$$\iint_{A_n} \sigma_{ij} dA = \int_{A_n} \sigma_{ik} n_k x_j dl \tag{12}$$

that is,

$$\langle \sigma_{ij} \rangle_{A_n} A_n = \langle \sigma_{ik} n_k x_j \rangle_{A_n} |A_n| \tag{13}$$

where n_k is the normal to the boundary $|A_n|$.

Furthermore, it is common practice to assume that the average strain ($\langle \varepsilon_{ij} \rangle_{A_n}$) and average stress ($\langle \sigma_{ij} \rangle_{A_n}$) are related in the same way as in a local field by the same material constants [*20*]. For matrix material,

$$\begin{aligned} \langle \sigma_{ij} \rangle_{A_m} &= C^m_{ijkl} \langle \varepsilon_{kl} \rangle_{A_m} && |\langle \sigma_{33} \rangle_{A_m} - \langle \sigma_{11} \rangle_{A_m}| \le \sigma_{ym} \\ \langle \varepsilon_{ij} \rangle_{A_m} &= \varepsilon^0_{ij} + C^{mp}_{ijkl}{}^{-1} [\langle \sigma_{kl} \rangle_{A_m} - \sigma^0_{kl}] && |\langle \sigma_{33} \rangle_{A_m} - \langle \sigma_{11} \rangle_{A_m}| > \sigma_{ym} \end{aligned} \tag{14}$$

where C^m_{ijkl} and C^{mp}_{ijkl} are the stiffness and the tangential stiffness of the matrix, and ε^0_{ij} and σ^0_{ij} are the average strains and stresses on the yield surfaces in the strain and the stress space, respectively, and Tresca yield criteria is used.

Yano et al. [*37*] stated that the lateral stress generated by the difference in Poisson's ratio is small with a Al/Al, Ni fiber-reinforced eutectic composite system which has a Poisson's ratio of $\nu_f = 0.16$ and $\nu_m = 0.33$. Since a SiC/Al system has a Poisson's ratio of $\nu_{SiC} = 0.19$ versus $\nu_{Al} = 0.33$, we shall adopt the statement. Therefore, if only the longitudinal normal stress is considered, Eq 14 will reduce to the following:

$$\begin{aligned} \langle \varepsilon_{33} \rangle_{A_n} &= \frac{\langle \sigma_{33} \rangle_{A_n}}{E_m} && \langle \sigma_{33} \rangle_{A_n} < \sigma_{ym} \\ \langle \varepsilon_{33} \rangle_{A_n} &= \frac{\langle \sigma_{33} \rangle_{A_n} - \sigma_{ym}}{E_{mp}} + \frac{\sigma_{ym}}{E_m} && \langle \sigma_{33} \rangle_{A_n} > \sigma_{ym} \\ A_n &= mt, mc \end{aligned} \tag{15}$$

From the above simplifications, it is easily revealed that the concept of volume mismatch has reduced to the mismatch between the whisker and the matrix at the whisker end. Because all the quantities we are interested in are along the X_3 axes, we may substitute a simpler notation for the element to be investigated, that is,

$$\langle \varepsilon_{33} \rangle_{A_n} = \langle \varepsilon_{A_n} \rangle; \qquad \langle \sigma_{33} \rangle_{A_n} = \langle \sigma_{A_n} \rangle \tag{16}$$

It is clear that Eqs 12 and 13 define the relationship between average stress over the area of one particular zone and the line average of the stress on the boundary $|A_n|$. Therefore, global equilibrium condition (equilibrium between zones) can be expressed in terms of volume average stress. The equilibrium within each zone is automatically satisfied when adapting Eq 13 [*37*]. Furthermore, during the entire analysis, the continuity condition at the interfaces between zones is satisfied on an average basis.

From the requirement of the condition of equilibrium of stresses, it may be shown that the average residual stress in the whisker is related to the average residual stress in the matrix by the following equation:

$$\langle \sigma'_w \rangle = -\frac{1 - V_w}{V_w} \langle \sigma'_m \rangle \tag{17}$$

where again, V_w refers to the volume fraction of the whiskers and $1 - V_w = V_{mc} + V_{mt} = V_m$ denotes the total volume fraction of the matrix. The overall average residual stress in the matrix is, in turn, related to the residual stress in the tensile part of the matrix, $\langle \sigma'_m \rangle$:

$$\langle \sigma'_m \rangle = \frac{V_{mt}}{1 - V_w} F_w \langle \sigma'_{mt} \rangle \tag{18}$$

where F_w is defined by:

$$F_w = \frac{V_w}{V_w + V_{mc}} \cong \frac{V_w}{1 - V_{mt}} \tag{19}$$

It may also be shown that the residual stress in the compressive part of the matrix is given by:

$$\langle \sigma'_{mc} \rangle = \frac{-V_{mt}}{1 - V_{mt}} \langle \sigma'_{mt} \rangle \tag{20}$$

Considering the cooling process, it is known that the mismatch of thermal expansion coefficients is large enough to induce plastic deformation around the reinforcement [*38*]. By considering equilibrium and compatibility, in an average sense, it can be seen that the following equations can be obtained when $|\Delta T_1| < |\Delta T| < |\Delta T_2|$ (the details of the derivation are shown in Appendix B and in Ref *36*) where:

$$\begin{aligned} |\Delta T_1| &= \frac{\sigma_{ym}\left[(1 + F_w)\frac{1}{E_m} - \frac{1 - 2V_{mt}}{1 - V_{mt}}\frac{F_w}{E_{mp}} + \frac{V_{mt}}{1 - V_{mt}}\frac{F_w}{E_w}\right]}{\Delta\alpha F_w} \\ |\Delta T_2| &= \frac{\sigma_{ym}\left[\frac{1}{E_m}\frac{1 - V_{mt}}{V_{mt}} + \frac{F_w}{E_m} + \frac{F_w}{E_w}\right]}{\Delta\alpha F_w} \end{aligned} \tag{21}$$

here, $|\Delta T_t|$ and $|\Delta T_c|$ represent the magnitude of the temperature change when matrix tensile zone (A_{mt}) and compressive zone (A_{mc}) become fully plastically deformed, respectively, by the thermal stresses. Therefore, the thermal residual stress along the longitudinal direction is:

$$\langle\sigma_m^r\rangle = \frac{V_{mt}F_w}{1 - V_w} \cdot \frac{\sigma_{ym}\left[\frac{1}{E_{mp}} - \frac{1}{E_m}\right](1 - F_w) + F_w|\Delta\alpha|\,|\Delta T|}{\frac{1}{E_m} + \frac{V_{mt}}{1 - V_{mt}}\left[\frac{1 - F_w}{E_{mp}} + \frac{F_w}{E_w}\right]} \quad (22)$$

This means that within a certain range of temperature variation ($|\Delta T_c| \le |\Delta T| < |\Delta T_t|$) plastic deformation will be introduced in the matrix. However, until $|\Delta T| \ge |\Delta T_t|$, the matrix will remain partially plastically deformed. For $|\Delta T| = 500°$ C, it is both predicted by Eq 2 and experimentally observed by Vogelsang et al. [39] in terms of generation of dislocations that the matrix is partially plastically deformed. The predicted average residual stress in the matrix is given by Eq 22.

It is of particular interest to evaluate the new residual stresses in the composite when a uniaxial loading (σ_{ca}) corresponding to the total applied strain (ε_{tot}) is applied along the axis of the whisker and is subsequently removed. Clearly, the applied stress changes the residual stress when plastic deformation is involved. If the conditions, as stated before, are such that only portions of the matrix have initially yielded because of the thermal residual stresses, it may be shown that when the applied load is tensile, the overall average residual stress in the matrix after unloading is given by (for derivation details, refer to Appendix B):

$$\langle\sigma_m^{ru}\rangle = \begin{cases} \langle\sigma_m^r\rangle & \varepsilon_{ca} \le 0 \\ \langle\sigma_m^r\rangle - \dfrac{V_w}{1 - V_w}\dfrac{E_w E_m}{(1 - F_w)E_w + F_w E_m}\left(\dfrac{\sigma_{ca}}{E_m} - \dfrac{1 - V_w}{V_w}\dfrac{\langle\sigma_m^r\rangle}{E_m} + \varepsilon_{cap1} - \dfrac{\sigma_{ca}}{E_{cc}}\right) & 0 < \varepsilon_{ca} < \varepsilon_{cap2} \\ \langle\sigma_m^r\rangle - \dfrac{V_w}{1 - V_w}\left[\dfrac{E_w E_{mp}(\varepsilon_{ca} - \varepsilon_{cap2})}{(1 - F_w)E_w + F_w E_{mp}} - \dfrac{E_w E_m}{(1 - F_w)E_w + F_w E_m}\left(\dfrac{\sigma_{ca}}{E_{cc}}\right)\right] & \varepsilon_{ca} > \varepsilon_{cap2} \end{cases} \quad (23a)$$

where

$$\varepsilon_{cap1} = \frac{1 - V_w}{V_w}\left[\frac{2(1 - F_w)E_w + 2F_w E_m}{E_w} + \frac{1 - V_{mt}}{V_{mt}}\right]\frac{\langle\sigma_m^r\rangle}{E_m} - \frac{\sigma_{ym}}{E_m} \quad (23b)$$

and

$$E_{cc} = \frac{(1 - V_{mt})E_w E_m}{(1 - F_w)E_w + F_w E_m} + V_{mt}E_m \quad (23c)$$

and E_{cc} represents the all-elastic modulus of the composite in the absence of any plastic thermal residual stresses.

When the applied load is compressive:

$$\langle\sigma_m^{ru}\rangle = \langle\sigma_m^r\rangle - \frac{V_w}{1 - V_w}\left[\frac{E_w E_{mp}\varepsilon_{tot}}{(1 - F_w)E_w + F_w E_{mp}} - \frac{E_w E_m}{(1 - F_w)E_w + F_w E_m}\left(\frac{\sigma_{ca}}{E_{cc}}\right)\right] \quad (23d)$$

Equation 23 clearly indicates that $\langle\sigma_m^{ru}\rangle$ is no longer a monotonic function. These equations, therefore, predict a non-monotonic change in the residual stresses in the composite depending on whether the system is subjected to a compressive or tensile uniaxial loading.

By considering applied composite stress (σ_{ca}) and the corresponding composite strain ($\varepsilon_{tot} = \Sigma_i \varepsilon_{cai}$)

$$\sigma_{ca} = \sum_i E_{ci}\varepsilon_{cai} \quad (24)$$

where E_{ci} is the Young's modulus or composite tangential Young's modulus of the composite depending on the nature of the strain (ε_{cai}), that is, elastic or plastic. The result is shown in Fig. 18. It is clear, by comparing with Fig. 4, that the most prominent features predicted by the FEM are reproduced by the volume mismatch model.

Using Eq 23, the average values of the residual stress in the matrix were plotted in Fig. 19 after the application of tensile and compressive loadings. For the purpose of comparison, the results of the finite-element analysis described before have also been superimposed on the same diagram.

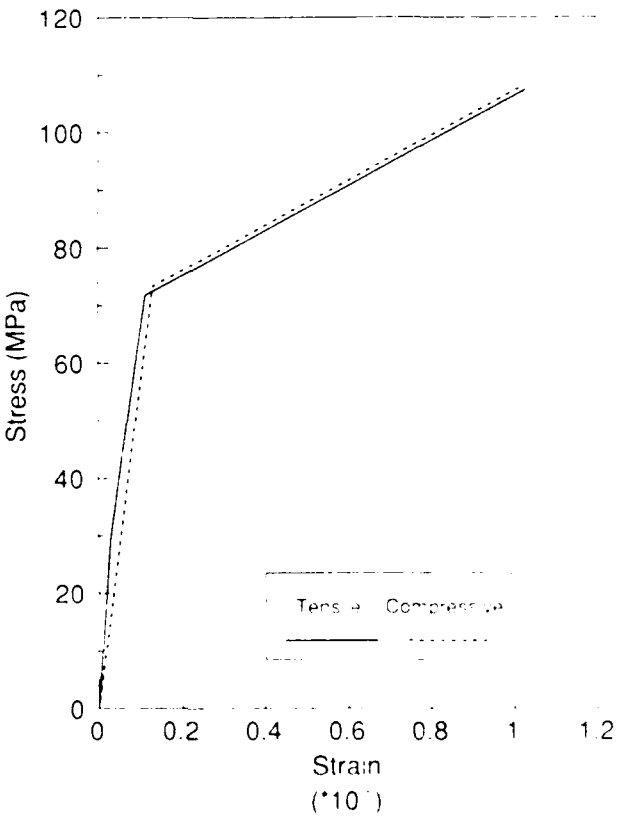

FIG. 18—*Stress-strain curves predicted by the volume mismatch model which are in general agreement with the FEM prediction shown in Fig. 4.*

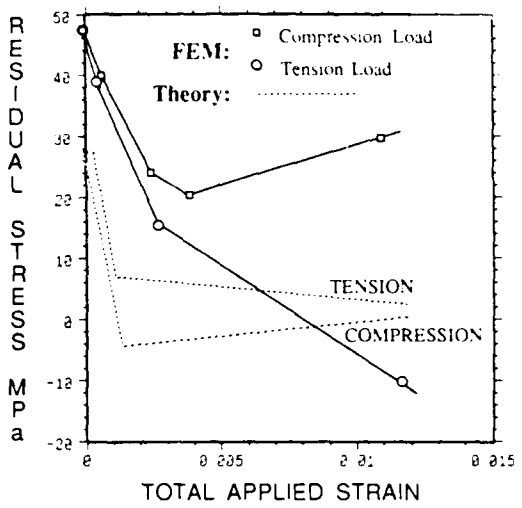

FIG. 19—*Comparison of average longitudinal residual stress predicted by FEM and the volume mismatch model. Note the similarities of slope change between the two models.*

Discussion

The results of the FEM modelling that have been duplicated by the phenomenological modelling indicate that residual stress produced by the ΔCTE and cooling is affected by the external load even at the initial loading stage. If the deformation is a result of compressive loading, the residual stress at first decreases and then increases with increasing deformation, whereas, if the deformation is the result of tensile loading, the residual stress decreases initially at a rapid rate and the rate slows upon further deformation. If the tensile deformation is continued, the residual stress changes sign from tensile to compressive.

From the phenomenological analyses, it is clear that the volume mismatch model gives qualitative agreement with the finite-element analysis on the general trend of the residual stress change. Not only the immediate drop of the average residual stress upon loading is apparent, but the slope change can also be predicted. Note that in the case of compressive loading, there is a sign change in the slope after the composite has started yielding, which was not predicted by the interface model. Furthermore, by comparing Figs. 4 and 18, the constitutive behavior of the composite predicted by FEM and the volume mismatch model are generally in agreement.

It should be pointed out that the predicted difference in the apparent Young's modulus under a loading scheme of different sense is a direct result of the asymmetric characteristic of the material under plastic deformation. When an additional deformation is imposed on a material that is already under plastic deformation, the relationship of the deformation to the applied load depends on whether the applied load represent a process of loading or unloading. In the composites, the matrix is plastically deformed as a result of thermal residual stress. As can be seen in this analysis, the nature of the longitudinal residual stress (tensile or compressive) is distinctly different depending on the location in the matrix. When an external load is applied, whether it is a process of loading or unloading at different locations in the matrix depends on the direction of the external load. Therefore, the apparent Young's modulus of the composites is different when the loading direction is different.

To understand the underlying mechanism for the change in residual stress, it is helpful to retrieve the argument of weighted residual stress in the section of FEM analysis. Since the ratio of the simple average stress over weighted average stress is greater than 1 (1.55), this means that the magnitude of the weighting factor (stress rate $\partial\sigma_{33}/\partial q$) is greater in the compressive region. Physically, it means that, to maintain compatibility between the matrix material at the whisker tip and the rest of the matrix, the compressive zone at the whisker tip responds faster than the rest of the matrix, that is, higher stress (strain) rate. This will result in localized plastic deformation before global yield. Since the gradient of plastic deformation in the material is mainly responsible for the deformation generated residual stress, the immediate change of the residual stress upon the initial external deformation is explained.

It is also interesting to note that the current Eshelby method does not predict such a residual stress reduction after an initial prestrain. Withers et al. [*20*] in their recent mean field investigation implied that the residual stress stays as a constant within a preglobal-yield region and that there is an overall monotonic change in residual stress as a result of prestraining. The discrepancy lies in that, in the mean field theory, the yielding criteria is satisfied in an average sense. However, well before the average global yielding criteria is satisfied, localized microyielding has already occurred, for example, at the whisker end, as pointed out previously, and incompatibilities between different parts of the matrix which are responsible for the generation of the matrix residual stress have already developed. Therefore, residual stress alteration is induced before the global yielding. However, by considering only a global average field, such localized microplastic deformation can not be taken into account. In the mean field theory, assumption was made that deformation was uniform in the matrix. Therefore, deformation generated matrix residual stresses are due only to the incompatibility between matrix and the reinforcement. The residual stresses as a result of the plastic deformation gradient in the matrix are not considered.

In the postyield regime, it is worthwhile to point out that in the case of compressive loading, there is a sign change in the slope $\partial(\sigma'_m)/\partial\varepsilon_{33}$ after the composite yielding, which is predicted by both FEM and the volume mismatch composite model. This is an indication that the interaction between the tensile and compressive zones becomes totally different. The original compressive load will produce a geometric compromise between the tensile and compressive zones, and therefore, there will be a reduction in residual stress. After the matrix material is completely deformed plastically by the applied compressive load, the two zones become more and more incompatible. Therefore, the residual stress increases again. It is also important to point out that while the trend of the residual stress change is in agreement with both FEM and volume mismatch models, the actual magnitude of the residual stresses predicted by the analytical model is much smaller than that predicted by the FEM. Furthermore, the relative positions between tensile and compressive curves predicted by FEM are not in agreement with the volume mismatch model. It is speculated that the absence of interfacial bonding in the model is the key reason for the discrepancy. For example, the discrepancy of relative positions of the curves of residual stress after tension and compression between the FEM and volume mismatch can be explained by the fact that the effect of interface will enhance the initial residual stress drop when under external tensile load and oppose such a drop when under compression.

Such an effect can be verified easily through Eq 10, which is directly derived from shear load transfer. However, the pattern of the residual stress changes is solely determined by the volume mismatch mechanism.

During the 2-D FEM analysis, an assessment was made that a 2-D plane-strain FEM analysis is a more economical way of modelling the generation of the residual stress. The incompatibility between matrix material at the tip of the whisker and the rest of the matrix during plastic deformation is responsible for the change in the residual stress. In a 2-D plane-strain approximation, this factor still remains because of the existence of the tensile and compressive zones in the matrix. Whereas, in a more realistic 3-D model, the only thing that makes it closer to reality is that the surface area of the reinforcement is significantly increased for the same volume fraction, which means that the mechanism of load transfer becomes more effective. However, it has been demonstrated that the effect of load transfer is only restricted to a small volume near the matrix-reinforcement interface in a whisker-reinforced composite, and the effectiveness of the load transfer does not change the fact that there is a higher stress concentration at the tip of the whisker. Therefore, in a 2-D plane-strain condition, while all the unnecessary complications are eliminated, the main mechanism of residual stress generation during plastic deformation is preserved. Considering the overall effect of interfacial load transfer and the effect of volume mismatch, it is suggested that the overall increase in the magnitude of the slope in the change of residual stress, shown in Fig. 15, is due to the enhanced effect of interfacial load transfer. This enhanced load transfer is believed to be a result of the increase of matrix-whisker interfacial area.

Conclusions

In summary:

1. The predicted change of the average residual stress is not monotonic with respect to the applied prestress (strain), that is, regardless of the sign of the loading. The average residual stress drops upon the initial elastic deformation, and the change of the residual stress as a result of the external load depends on whether the loading history is compressive or tensile.
2. The results predicted by FEM are generally comparable to those predicted by the theoretical model which is based on the volume mismatch between the reinforcement and the matrix. This indicates that the volume incompatibility is the controlling factor regarding the change in residual stress.
3. The FEM and theoretical results indicate that the asymmetrical constitutive behavior of whisker-reinforced SiC/Al composites is primarily due to the presence of the thermal residual stress.
4. A 2-D plane-strain analysis is an adequate and yet more economical approach than the actual time consuming 3-D FEM analysis in understanding the generation of the residual stress caused by external deformation.

Acknowledgment

This research was supported in part by the Office of Naval Research under Contract N00014-85-K-0007. The authors wish to acknowledge the continued support and encouragement of Dr. S. Fishman of the Office of Naval Research. The authors would also like to thank Prof. C. Schwartz of the University of Maryland for his encouragement in using the ADINA program and the Computer Science Center of the University of Maryland for its support of computer time.

APPENDIX A

Modified Shear Log Model

In this appendix, a modified shear lag model is derived. A more complete form can be found in Ref 35.

Considering equilibrium, the following equation can be obtained:

$$\frac{d\sigma'_m}{dz} = -\frac{4\tau_0}{d} \tag{A1}$$

Assuming that the aluminum matrix follows the bilinear stress-strain relationship and considering displacement-strain transformation equation, the displacement can be related to interfacial shear stress in the following manner:

$$h(|\Delta\alpha|\,|\Delta T|z + \Delta w - \Delta w_0) = \frac{4}{d}\left(\frac{D}{d}\frac{\sigma_{z,m}}{2} - \tau_0\right) \tag{A2}$$

Combining Eqs A1 and A2:

$$\frac{d\sigma'_m}{dz} = h(|\Delta\alpha|\,|\Delta T|z + \Delta w - \Delta w_0) - \frac{2D}{d^2}\sigma_{z,m} = -\frac{4\tau_0}{d} \tag{A3}$$

considering $\sigma_{z,m} \propto \Delta w_0$, and solving Eq A3 in a similar fashion as described in Ref 35, σ'_m can be obtained as:

$$\sigma'_m = E_m(\varepsilon'_m) - |\Delta\alpha|\,|\Delta T|)\left(1 - \frac{\cosh \beta z}{\cosh \beta l}\right) \tag{A4}$$

where (ε'_m) is the averaging matrix thermal residual strain, and β can be defined as:

$$\beta = \sqrt{\frac{h}{E_m}}$$

Averaging σ'_m by means of the continuum form of Eq 3:

$$(\sigma'_m) = E_m\left[1 - \frac{\tanh\left(\frac{\beta l}{2}\right)}{\left(\frac{\beta l}{2}\right)}\right](\varepsilon'_m) - \Delta\alpha\,\Delta T) \tag{A5}$$

where

$$(\sigma'_m)V_f + (\sigma'_m)(1 - V_m) = 0 \tag{A6}$$

Rearranging Eqs A5 and A6 and considering the following:

$$(\varepsilon'_m) = \frac{\sigma_{mx}}{E_m} + \frac{(\sigma'_m) - \sigma_{mx}}{E_{mp}}$$

the following equations can be obtained:

$$\langle\sigma'_w\rangle = E_w\left[1 - \frac{\tanh\left(\frac{\beta l}{2}\right)}{\left(\frac{\beta l}{2}\right)}\right]\left[\sigma_{ym}\left(\frac{1}{E_m} - \frac{1}{E_{mp}}\right) + \Delta\alpha\ \Delta T\right] \Big/ \left\{1 + \frac{V_w}{1 - V_w}\frac{E_w}{E_{mp}}\left[1 - \frac{\tanh\left(\frac{\beta l}{2}\right)}{\left(\frac{\beta l}{2}\right)}\right]\right\} \quad \text{(A7)}$$

$$\langle\sigma'_w\rangle V_w + \langle\sigma'_m\rangle(1 - V_w) = 0$$

It is likely that the matrix is fully plastically deformed as a result of thermal residual stress. Therefore, h and β can be determined as:

$$h = \frac{8G_{mp}}{d^2 \ln\left(\frac{D}{d}\right)}$$

$$\beta = \frac{2\sqrt{2}}{d}\sqrt{\frac{G_{mp}/E_w}{\ln\left(\frac{D}{d}\right)}}$$

When a longitudinal applied stress (σ_{ca}) is imposed, the matrix is plastically deformed when the matrix stress is larger than the yield strength of the matrix. Considering the corresponding applied plastic strain ($\varepsilon_{ca,ap}$), the residual stress after unloading can be determined as:

$$\langle\sigma''_m\rangle = \langle\sigma'_m\rangle + \varepsilon_{ca,ap}E_{mp} - \langle\varepsilon_{unload}\rangle E_m \quad \text{(A8)}$$

$$\langle\sigma''_w\rangle = \langle\sigma'_w\rangle + E_w\varepsilon_{ca,ap}\left[1 - \frac{\tanh\left(\frac{\beta l}{2}\right)}{\left(\frac{\beta l}{2}\right)}\right] - E_w\langle\varepsilon_{unload}\rangle\left[1 - \frac{\tanh\left(\frac{\beta l}{2}\right)}{\left(\frac{\beta l}{2}\right)}\right] \quad \text{(A9)}$$

$$\langle\sigma''_m\rangle = -\frac{V_w}{(1 - V_w)}\langle\sigma''_w\rangle \quad \text{(A10)}$$

where $\langle\varepsilon_{unload}\rangle$ is the average strain resulting from unloading. Eliminating $\langle\varepsilon_{unload}\rangle$ from Eqs A8 through A10, the final form of the residual stress is obtained:

$$\langle\sigma''_m\rangle = \langle\sigma'_m\rangle - \varepsilon_{ca,ap}V_wE_w\left[1 - \frac{\tanh\left(\frac{\beta l}{2}\right)}{\left(\frac{\beta l}{2}\right)}\right](E_m - E_{mp}) \Big/ E_c$$

$$\langle\sigma''_w\rangle = -\frac{1 - V_w}{V_w}\langle\sigma''_m\rangle \quad \text{(A11)}$$

$$\beta = \frac{2\sqrt{2}}{d}\sqrt{\frac{G_{mp}/E_w}{\ln\left(\frac{D}{d}\right)}}$$

APPENDIX B

Volume Mismatch Model

In this Appendix, the volume mismatch model is derived. A more complete form can be found in Ref *35*.

On satisfying global compatibility, the thermal residual stress can be obtained. If the temperature change is small so that the matrix remains elastic, the global compatibility and equilibrium condition can be obtained as:

$$\begin{cases} \dfrac{\langle\sigma'_{mt}\rangle}{E_m} - \dfrac{\langle\sigma'_{mc}\rangle}{E_m}(1 - F_w) - \dfrac{\langle\sigma'_w\rangle}{E_w}F_w = |\Delta\alpha|\,|\Delta T|F_w \\ \langle\sigma'_{mc}\rangle = -\dfrac{V_{mt}}{1 - V_{mt}}\langle\sigma'_{mt}\rangle \end{cases} \quad \text{(B1)}$$

The corresponding matrix thermal residual stress is:

$$\langle\sigma'_m\rangle = \frac{V_{mt}F_w}{1 - V_w}\frac{|\Delta\alpha|\,|\Delta T|F_w}{\frac{1}{E_m} + \frac{1 - F_w}{E_m}\frac{V_{mt}}{1 - V_{mt}} + \frac{F_w}{E_w}\frac{V_{mt}}{1 - V_{mt}}} \quad \text{(B2)}$$

When the temperature change is small, there is no thermally induced plasticity in the matrix. When the temperature change is smaller than the critical temperature, the matrix remains elastic, that is,

$$|\Delta T| \le |\Delta T_c|$$

where the critical temperature change (ΔT_c) can be obtained as:

$$|\Delta T_c| = \frac{\sigma_{ym}\left(\frac{1}{E_m}\frac{1 - V_{mt}}{V_{mt}} + \frac{1 - F_w}{E_m} + \frac{F_w}{E_w}\right)}{|\Delta\alpha|F_w} \quad \text{(B3)}$$

When the temperature change is large enough, the matrix at the tip of the whisker starts to yield. The variation of the temperature change for such a condition if given by:

$$|\Delta T_c| < |\Delta T| < |\Delta T_l|$$

and

$$|\Delta T_l| = \frac{\sigma_{ym}\left[\frac{(2 - F_w)}{E_m} - \frac{1 - 2V_{mt}}{1 - V_{mt}}\frac{1 - F_w}{E_{mp}} + \frac{V_{mt}}{1 - V_{mt}}\frac{F_w}{E_w}\right]}{|\Delta\alpha|F_w} \quad \text{(B4)}$$

Considering a compatibility condition similar to Eq B1, the thermal residual stress can be obtained:

$$\langle\sigma'_m\rangle = \frac{V_{mt}F_w}{1 - V_w}\frac{\sigma_{ym}\left(\frac{1}{E_{mp}} - \frac{1}{E_m}\right)(1 - F_w) + F_w\Delta\alpha\ \Delta T}{\frac{1}{E_m} + \frac{V_{mt}}{1 - V_{mt}}\left(\frac{1 - F_w}{E_{mp}} + \frac{F_w}{E_w}\right)} \quad \text{(B5)}$$

For an elastic matrix, when an external load is applied, the following equations can be constructed:

$$\frac{\sigma_{ca}}{E_{ce}} = \frac{\langle\sigma_w\rangle}{E_m}(1 - F_w) + \frac{\langle\sigma_w\rangle}{E_w}F_w$$

$$\sigma_{ca} = \langle\sigma_w\rangle(1 - V_{mt}) + \frac{V_{mt}^2 F_w}{1 - V_w}\langle\sigma_m\rangle \tag{B6}$$

$$\frac{V_{mt}F_w}{1 - V_m}\frac{\langle\sigma_m\rangle}{E_m} = \frac{\sigma_{ca}}{E_{ce}}$$

where $\langle\sigma_w\rangle$ and $\langle\sigma_m\rangle$ are average stress in the whisker and matrix, respectively. Solving Eq B6, the Young's modulus can be obtained as:

$$E_{ce} = \frac{(1 - V_{mt})E_m E_w}{E_w(1 - F_w) + F_w E_m} + V_{mt}E_m \tag{B7}$$

With a presence of thermally induced matrix plasticity, when an applied load is imposed on the composites, the stress state in the composites can be expressed as:

$$\begin{cases}\langle\sigma_w\rangle = \langle\sigma'_w\rangle + \langle\sigma''_w\rangle \\ \langle\sigma_m\rangle = \langle\sigma'_m\rangle + \langle\sigma''_m\rangle\end{cases} \tag{B8}$$

where $\langle\sigma''_w\rangle$ and $\langle\sigma''_m\rangle$ are the average stresses in the whisker and the matrix as a result of applied load, respectively, and their value is different under different loading directions.

The total applied strain can be related to the average whisker strain and the strain in the matrix at the tip of the whisker:

$$E_{tot} = F_w(\varepsilon_w) + (1 - F_w)(\varepsilon_m) \tag{B9}$$

Equation B9 has provided a relationship between average strains from different locations in the matrix.

To consider the stress gradient, the matrix average stresses in the initial compressive zone ($\langle\sigma_{m_c}\rangle$) and tensile zone ($\langle\sigma_{m_t}\rangle$) should be considered separately. Using the equilibrium condition, the following equations can be obtained:

$$\begin{cases}\langle\sigma_m\rangle = \dfrac{V_{mt}}{1 - V_w}\langle\sigma_{m_t}\rangle + \dfrac{V_{m_c}}{1 - V_w}\langle\sigma_{m_c}\rangle \\ \sigma_{ca} = (1 - V_w)\langle\sigma_m\rangle + V_w\langle\sigma_w\rangle\end{cases} \tag{B10}$$

Because of the thermally induced matrix plasticity, the response of the composites to a uniaxial tensile load is different from a compressive load. Considering Eqs B9 and B10, and following the development of the matrix plasticity, the response of the composites to the external applied strain can be derived.

For a tensile load, the following equations can be obtained:

$$\langle\sigma''_{mt}\rangle = \begin{cases} E_m\varepsilon_{tot} & \varepsilon_{cap} = 0 \\ \sigma_{ym} - \dfrac{1 - V_w}{F_w V_{mt}}\langle\sigma'_m\rangle + E_{mp}\varepsilon_{cap} & \varepsilon_{cap} > 0\end{cases} \tag{B11}$$

$$\langle\sigma''_{mc}\rangle = \begin{cases} \dfrac{E_w E_m}{(1 - F_w)E_w + F_w E_m}\varepsilon_{tot} & \varepsilon_{cap} \le \varepsilon_{cap1} \\ -2\langle\sigma'_w\rangle + \dfrac{E_{mp}E_w}{(1 - F_w)E_w + F_w E_{mp}}\varepsilon_{cap} & \varepsilon_{cap} > \varepsilon_{cap1}\end{cases}$$

and

$$\varepsilon_{cap1} = \frac{1 - V_w}{V_w}\left\{\frac{2[(1 - F_w)E_w + F_w E_m]}{E_w} + \frac{1 - V_{mt}}{V_{mt}}\right\}\frac{\langle\sigma'_m\rangle}{E_m} - \frac{\sigma_{ym}}{E_m}$$

When the composites are under compression, the internal stress is given by:

$$\langle\sigma''_{mt}\rangle = \begin{cases} E_m\varepsilon_{tot} & \varepsilon_{cap} = 0 \\ -\left(\dfrac{(1 - V_w)}{V_{mt}F_w}\langle\sigma'_m\rangle + \sigma_{ym}\right) + \varepsilon_{cap}E_{mp} & |\varepsilon_{cap}| > 0\end{cases} \tag{B12}$$

$$\langle\sigma''_{mc}\rangle = \frac{E_w E_{mp}}{(1 - F_w)E_w + F_w E_{mp}}\varepsilon_{tot}$$

After the external applied stress is removed from the composites, deformation-induced residual stresses in the matrix can then be determined. Considering Eq B8, the residual stress state can be obtained:

$$\begin{cases}\langle\sigma'^{ru}_w\rangle = \langle\sigma'_w\rangle + \langle\sigma''_w\rangle + \langle\sigma^{unload}_w\rangle \\ \langle\sigma'^{ru}_m\rangle = \langle\sigma'_m\rangle + \langle\sigma''_m\rangle + \langle\sigma^{unload}_m\rangle\end{cases} \tag{B13}$$

where, by considering Eqs 15 and B8 through B10, and paying special attention to the stress state at each zone, that is, $\langle\sigma_{m_t}\rangle$, $\langle\sigma_w\rangle$, and $\langle\sigma_{m_c}\rangle$, the matrix stress as a result of unloading ($\langle\sigma^{unload}_m\rangle$) can be determined as:

$$\langle\sigma^{unload}_m\rangle = -\frac{V_w}{1 - V_w}\frac{E_w E_{mp}}{(1 - F_w)E_w + F_w E_{mp}}\frac{\sigma_{ca}}{E_{ce}} \tag{B14}$$

Substituting Eqs B5, B11 (or B12), and B14 into Eq B13, and with a consideration of Eqs B9 and B10, the matrix residual stress can be generated.

For compressive load:

$$\langle\sigma'^{ru}_m\rangle = \langle\sigma'_m\rangle - \frac{V_w}{1 - V_w}\left[\frac{E_w E_{mp}\varepsilon_{tot}}{(1 - F_w)E_w + F_w E_{mp}} - \frac{E_w E_m}{(1 - F_w)E_w + F_w E_m}\frac{\sigma_{ca}}{E_{ce}}\right] \tag{B15}$$

For tensile load:

$$\langle\sigma'^{ru}_m\rangle = \begin{cases} \langle\sigma'_m\rangle & \varepsilon_{cap} = 0 \\ \langle\sigma'_m\rangle - \dfrac{V_w}{1 - V_w}\dfrac{E_w E_m}{(1 - F_w)E_w + F_w E_m}\left[\dfrac{\sigma_{ym}}{E_m} - \dfrac{1 - V_w}{V_w}\dfrac{\langle\sigma'_m\rangle}{E_m} + \varepsilon_{cap} - \dfrac{\sigma_{ca}}{E_{ce}}\right] & \varepsilon_{cap} < \varepsilon_{cap1} \\ \langle\sigma'_m\rangle - \dfrac{V_w}{1 - V_w}\left[\dfrac{E_w E_{mp}(\varepsilon_{cap} - \varepsilon_{cap1})}{(1 - F_w)E_w + F_w E_{mp}} - \dfrac{E_w E_m}{(1 - F_w)E_w + F_w E_m}\dfrac{\sigma_{ca}}{E_{ce}}\right] & \varepsilon_{cap} > \varepsilon_{cap1}\end{cases} \tag{B16}$$

REFERENCES

[1] Arsenault, R. J. and Wu, S. B., *Materials Science and Engineering*, Vol. 96, 1987, p. 77.

[2] Cao, H. C., Thouless, M. D., and Evans, A. G., *Acta Metallurgica*, Vol. 36, No. 8, 1988, pp. 2037–2046.

[3] Flom, Y. and Arsenault, R. J., *Acta Metallurgica*, Vol. 37, 1989, p. 2413.

[4] Mura, T. and Taya, M., in *Recent Advances in Composites in the United States and Japan, ASTM STP 864*, J. R. Vinson and M. Taya, Eds., American Society for Testing and Materials, Philadelphia, 1985.

[5] Dvorak, G. J. and Rao, M. S. M., *Journal of Applied Mechanics*, Vol. 98, No. 4, Dec. 1976, pp. 619–624.

[6] Garmong, G., *Metallurgical Transactions S*, Oct. 1974, pp. 2183–2190.

[7] Takao, Y., *Journal of Composite Materials*, Vol. 21, No. 2, Feb. 1987, pp. 140–156.

[8] Hoffman, C. A., *Journal of Engineering Materials*, Vol. 1, 1974, pp. 55–62.

[9] Levy, A. and Papazian, J. M., *Metallurgical Transactions*, Vol. 21A, Feb. 1990, pp. 411–420.

[10] Dutta, I. and Bourell, D. L., *Journal of Composite Materials*, Vol. 22, Sept. 1988, pp. 829–849.

[11] Christman, T., Needleman, A., and Suresh, S., "An Experimental and Numerical Study of Deformation in Metal-Ceramic Composites," Brown University Report NSF-ENG-8451092-1-89, Brown University, Providence, RI, 1989.

[12] Flow, E. C., *Military Application*, Sept. 1988, pp. 1–5.

[13] Arsenault, R. J., Shi, N., Feng, C. R., and Wang, L., submitted to *Materials Science and Engineering*, Vol. A131, 1991, pp. 55–68.

[14] Aboudi, J., *Solid Mechanical Archives*, Vol. 11, No. 3, 1986, pp. 141–183.

[15] Teply, J. and Dvorak, G. J., *Journal of Mechanical Physical Solids*, Vol. 36, No. 1, 1988, pp. 29–58.

[16] Tvergaard, V., *Acta Metallurgical Materials*, Vol. 38, No. 2, 1990, pp. 185–194.

[17] Tandon, G. P. and Wong, G. J., *Journal of Applied Mechanics*, Vol. 55, March 1988, pp. 126–135.

[18] Clegg, N. J., *Acta Metallurgica*, Vol. 36, No. 8, 1988, pp. 2141–2149.

[19] Arsenault, R. J. and Taya, M., *Acta Metallurgica*, 35, 1987, p. 651.

[20] Withers, P. J., Stobbs, W. M., and Pedersen, O. B., *Acta Metallurgica*, Vol. 37, No. 11, 1989, pp. 3061–3084.

[21] Eshelby, J. D., *Proceedings of the Royal Society*, Vol. 241A, 1957, p. 376.

[22] Eshelby, J. D., *Proceedings of the Royal Society*, Vol. 252A, 1959, p. 561.

[23] Takao, Y. and Taya, M., *Journal of Composite Materials*, Vol. 21, 1987, p. 140.

[24] Papazian, J. M. and Adler, P. N., *Metallurgical Transactions A*, Vol. 21A, 1990, pp. 401–410.

[25] Arsenault, R. J., *Materials Science and Engineering*, Vol. 64, 1984, pp. 171–181.

[26] McDaniels, D. L., *Metallurgical Transactions A*, Vol. 16A, June 1985, p. 1105.

[27] Ledbetter, H. M. and Austin, M. W., *Materials Science and Engineering*, Vol. 89, 1987, p. 53.

[28] Majumdar, S., Kupperman, D., and Singh, J., *Journal of the American Ceramics Society*, Vol. 71, [10] 1988, p. 858.

[29] Pedersen, O. B., *Acta Metallurgica*, Vol. 31, No. 11, 1983, pp. 1795–1808.

[30] Sato, N., Kurauchi, T., Sato, S., and Kamigaito, O., *Journal of Composite Materials*, Vol. 22, Sept. 1988, pp. 850–873.

[31] Cox, H. L., *Journal of Applied Physics*, Vol. 3, 1952, p. 72.

[32] Nairn, J., *Journal of Composite Materials*, Vol. 22, June 1988, pp. 561–587.

[33] Nardone, V. C. and Prewo, K. M., *Scripta Metallurgica*, Vol. 20, 1986, pp. 43–48.

[34] Taya, M. and Arsenault, R. J., *Scripta Metallurgica*, Vol. 21, 1987, pp. 349–354.

[35] Shi, N., "Thermomechanical Behavior of SiC Al Composites," Ph D. thesis, University of Maryland, College Park, 1991.

[36] Kelly, A., *Strong Solid*, 2nd ed., Clarendon Press, Oxford, 1973.

[37] Yano, T., Yanagisawa, O., and Ohmori, M., *Metallurgical Transactions of JIM*, Vol. 30, No. 5, 1986, pp. 345–353.

[38] Arsenault, R. J. and Shi, N., *Materials Science and Engineering*, Vol. 81, 1986, pp. 175–187.

[39] Vogelsang, M., Arsenault, R. J., and Fisher, R. M., *Metallurgical Transactions A*, Vol. 17A, 1986, pp. 379–389.

Fracture toughness of discontinuous metal matrix composites

R.J. Arsenault

Metallurgical Materials Laboratory, Materials and Nuclear Engineering Department, University of Maryland, College Park, MD 20742-2115

Abstract

The various theories that have been proposed to account for fracture toughness of discontinuous metal matrix composites, or the lack there of, are examined. It has been observed that the fracture toughness is independent of particle size and the fracture proceeds through the matrix. A significant factor which has not been considered in the past is that the matrix is in a severely cold worked condition. The cold worked state is the major factor contributing to the low fracture toughness of discontinuous metal matrix composites.

1. Introduction

The fracture toughness of discontinuous metal matrix composites (DMMC) is always less than the fracture toughness of the matrix, in the same heat treatment or annealed condition. If a specific case is considered, a 20 V% SiCp/6061 composite aged to the T-6 condition has a fracture toughness (K_{IC}) of ~ 10 MPa· $m^{½}$, where as 0 V% 6061 may have a K_{IC} of > 40 MPa· $m^{½}$. There may be obvious reasons why the K_{IC} of the composite is less than that of matrix alloy, but there are still numerous questions associated with the fracture characteristics of DMMC.

During the past several decades there have been a considerable number of investigations of the fracture characteristics of two phase alloys where the second phase is a discrete precipitate or particulate[1-18]. The precipitate particle is usually assumed not to plastically deform and the matrix is assumed to be ductile. DMMC meet the criterion of these assumptions very well. The review by Schwalbe [13] and more recent publications by Bates [15], Gerberich [16] and Firrao and Roberti [17] are very

informative on this subject. In ductile fracture, characterized by void nucleating and growth (VNG), the spacing between the void nucleating particles is generally considered to be a critical microstructural parameter and taken together with the tensile properties controls the toughness of a given material [11-17]. This can be represented by the following simplified expression [17]

$$K_{IC} = [a\sigma_y \epsilon^*_f E_f(N)]^{1/2} s^{1/2} \quad (1)$$

where K_{IC} is the plane strain fracture toughness, a is a numerical coefficient, σ_y is the yield stress, ϵ^*_f is the maximum strain acting at the crack tip, E is the Young's modulus, f(N) is some function of the strain-hardening exponent and s is the average inclusion spacing in the matrix. The experimental data collected by various investigators are usually given in terms of the volume fraction of the second phase particles (V) or less often in terms of s (see Fig.1)

Therefore, it appears that the fracture toughness of SiC/Al composites can be improved when the size of the SiC particles is increased, providing that at least one of the two following assumptions is met:

(1). voids are nucleated by SiC particles and/or

(2). the response of the matrix to change of s remains the same regardless of whether this change is caused by varying the volume fraction or the size of the SiC particles.

Crack initiation and propagation, i.e. the separation mechanism, in SiC/Al composites has been investigated to some extent over the last few years. Essentially, there are three different questions that have been raised concerning the crack initiation and propagation. These are: (1) Does the fracture of the SiC particles contribute to the separation of the composite, i.e. are they an integral part of the fracture mode? (2) Does void nucleation at the SiC whisker or particle and growth contribute to the fracture process? (3) What is the significance of cracked tip opening displacement?

The fracture of SiC whiskers or particles can conceivably initiate fracture of the composite. If the particle or whisker were large enough, then a crack of critical length could form and if the dynamic K_{IC} of matrix were low enough, the crack would continue to propagate into the matrix leading to failure of the composite [19]. Embury et al [20] have also developed a damage initiation model, i.e. cracking of SiC particles, as a fracture mechanism of SiC/Al composites.

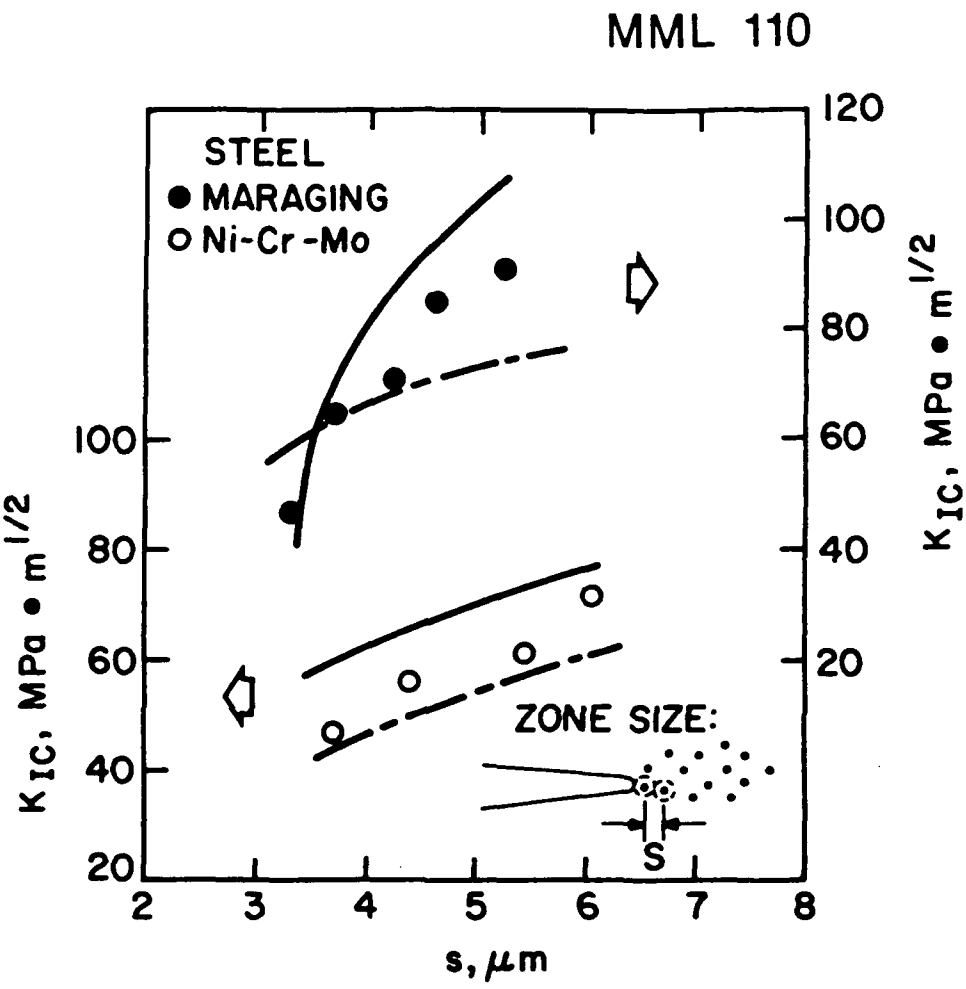

Fig.1 Fracture toughness as a function of "process" zone size. When VNG mechanism is active the process zone size is equated with the average spacing, s,between void nucleating particles(Gerberich, Ref.[16]). Various forms of equation(1) are employed by Gerberich to predict the fracture toughness values (solid and dashed lines) and compare them with the experimental data reported by Schwalbe and Spitzig.

If the fracture of SiC could initiate fracture, then the fracture of SiC should aid in the propagation of the crack. It has been shown that large intermetallic inclusions can act as a fracture initiation site in SiC/Al composites [1]. However, in an experiment to measure the bond strength between SiC and Al, a tensile sample of 99.99% Al was fabricated which contained a 3 mm diameter sphere of SiC in the center of the gage section. The gage section was 25 mm long and had a diameter of 6 mm.

When the sample was tested, shortly after macro-yielding, the SiC sphere fractured perpendicular to the tensile axis with a small drop in load. The test was continued and the sample finally failed, but the sample did NOT fail by extension of the crack in the SiC into the Al matrix, even though there was a 25% reduction in the cross sectional area as a result of the fractured SiC sphere. The sample failed at another place in the gage length [22].

Another factor which should be examined in a consideration of the fracture toughness of DMMC is difference in the microstructure of the matrix alloy (in the composite) vs the microstructure of non-reinforced matrix alloy. The microstructure of the composite matrix is almost the same as a cold worked microstructure. The composite matrix microstructure has a *higher* dislocation density than the cold worked matrix alloy. In the specific case of 20 V% SiC_p/1100 composite (5μm SiC particles) the dislocation density is higher than that of 1100 Al cold rolled (rolled at room temperature) 95 % reduction in thickness. Therefore, it is probably only meaningful to compare the fracture toughness of DMMC with cold worked matrix alloy [23].

In the remainder of this paper, , a discussion will be undertaken of the three major points raised in the introduction.

2. Particle Size Dependance

In the investigation by Flom and Arsenault [24], compact tension samples (CTS) were tested using the single specimen J-integral test method per ASTM standard E 813. Also, the energy separation technique (EST) was utilized as an additional tool in the load-unload records analysis [25]. The EST enables one to obtain values of plastic, I, and elastic, G, contributions to the total value of J-integral. It implies that the area under the load vs displacement curve which corresponds to the work done by external force can be separated into the stored elastic strain (potential) energy, U_S, the elastic energy, U_E, released during crack extension, and plastic energy, U_p, dissipated during the crack extension, as schematically shown in Fig.2. A more detailed description of the EST can be found elsewhere [25]. The rate of plastic energy dissipation, $I = 1/B_n dU_p/da$, and the elastic energy release rate, $G = 1/B_n dU_E/da$, represent the plastic and elastic parts of the J-integral, i.e. $J = I + G$, where B_n is the thickness of the CTS between the side groove and a is the crack length. Crack initiation fracture toughness can be determined as [25]

$$K_{IC} = \left(\frac{GE_c}{1-\nu^2}\right)^{1/2} \qquad (2)$$

where E_c is the composite Young's modulus and ν is the Poisson ratio (ν = 0.31). Also a direct evaluation of K_{IQ} is possible by taking maximum load P_m from the load-unload record and substituting into the expression[26]

$$K_{IQ} = \frac{P_m f(a/w)}{B_n (w)^{1/2}} \qquad (3)$$

where W is the width of the CTS as shown in Fig.5.4(a) and values of f(a/w) are readily available. Crack growth fracture toughness is evaluated by a dimensionless tearing modulus, T, which is equal to [27]

$$T = \frac{E_c}{\sigma_y^2} \frac{dJ}{da} \qquad (4)$$

where σ_y is the composite yield stress and dJ/da is the slope of the stable crack extension portion of J vs a plot constructed in accordance with ASTM E813. Crack extension was determined by using the unloading compliance technique [27]. In order to verify the calculated crack extension values, the tested CTS were exposed to elevated temperature and then fractured (heat tinting method). Experimentally measured crack lengths were found to be within 5-10% from the values calculated by a compliance technique.

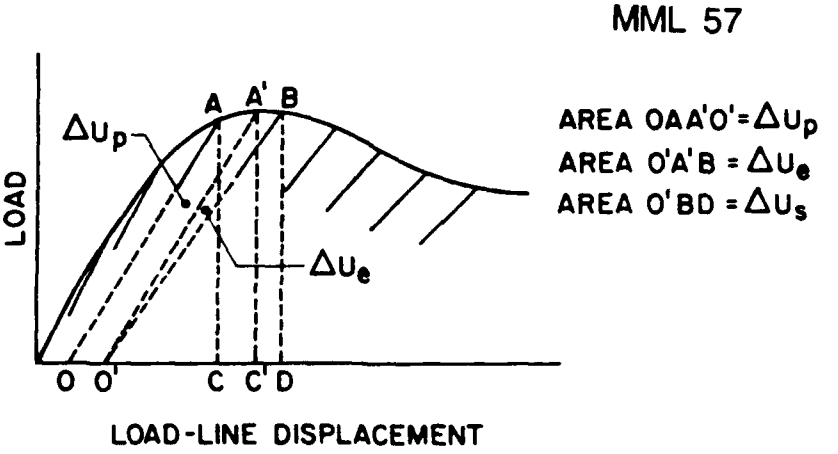

Fig.2 Schematic of the energy separation principle between two successive unloadings.

Crack initiation fracture toughness measured as K_{IC} and K_{IQ} is plotted as a function of the average SiC particle size and shown in Fig.3. The fact that both K_{IC} and K_{IQ} show the same trend, i.e. no dependence on the size of the SiC particles, increases the confidence in the results obtained and supports the energy separation method as a new and powerful tool.

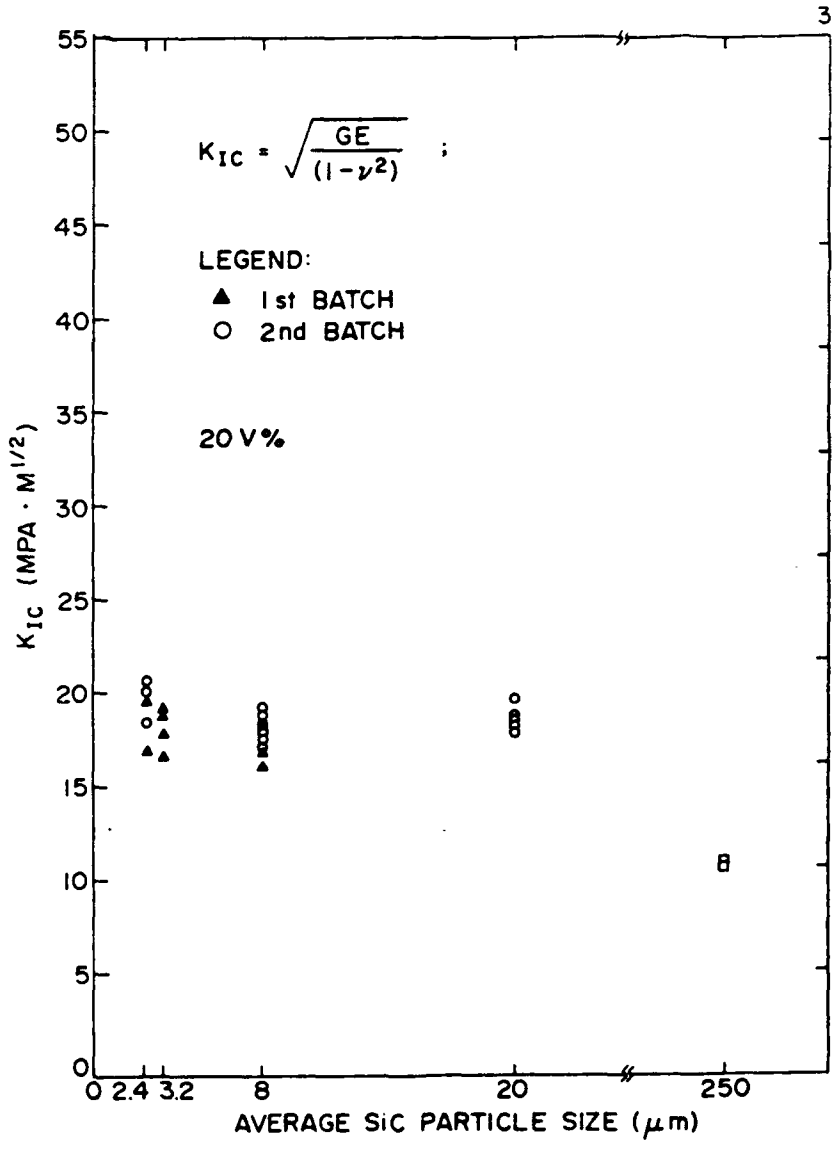

Fig.3 Crack initiation fracture toughness of SiC/Al composites measured as K_{IC} as a function of average SiC particle size.

The numerical difference ($K_{IC} \approx 18$ MPa$\cdot$ m$^{1/2}$ and $K_{IQ} \approx 23$ MPa$\cdot$ m$^{1/2}$) between the values of K_{IC} and K_{IQ} can be explained as follows. A finite notch with a root radius of $\approx 150\mu$m was machined in CTS in order to start the crack (in contrast with ASTM E 399 requirement of a fatigue precracking to form a geometrically sharp crack). Thus it is reasonable to related to the microstructure. Substituting values for $K_{IC(r)} = 23$ MPa$\cdot$ m$^{1/2}$, $K_{IC} = 18$ MPa$\cdot$ m$^{1/2}$ and $r \approx 150\ \mu$m, we obtain $c = 20\ \mu$m. This value is within the range of the microcracking ahead of the crack tip in a 2.4 μm average SiC particle size composite.

Initiation fracture toughness of a 250 μm SiC/Al composite is almost a factor of 2 less than the rest of the tested composites. This is apparently due to the premature cracking of 250 μm SiC particles.

Crack growth fracture toughness defined as tearing modulus, T versus the average size of SiC particles is plotted in Fig.4. The increase of the crack growth toughness with an increase of the SiC particle size means that more energy is dissipated during crack extension in the composite with a larger size of SiC particles.

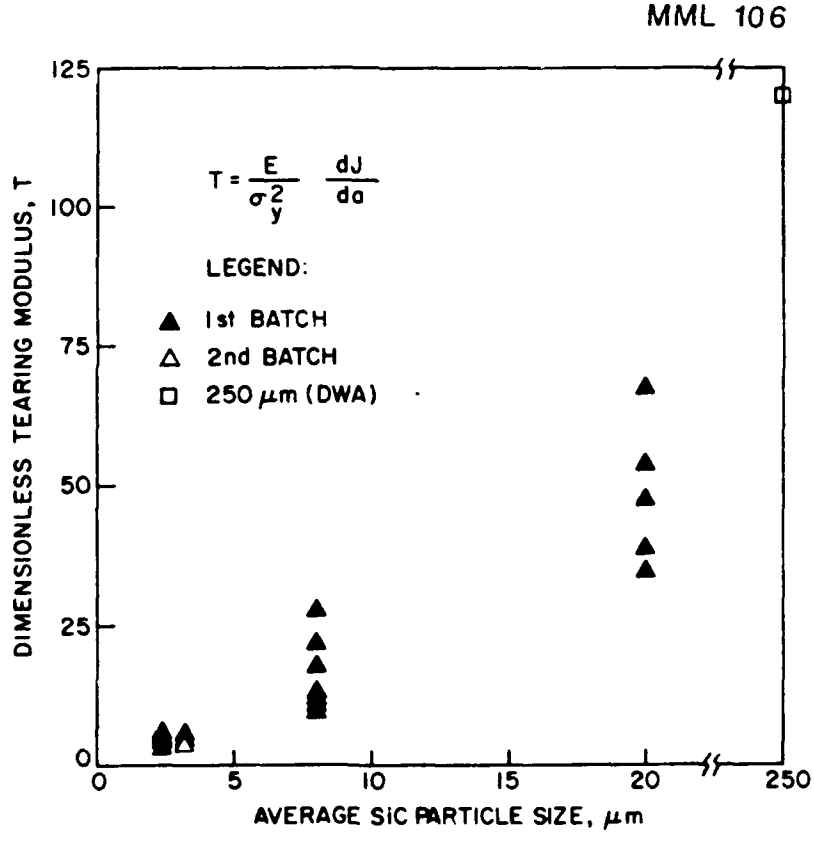

Fig.4 Crack growth fracture toughness of SiC/Al composites measured as T as a function of average particle size at a constant volume fraction of 20%.

The above experimental results indicate that crack initiation fracture toughness K_{IC} is independent of the SiC particle size (within the range of SiC sizes tested). In order to understand this result it is instructive to consider local energy dissipation mechanisms associated with the crack extension in SiC/Al composite. We are using the term "local" to emphasize the area in the vicinity of the crack tip. The plastic deformation in the bulk of the SiC/Al specimen is not included since it is separated out by using the energy separation technique (EST).

The elastic energy release rate G consists of the several terms that account for energy dissipation . These terms can be identified as

$$G = \gamma_S + \gamma_V + \gamma_{PLzone} + \gamma_{CTS} \qquad (6)$$

where γ_S is the energy consumed in creation of the new surfaces, γ_V is the energy consumed in the formation of the void sheet, γ_{PLzone} is the energy dissipated into plastic deformation around the crack tip and γ_{CTS} represents crack tip shielding effects described by Ritchie and Yu [28].

It can be shown, that most of the energy is absorbed within the plastic zone around the crack tip (γ_{PLzone}). In order to estimate this energy one has to know the distribution of the plastic strain in a direction perpendicular to the direction of crack propagation [29]. The data indicates that in the region immediately adjacent to the crack the plastic strain is large, as evidenced by very large dislocation density [30]. Also it was observed that the dislocation density is the same in the immediate region of fracture for two different volume fractions of SiC reinforcements [30] (SiC particle size was the same). Based on these results we can assume that as the particle size increases, i.e. an interparticle spacing increases (V = const.), the density of dislocation in the immediate region of the crack remains the same. Therefore γ_{PLzone} is independent of particle size.

The increase in crack growth fracture toughness (measured as I and T) with an increase of the SiC particle size can be treated on the basis of the relationship between the dislocation density and the spacing of the SiC particles demonstrated by Arsenault and Shi [31]. From their work one can see that the increase in the tearing modulus with an increase in particle size is the result of the increased plastic deformation that can be accommodated in the matrix as the interparticle spacing increases.

The data discussed above can not support a mechanism based on VNG at the interface of SiC and the matrix [18, 32] for these mechanism predict and increase in K_{IC} with an increase in particle size at a constant volume fraction. Also, the damage

mechanism of Embury et al. [20] which predicts on increase in particle cracking with an increase in particle size. This would suggest as the particle size increases the fracture toughness should decrease. This indeed happens when very larger particles are involved i.e. 250 μm particle size. However, in the particle size range of 0.5-20 μm there is no decrease in K_{IC}, which would indicate that particle cracking is playing a very small role in the fracture process.

3. Separation Mode

As discussed in the introduction, the mode of crack propagation is area of some controversy. An investigation was undertaken to determine how the crack propagates [33]. Precracked, polished compact tension samples (CTS) loaded in a mini-tensile stage within the scanning electron microscope. The stage was capable of incrementally loading the CTS, which allowed examination of the crack tip under load.

The crack tip region was then photographed, produce a map for the purpose of determining where and which of the SiC particles were fractured. Then, the crack was advanced by loading the sample, and then rephotographed.

Composite samples containing various size of SiC particulates were investigated; however, only a few of them will be considered here.

The specific case to be discussed in detail is a composite containing 20 V% 8 μm SiC particles. After the crack had been propagated a considerable distance, the crack has stopped in front of a rather large particle (Fig.5). Continued loading of the sample results in no apparent change in the crack, except that the crack tip has opened further. The crack opening is extremely small; even at a distance of 5 to 10 μm behind the crack tip, the crack opening displacements is < 1 μm and probably < 0.1 μm. Also, the large particle at the tip of the crack did not fracture, the crack proceeded around the large particle.

Upon further loading of the sample, as shown in Fig.6, the crack tip has stopped somewhere in front of a particle which apparently is cracked in three different locations. The crack proceeds, as shown in Fig.7, through one of preexisting cracks in the cracked sample. Figures 8 and 9 are continuations of the crack.

From a consideration of the above experimental results it is obvious that there are differences with some of the previously generated data on the fracture characteristics of SiC/Al composites, but these differences can be readily accounted for. Also, a clearer explanation of some of the previous data is now possible.

Fig.5 A scanning electron microscope micrograph of a propagation of a crack of a 20 V% 8 μm SiC particulate/1100 Al matrix composite.

The previous data from matching fracture surfaces and unloaded propagated cracks supported the concept that fracture of SiC particles in front of the advancing crack played a significant role in the fracture process and can be readily explained or accounted for. The above mentioned previous data is based on the examination of postmortem samples. The basic problem associated with examining postmortem samples is that it is impossible to know whether the SiC particle or whisker was broken due to processing prior to the actual fracture test. In the present investigation there was no case where it could be shown that the advancing crack resulted in the fracture of SiC particles.

It was clearly observed that as the crack advances, it has a distinct preference to proceed through existing cracked SiC particles. This would be entirely logical, since with the crack advancing through existing cracked SiC particles there is no need to create two new surfaces since they already exist. Therefore, matching fracture surfaces would have a matching "fractured" SiC particle. Also, the observation by Flom and Arsenault [24] that the number of SiC particles along the fracture path is greater than a random line through the composites is simply a consequence that the crack would rather propagate through an existing cracked (fractured) SiC particle.

Fig.6 A scanning electron microscope micrograph of a propagation of a crack of a 20 V% 8 μm SiC particulate/1100 al matrix composite.

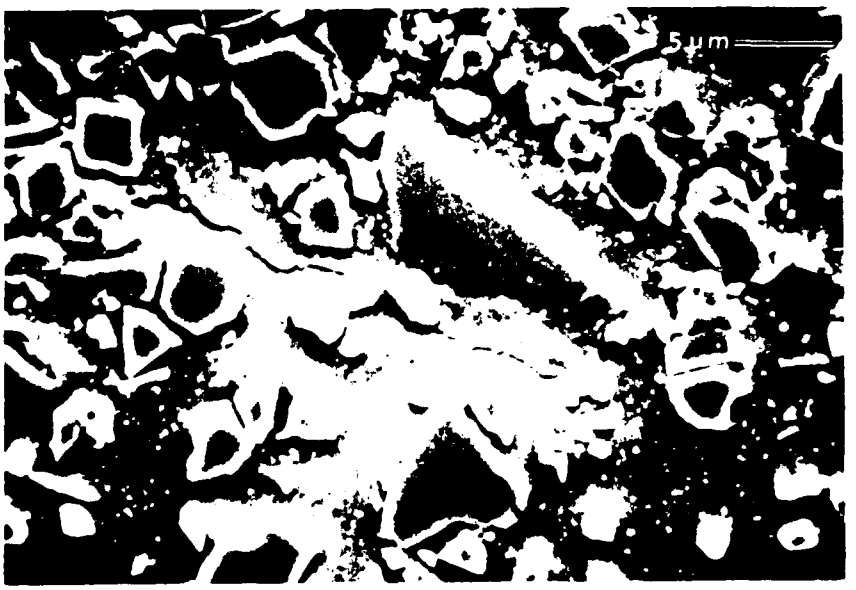

Fig.7 A scanning electron microscope micrograph of a propagation of a crack of a 20 V% 8 μm SiC particulate/1100 matrix composite.

Fig.8 A scanning electron microscope micrograph of a propagation of a crack of a 20 V% 8 μm SiC particulate/1100 Al matrix composite.

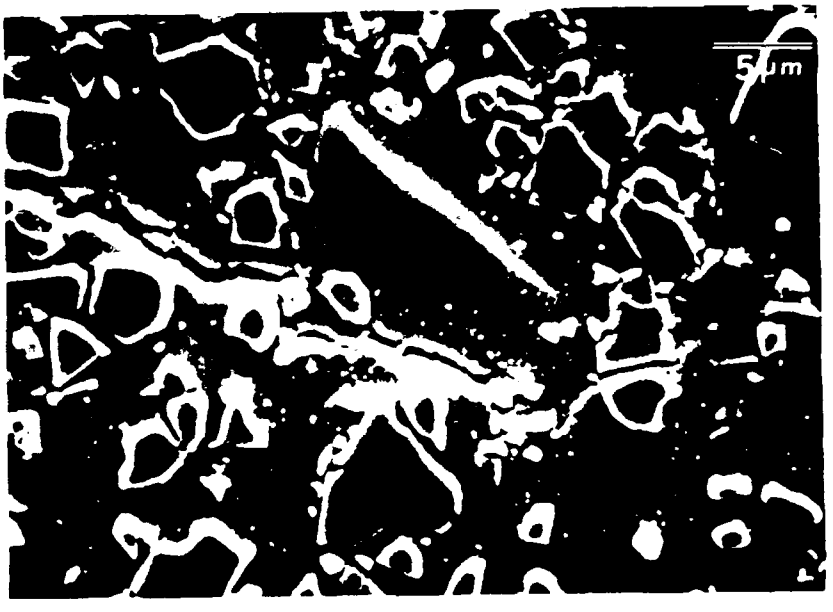

Fig.9 A scanning electron microscope micrograph of a propagation of a crack of a 20 V% 8 μm SiC particulate/1100 Al matrix composite.

In terms of the sharpness of the crack tip in the composites, i.e., lack of crack tip blunting, this can be traced back to the lack of plastic deformation which does not occur in these composites. In order to have crack tip blunting, it is necessary to have in-plane plastic deformation. If plastic deformation in the crack tip region (which can occur) is very small, there will be no blunting. Considering a very simple case, if the crack was initially very sharp and then blunted to a crack tip opening displacement of 2 μm, as in the case of the cold rolled 6061 Al alloy, the effective plastic strain required would be 15 - 30% as obtained by McMeeking [34] in an FEM investigation of crack tip blunting. It may be argued that the analysis of McMeeking is not valid since his analysis is for a stationary crack. The cracks in the SiC/Al composite propagate in a discontinuous manner. The major component of this effective plastic strain is a tensile strain perpendicular to the crack plane. However, Davidson [35] believes that the tensile strain is very small in SiC/Al composites. The tensile strain is small due to the elastic constraint of the high modulus (in comparison to Al) SiC particulate present in the composite, and the fact that the matrix within the composite has a very high dislocation density, i.e., equivalent to a highly cold worked condition.

Even though the 6061 Al alloy was cold rolled 75%, it is still possible to have significant plastic strain occurring at the crack tip in the plane-stress condition. Prior to slicing the sample in half, the crack propagates in a nearly plain-strain condition. As a result of the greater plastic strain, there is significant crack tip opening (several orders of magnitude) in comparison to the SiC/Al composites.

The lack of void nucleation and growth at the SiC matrix interface is more than likely due to a very high bond strength [36] between SiC and Al.

4. Matrix Microstructure Effect

A general observation is that fracture toughness of a metal or alloy decrease with increase in cold work. In other words, the fracture toughness is generally greater than the annealed condition as compared to the cold worked condition.

The microstructure of the matrix of an annealed or precipitation hardened SiC/Al composite is similar to matrix cold worked 90 %. This would suggest that if the matrix material was cold worked 90 %, then the fracture toughness of the matrix material would be comparable to that of the 20 V% SiC_p/Al alloy composite.

A preliminary investigation showed (Table 1) that cold rolling 6061 Al alloy to 69% resulted in nearly a factor of two reduction in K_{IC}, and in the case of 139% cold rolling there is further reduction in K_{IC}. At this level the K_{IC} value of the cold rolled matrix alloy is comparable to the 20 V% SiC_p/6061 Al alloy composite.

Table 1
Fracture toughness vs cold work

Material	Percentage of cold work	K_{IC} MPa.$m^{1/2}$
6061 Al T6	0	43
6061 Al T6	15	31
6061 Al T6	69	27
6061 Al T6	139	~20

In another investigation [37] in which correlation between K_{IC} and yield stress was determined, it was shown that as the yield stress increased (due to cold work) the fracture toughness decreased. At a yield stress (of the cold worked matrix alloy) corresponding to yield stress of 20 V% SiC_p/6061 Al alloy composite, the cold work 6061 Al alloy has the same K_{IC} value as the 20 V% SiC_p/6061 Al alloy composite.

5. Conclusions

From a consideration of the data discussed above, it possible to arrive at several conclusions.

1. An increase of SiC particle size did not improve K_{IC} fracture toughness of SiC/Al composite. K_{IC} was independent of SiC particle size up to 20 μm average size.

2. The crack growth toughness, i.e. the tearing modulus and plastic work, increased as the SiC particle size increased.

3. No evidence of void nucleation at SiC particles was found.

4. SiC/Al composite is a more complicated system than it appears: (1) the sites of void nucleation were not well defined, and (2) the two alternative ways of increasing interparticle spacing did not produce the same results:

- If the particle size was constant, and the volume fraction was increased and spacing decreased, then K_{IC} decreased.
- If the particle size and spacing were increased, and volume fraction was held constant, then K_{IC} remained constant.

5. The crack appears to go around intact SiC particles leaving a distinct outer coati- on the SiC particles which is in agreement with in situ TEM investigations of crack propagation in this particular material.

6. The observance of cracking of the SiC particles in front of the crack tip due to the advance of the crack tip is a rare event. If there are preexisting fractured SiC particles, the crack proceeds through the precracked SiC particles.

7. The crack tip opening displacement at the crack tip and 5-15 μm behind the crack tip as it initially propagates in the composites containing 2.4-20 μm size SiC particles was extremely small, i.e., less than 0.1 μm.

8. An important factor where considering the fracture toughness of SiC/Al composites is that matrix has a high dislocation density and a small subgrain size, even where the composite is in the annealed condition. Therefore the matrix of the composite can be equated to a cold worked condition. Cold working always reduce the fracture toughness.

6. Acknowledgements

The author wishes to acknowledge the continued support of the Office of Naval Research under grant No. N00014-91-5-1353 and continued encouragement of Dr. S. Fishman, program manager.

References

1. B.I.Edelson and W.M.Baldwin, Trans.Am.Soc.Metals 55 (1962) 230.
2. J.Gurland and J.Plateau, Trans.Am.Soc.Metals 56 (1963) 442.
3. A.Gangullee and J.Gurland, Trans.Metall.Soc.A.I.M.E.239 (1967) 269.
4. J.Gurland, Trans.Metall.Soc. A.I.M.E.227 (1963) 1146.
5. C.T.Liu and J.Gurland, J.Trans.Metall.Soc.A.I.M.E. 224 (1968) 1535.
6. C.T.Liu and J.Gurland, Trans.Am.Soc.Metals 61 (1968) 156.
7. J.Gurland, in Modern Composite Materials, edited by L.J.Broutman and R.H.Krock , Adison-Wesley, Reading, Mass. 1969.
8. I.L.Mogford, Metall.Rev. 114, 12 (1967) 49.
9. R.H.Van Stone, R.H.Merchant and J.R.Low Jr, ASTM STP 556 (1974) 93.
10. T.B.Cox and J.R.Low, Metall. Trans. 5 (1974) 1457.
11. G.T.Hahn and A.R.Rosenfield, Metall.Trans. A6 (1975) 653.
12. G.G.Garret and J.F.Knott, Metall.Trans. A9 (1978) 1187.
13. K.H.Schwalbe, Engng Fract. Mech. 9 (1977) 795.

14. G.LeRoy, J.D.Embury, G.Edwards and M.F.Ashby, Acta Metall.29 (1981) 1509.
15. R.C.Bates, in Proc. 113th AIME Conf., P.117, edited by J.M.Wells and J.B.Landes, 1985.
16. W.W.Gerberich, in Proc. 113th AIME Conf., P49, edited by J.M.Wells and J.B.Landes, 1985.
17. D.Firrao and R.Roberti, in Proc. 113th AIME Conf., p165, edited by J.M.Wells and J.B.Landes, 1968.
18. T.Christman, A.Needleman, S.R.Nutt and S.Suresh, Acta Metall 107 (1989) 49.
19. G.T.Hahn, Metall.Trans. 15A (1984) 947.
20. Y.Brechet, J.D.Embury, S.Tao and L.Luo, Acta Metall. 39 (1991) 1781.
21. Y.Flom and R.J.Arsenault, J.Metal 38 (1986) 31.
22. Y.Flom, Master's Thesis, University of Maryland, 1984.
23. R.J.Arsenault, L.Wang and C.R.Feng, Acta Met. 33 (1991) 47.
24. Y.Flom and R.J.Arsenault, Acta Metall. 37 (1989) 2413.
25. M.F.Mecklenburg, J.A.Joyce and P.Aprecht, presented at : 3rd Int. Symp. on Nonlinear Fracture Mechanics, ASTM, Knowville, Tenn. 1986.
26. 1986 Annual Book of ASTM Standards, Section 3, Vol 03.01, Standard E 399.
27. D.G.H.Latzo, C.E.Turner, J.D.Landes, D.E.McCabe and T.K.Hellen, Post Yield Fracture Mechanics, 2nd edn. Elsevier, Amsterdam, 1984.
28. R.O.Ritchie and W.Yu, In Small Fatigue Cracks, edited by R.O.Ritchie and J.Lankford, TMS-AIME, Warrendale. Pa. 1986.
29. D.L.Davidson, Metall.Trans.18A (1987) 2115.
30. R.J.Arsenault, N.Shi, C.R.Feng and L. Wang, Mater.Sci.Eng., A131 (1991) 55.
31. R.J.Arsenault and N.Shi, Mater.Sci.Engng.81 (1986) 175.
32. C.R.Crowe, R.A.Gray and D.F.Hasson, Proc.ICCM-5, P.843, edited by W.Harigan, 1985.
33. S.B.Wu and R.J.Arsenault, Mater.Sci.Eng. A138 (1991) 227.
34. R.M.McMeeking, J.Mech.Phys. Solids, 25 (1977) 357.
35. D.L.Davidson, Annual Report to ONR Report No. 06-8602/5, Jan.1989 and private communication, March 1990.
36. Y.Flom and R.J.Arsenault, Mater.Sci.Eng., 77 (1986) 191.
37. J.Glazer, S.L.Verzasconi, R.R.Sawtell and J.W.Morris Jr., Metall.Trans. 18A (1987) 1695.

Influence of the Thermally Induced Plasticity and Residual Stresses on the Deformation of SiC/Al Composites

N. Shi and R. J. Arsenault

ABSTRACT

The Finite Element Method (FEM) was employed to investigate the matrix plastic flow in a whisker reinforced SiC/Al composite under external tensile load. It was found that the plastic zone induced by the plastic relaxation of thermal stresses expands under the external tensile load. The overall matrix plastic flow was characterized by the expansion and interconnection of the plastic zones around whiskers. This process can be divided into several characteristic stages, and related to the global stress-strain relationship. It was also found that composite asymmetric constitutive response to external tensile and compressive loads as well as the composite asymmetric Bauschinger behavior was due to the thermally induced plasticity and residual stresses.

1 INTRODUCTION

Arsenault *et al.* proposed that a high dislocation density due to the difference in coefficients of thermal expansion (ΔCTE) should account for the strengthening of composites [1] Miller *et al.* suggested that the strengthening of SiC/Al composites may result from the Orowan mechanism [2]. However, it is still unclear as how the thermally induced plasticity affects the evolution of the matrix plastic flow which is important to the understanding of the composite strengthening.

When SiC/Al composites are subjected to either a tensile or compressive load, their constitutive behavior is distinctly different. It was generally found that the compressive yield strength of these composites was larger than that of the tensile yield strength, while the apparent Young's modulus for compression was smaller than that for tension [3]. If a material is initially plastically deformed in tension, then reverse deformed in compression, a difference in stress is required to initiate plastic deformation in the reverse cycle. Usually, the magnitude of the yield stress in the reverse cycle is less than the flow stress in the forward cycle. This reduction in stress (or the strain necessary to reach the previous level of flow stress) is defined as the Bauschinger Effect. In the case of monolithic Al, the direction of initial deformation (*i.e.*, tensile or compressive) does not have any influence on the Bauschinger Effect. The SiC/Al composites, however, exhibit a remarkable characteristic, *i.e.*, the flow stress drop (or alternatively, the Bauschinger strain) is larger when the composite deforms in a compression-tension sequence than vise versa [3].

In this investigation, FEM modeling was performed on the evolution of matrix plastic flow of a SiC whisker (SiC_w) reinforced annealed 6061 Al by monitoring the load-induced

[1]N. Shi and R. J. Arsenault, graduate student and professor, respectively, Metallurgical Materials Laboratory, Department of Materials and Nuclear Engineering, University of Maryland, College Park, MD 20742-2115.

changes of the plastic zone generated by ΔCTE, and then a correlation was determined between the matrix microplastic flow and the global composite tensile stress-strain curve. Based on the knowledge of the evolution of the matrix plasticity, a fundamental quest leading to an understanding of the asymmetric composite constitutive behavior was initiated, especially the asymmetric apparent Young's modulus and the Bauschinger Effect.

2 FEM ANALYSIS

In this investigation, a 2-D plane strain FEM thermo-elasto-plastic analysis was performed, in which the Von Mises yield criteria and the incremental flow rule were employed [4]. The composite was assumed to be a 2-D infinite periodic array of hexagonally distributed SiC whiskers of 20V% embedded in the matrix (or the staggered array), as shown in Fig. 1. An aspect ratio of four was selected. This value is a typical average from experimental observations [5, 6]. Due to symmetry conditions, a unit cell, as shown in Fig. 1, may be selected. The details of the boundary conditions along the unit cell boundary were published elsewhere [7].

To account for the thermally generated plasticity due to cooling from the annealing temperature, a temperature change, ΔT, was applied to the FEM unit cell. The materials properties were obtained from Ref. [8, 9] During modeling, neither thermal gradient nor matrix creep was considered. Due to a large ΔCTE, thermally induced matrix plastic flow from $\Delta T = 480°C$ is likely to spread over the entire matrix. To better understand the evolution of the matrix plasticity, two temperature changes of $\Delta T = 30$ and $480°C$ were employed, respectively.

It has been reported previously that the matrix longitudinal thermal residual stress is compressive at the tip of the whisker, and tensile in the rest of the matrix [10]. Therefore, in the current analysis, the matrix is categorized into two different zones: the initial compressive and tensile zones at the tip of and along the longitudinal sides of the whiskers, respectively. The schematics of this partition is shown in Fig. 1.

3 RESULTS AND DISCUSSIONS

3.1 THE BEHAVIOR OF THE PLASTIC ZONE

Following the temperature change of $\Delta T = 30°C$, longitudinal loading is applied to $\overline{AB}$ (in Fig. 1) incrementally. Fig. 2 shows the behavior of the thermally induced matrix plastic zone in a 20V% composite under external tensile loading. In this diagram, the locations of plastic zone boundary are plotted at different load levels, the label on each line represents the level of the applied traction in MPa, The hatched side of the line represents matrix that is *currently plastically deforming*, and we refer this enclosure as the *plastic zone*. Prior to external loading, the matrix has partially plastically deformed around the whisker due to plastic relaxation of the thermal stresses. When a tensile load is imposed, the shape of the plastic zone changes. It expands along the longitudinal whisker-matrix interface, while unloading from the initial residual compression occurs at the tip of the whisker.

As the applied load increases, plastic zones around two adjacent whiskers attract each other. This is characterized by the bowing-out of the plastic zone boundary shown in Fig. 2 when applied stress reaches 35.5 MPa.

When the external load reaches about 36 MPa, the plastic zone boundaries interconnect along $\overline{BC}$. Upon further load increases (*e.g.* to 44 MPa in Fig. 2), the only part of the matrix behaving elastically is at the tip of the whisker where it is still going through unloading and loading in reverse direction with respect to the compressive longitudinal thermal residual stress. When the internal stresses gradually reach the matrix flow stress,

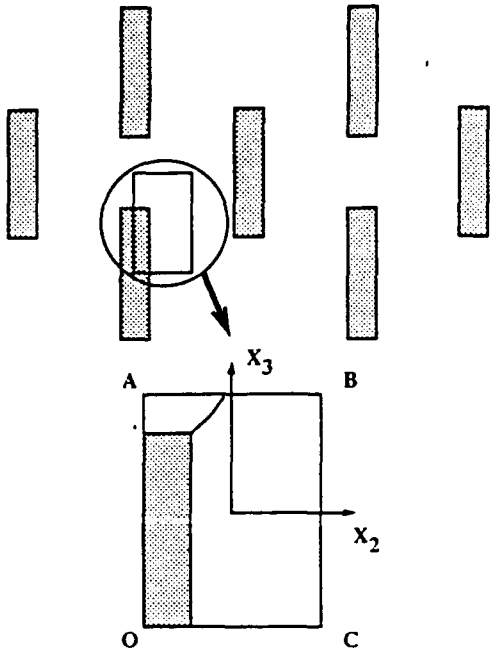

Figure 1. Schematics of an unit cell taken from an infinite hexagonally distributed array. In this unit cell, the boundary between the initial compressive and tensile zones is shown.

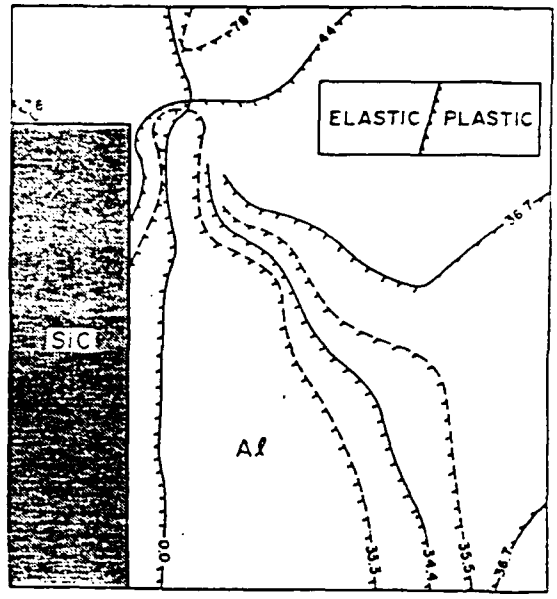

Figure 2. Sequence of the plastic zone expansion in the matrix of a 20V% whisker reinforced SiC-6061 Al composite with a thermal history of $\Delta T = 30°C$. An external load in MPa is applied incrementally.

the plastic zone starts to propagate into the initial compressive zone. The emergence of the load-induced plastic flow in the initial compressive zone then breaks the remaining elastic region into two "elastic pockets" — one immediately next to the matrix-whisker interface at the tip of the whisker, the other some distance away from the corner of the whisker.

To summarize, the entire process of plastic zone expansion can be divided into four stages: (1) plastic zone expansion in the initial tensile zone; (2) plastic zone interconnection along the cell boundary $\overline{BC}$; (3) overcoming the compressive thermal residual stresses at the tip of the whisker; (4) fragmentation of the elastic matrix to form remnant elastic pockets at SiC_w tip surrounded by the matrix plastic flow.

The matrix microplasticity is also correlated to the composite mechanical properties. Fig. 3 shows the initial portion of the stress-strain curve produced by FEM, and how it is related to the plastic zone expansion process. At the start, the stress-strain relationship is approximately linear. However, because of the thermally induced plasticity in the matrix, the thermally induced plastic zone expands even within this approximately linear region as shown in Fig. 2. As the plastic zones attract to each other and interconnect, the stress-strain curve goes quickly out of the approximate linearity. Once the entire initial tensile zone is plastically deforming, the slope of the stress-strain curve approaches a constant again (Fig. 3). This is due to the fact that the rate of propagation of the plastic zone boundary is greatly reduced because of the ongoing process of overcoming the compressive residual stress in the initial compressive zone.

As the load further increases, onset of the composite global yielding is characterized by the formation of the remnant elastic pockets. At .2% yield stress, the entire matrix is plastically deforming except within the elastic pocket away from the corner of the whisker.

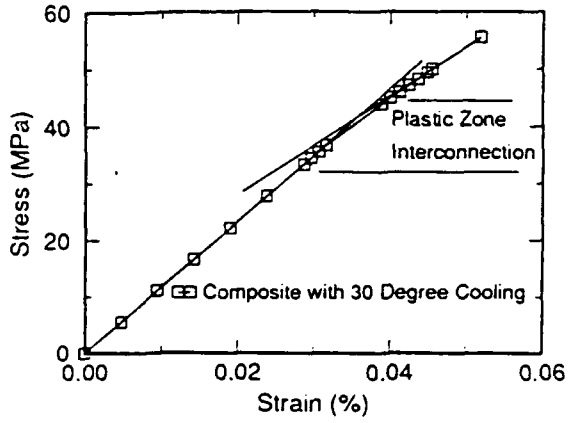

Figure 3. Initial response of a 20V% composite with $\Delta T = 30°C$, where the deviation from the approximate linearity is characterized by the plastic zone interconnection in the initial tensile zone.

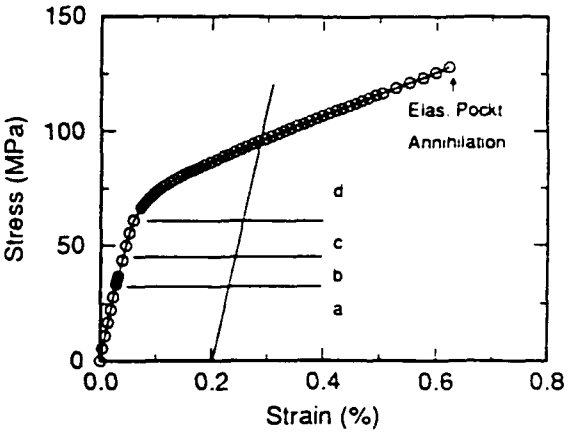

Figure 4. Four stages of the plastic zone expansion and their chara cteristics reflected on the tensile behavior of a 20V% SiC_w/Al composites with a thermal history of $\Delta T = 30°C$, *a*: expansion of the initial tensile plastic zone; *b*: interconnection of the initial tensile plastic zones; *c*: deformation-induced plastic flow in the initial compressive plastic zone; *d*: fragmentation of the the remnant elastic matrix.

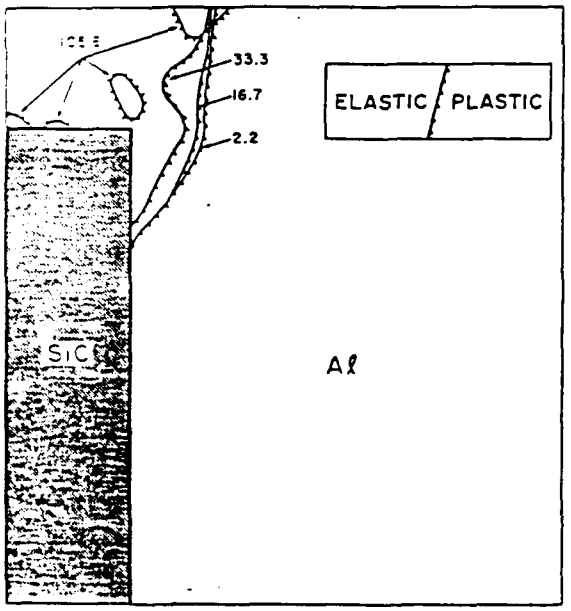

Figure 5. Process of the plastic zone expansion and interconnection in the matrix of a 20V% SiC_w/Al composites with a thermal history of $\Delta T = 480°C$. The applied stress(MPa) is applied incrementally.

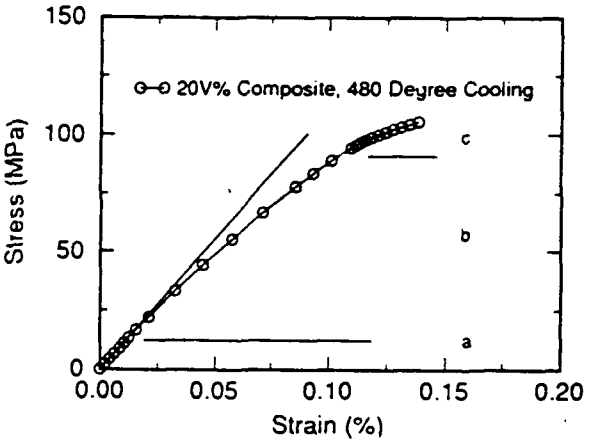

Figure 6. Different stages of plastic deformation and the tensile behavior of a 20V% SiC_w/Al composites with a thermal history of $\Delta T = 480°C$, *a*: steady plastic zone size; *b*: consumption of elastic matrix at the tip of the whisker by incremental plastic flow; *c*: fragmentation of the remnant elastic matrix.

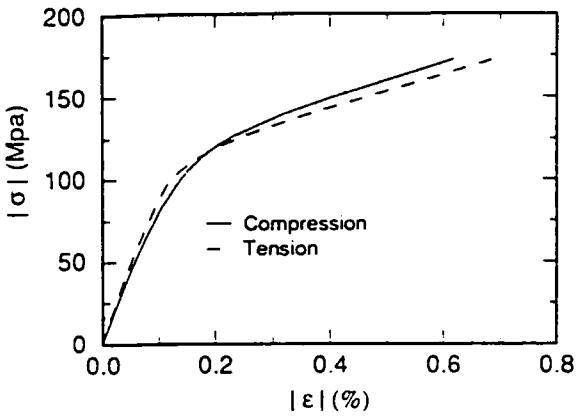

Figure 7. Stress-strain curves under tension and compression predicted by the FEM, where the apparent young's modulus of the composite is higher when it is uder tension, whereas the yield strength is greater when it is under compression.

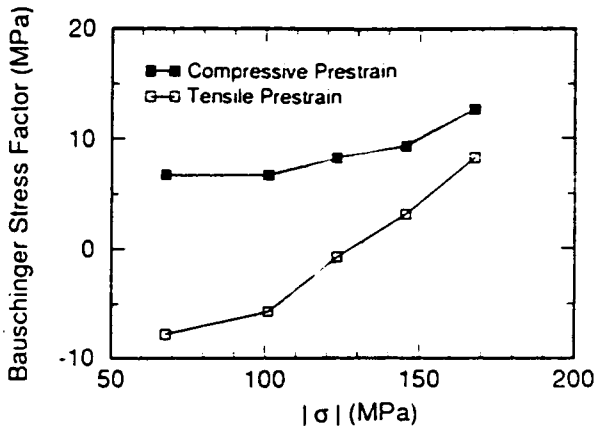

Figure 8. FEM prediction of the Bauschinger stress factor, σ_b, as a function of the applied forward strain, where σ_b is larger if the forward load is in compression, and the initial value of σ_b is negative.

As will be seen during the remainder of this study, the final location of the remaining elastic zone is a strong function of reinforcement concentration. The correlation of each stage of the plastic zone expansion with the stress-strain relationship is shown in Fig. 4.

For $\Delta T = 480°C$, which is a more realistic temperature change when cooling from the annealing temperature, the evolution of the matrix plasticity is shown in Fig. 5, where the same convention, as employed in Fig. 2, is used. Due to a larger ΔT, the thermally induced plastic flow has spread over the entire matrix prior to any external loading. As compared with the cooling of $\Delta T = 30°C$, the development of matrix plasticity due to a tensile load is the same in characteristics except that the first two stages of the plastic zone expansion occur during "thermal loading", which leads to that the changes of the matrix plasticity is concentrated at the tip of the whiskers.

Fig. 6 shows the predicted stress-strain curve of the composite along with the corresponding characteristics of the plastic zone. Comparing with Fig. 3, the "proportional limit" is considerably smaller, the difference comes from the fact that, for $\Delta T = 480°C$, the matrix is experiencing a different stage of plastic zone expansion. When the initial loading is applied within the approximate proportional limit, the matrix is unloading in the initial compressive zone, where the boundary of the plastic zone is insensitive to the external deformation. However, it takes significantly more additional work to spread the deformation-induced plasticity to reach the stage of fragmentation of remnant elastic matrix. This is due to the increase of compressive residual stress and the amount of thermally induced work hardening when ΔT is larger, *i.e.*, the thermally induced dislocations due to ΔCTE.

3.2 COMPOSITE ASYMMETRIC CONSTITUTIVE BEHAVIOR AND THE THERMALLY INDUCED PLASTIC FLOW

Fig. 7 displays the uniaxial stress-strain curves generated by FEM when a 20V% composite is under tensile and compressive loads, respectively. Fig. 8 shows the Bauschinger stress factor, σ_b, as a function of the applied forward strain. Here, the Bauschinger stress factor is defined as $\sigma_b = \sigma^F - \sigma^R$, where σ^F and σ^R represent the forward and reverse flow stresses, respectively. In this figure, σ_b is consistently larger when forward applied stress is in compression. These results match the observations by Arsenault *et al.* [3].

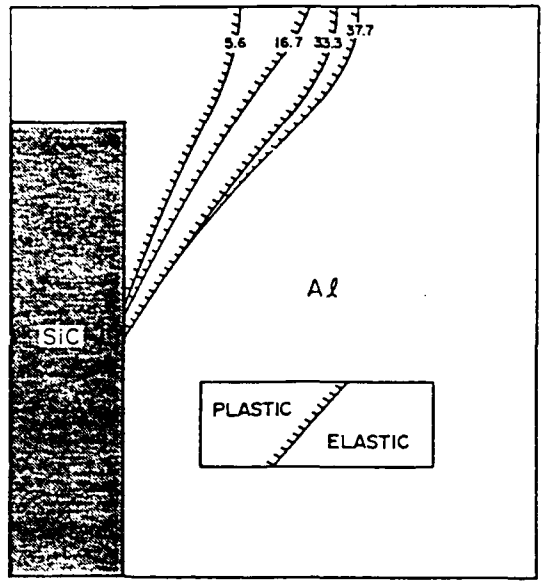

Figure 9. Matrix plastic zone expansion process of a 20V% SiC_w/Al composite under compressive loading condition with a thermal history of $\Delta T = 480°C$.

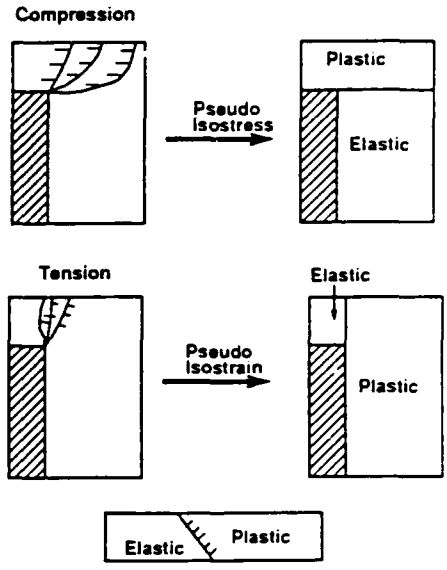

Figure 10. Schematics of the morphologies of the plastic zone under different loading conditions, where tensile loading will produce a pseudo-isostrain condition and compressive loading will produce a pseudo-isostress condition.

In addition, FEM analysis also predicts that the Bauschinger stress factor is initially negative ($\sigma_b < 0$), which means that there is an initial reverse strain hardening rather than normally observed reverse strain softening.

3.2.1 Asymmetric Apparent Young's Modulus

It is commonly believed that the asymmetric composite apparent Young's modulus is related to the asymmetric development of the shear stresses at the interface near the tip of the whisker [11, 12]. From FEM modeling, Levy *et al.* found that the interfacial thermal residual shear stress near the end of the whisker increases with compressive loading, and decreases with tensile loading [12]. Therefore, they argued that micro-plastic flow induced by the asymmetric development of the shear stress near the longitudinal interface produces early micro-yielding during compressive loading, so that the apparent Young's modulus is lower. However, this theory cannot explain how the asymmetric development of matrix shear stress leads to a higher compressive composite yield strength as shown in Fig. 7.

On initial tensile deformation, the development of the interfacial shear stresses induces unloading in the matrix. However, from the evolution of the matrix plastic flow shown in Fig. 5, the effect of such unloading is restricted to the immediate proximity along the longitudinal interface near the tip of the whisker, and its influence remains at small applied load, *e.g.*, at a load as small as 2.2 MPa, the plastic zone starts to expand toward the tip of the whisker.

Fig. 9 shows the characteristics of the plastic zone under a compressive load. Comparing the morphologies of the plastic zone under tensile and compressive loading, respectively, as shown in Figs. 5 and 10, the unit cell may be divided into three distinct regions:

elastic, plastic deforming regions and the whisker. Fig. 10 display an idealization based on this partition. If we consider the two stiffer regions to be an imaginary phase, we may define the morphology of the initial development of matrix plastic zone under tension and compression as pseudo-isostrain and pseudo-isostress conditions, respectively, in reference to the isostrain and isostress loading.

For isostrain condition:

$$E_c = E_1(1 - V_2) + E_2V_2. \tag{1}$$

For isostress condition:

$$E_c = \frac{E_1E_2}{(1 - V_2)E_2 + E_1V_2}. \tag{2}$$

where E_i $(i = 1, 2)$ and E_c are the Young's moduli of constituent phase i and the composite, respectively. V_i is the volume fraction of constituent phase i.

For the pseudo-isostrain model (Fig. 10), the stiffness can be evaluated by substituting Eq. 1 with the equations shown below:

$$E_1 = \frac{E_wE_m}{V_p^\sigma E_w + (1 - V_p^\sigma)E_m}; \tag{3}$$

$$E_2 = E_{mp}, \tag{4}$$

where V_p^σ corresponds to the volume fraction of the plastic zone in the pseudo-isostress model; E_m and E_w are the Young's moduli of the matrix and whisker, respectively; E_{mp} is the matrix work hardening rate. Substitute Eqs. 3 and 4 into Eq. 1 and consider $V_2 = V_p^\epsilon$ where V_p^ϵ corresponds to the volume fraction of the plastic zone in the pseudo-isostrain model, the modulus, E_c^ϵ, of the pseudo-isostrain model can be obtained:

$$E_c^\epsilon = \frac{(1 - V_p^\epsilon)E_wE_m}{V_p^\sigma E_w + (1 - V_p^\sigma)E_m} + E_{mp}V_p^\epsilon \tag{5}$$

For the pseudo-isostress model (Fig. 10), $E_1 = (1 - V_p^\epsilon)E_w + V_p^\epsilon E_m$, $E_2 = E_{mp}$, and $V_2 = V_p^\sigma$. Substitute E_1 and E_2 into Eq. 2, we obtain:

$$E_c^\sigma = \frac{(1 - V_p^\epsilon)E_wE_{mp} + V_p^\epsilon E_mE_{mp}}{(1 - V_p^\sigma)E_{mp} + (1 - V_p^\epsilon)V_p^\sigma E_w + V_p^\epsilon V_p^\sigma E_m} \tag{6}$$

where E_c^σ is the modulus for the pseudo-isostress condition. Considering material properties: $E_m = 68.3$ GPa; $E_{mp} = 2.08$ GPa; $E_w = 483$ GPa [9], and for a unit cell shown in Fig. 1 which corresponds to a 20V% composite, we obtain $E_c^\sigma = 9.887$ GPa; $E_c^\epsilon = 50.09$ GPa, *i.e.*, $E_c^\epsilon > E_c^\sigma$. The magnitude of the asymmetry of the Young's modulus is exaggerated because, as compared with that of the actual plastic zone shown in Fig. 9, the morphology of the plastic zone shown in Fig. 10 during compression leads to a lower bound for the composite stiffness.

From this result, it can be seen that the asymmetric apparent composite Young's modulus is due to an asymmetric plastic zone expansion which induces isostress or isostrain type of loading. This process continues until the morphology of the plastic zone can no longer be represented by the idealization shown in Fig. 10, that is, when the applied stress is approaching the composite yield stress.

3.2.2 Asymmetric Bauschinger Effect

In explaining the phenomenon of asymmetric Bauschinger stress factor, the "back

stress" model can be modified [13], in which the forward (σ_f^F) and reverse (σ_f^R) flow stresses can be expressed as:

$$|\sigma_f^F| = \sigma_y + \Delta\sigma_b^F + |\Delta\sigma_{fh}| \quad (7)$$

$$|\sigma_f^R| = \sigma_y - \Delta\sigma_b^R + |\Delta\sigma_{fh}| \quad (8)$$

where σ_y is the yield strength; $\Delta\sigma_b^F$ and $\Delta\sigma_b^R$ are the contributions of the back stress during forward and reverse cycle, respectively; $\Delta\sigma_{fh}$ is the plastic friction.

From Eq. 7 and 8, the Bauschinger stress factor can be expressed as: $\sigma_b = |\sigma_f^F| - |\sigma_f^R| = \Delta\sigma_b^F + \Delta\sigma_b^R$. Approximating the back stress as the matrix residual stress, we obtain the following equations:

$$\Delta\sigma_b^F \approx -\frac{\varepsilon^F}{|\varepsilon^F|}\langle\sigma_m^r\rangle; \quad (9)$$

$$\Delta\sigma_b^R \approx -\langle\sigma_m^{ru}\rangle = -C(\varepsilon^F)\frac{\varepsilon^F}{|\varepsilon^F|}\langle\sigma_m^r\rangle, \quad (10)$$

where $\langle\sigma_m^r\rangle$ is the thermal residual stress; $C(\varepsilon^F)$ is a function of forward applied strain, ε^F. $\langle\sigma_m^{ru}\rangle$ represents the changes of residual stress induced by the external deformation. Then the Bauschinger stress factor is

$$\sigma_b \approx -\left[1 + C(\varepsilon^F)\right]\frac{\varepsilon^F}{|\varepsilon^F|}\langle\sigma_m^r\rangle \quad (11)$$

Considering $C(\varepsilon^F) = 1 - k\varepsilon^F + O(\varepsilon^F)$, where $k > 0$, and $O(\varepsilon^F)$ represents the terms with higher order than ε^F. For the first order approximation, $O(\varepsilon^F)$ may be neglected, that is, $C(\varepsilon^F) = 1 - k\varepsilon^F$. Substituting C into Eq. 11, we obtain:

$$\sigma_b \approx (k\varepsilon^F - 2)\frac{\varepsilon^F}{|\varepsilon^F|}\langle\sigma_m^r\rangle \quad (12)$$

Eq. 12 reflects the general trend of the changes predicted by the FEM shown in Fig. 8. For tension-compression loading scheme ($\varepsilon^F > 0$),

$$\sigma_b \begin{cases} < 0 & \varepsilon^F < \frac{2}{k}; \\ \geq 0 & \varepsilon^F \geq \frac{2}{k}. \end{cases} \quad (13)$$

For compression-tension loading scheme ($\varepsilon^F < 0$), $\sigma_b > 0$. In both cases, $\frac{d\sigma_b}{d|\varepsilon^F|} = k > 0$.

4 CONCLUSIONS

From the above analysis, the following conclusions can be reached:

(1) The evolution of the matrix plasticity in a whisker reinforced SiC/Al composite is characterized by the expansion and interconnection of the thermally induced plastic zones.

(2) The process of plastic zone expansion can be divided into four different stages. Plastic zone expansion in the initial tensile zone; plastic zone interconnection in the initial compressive zone; overcoming the longitudinal compressive matrix thermal residual stress at the tip of the whisker; and the fragmentation of the remnant elastic matrix into pockets.

(3) The onset of global yielding is characterized by the fragmentation of the remnant elastic matrix at the tip of the whisker, where isolated remnant elastic pockets remain.

(4) The composite asymmetric constitutive behavior, the asymmetric Bauschinger effect and the apparent Young's modulus, can be related to the asymmetric matrix plastic flow due to the thermally induced plasticity and residual stresses.

5 ACKNOWLEDGEMENTS

N.S. and R.J.A. would like to acknowledge the Crystal Growth and Materials Testing Associates and the Office of Naval Research, respectively, for their partial financial support.

REFERENCES

1. Arsenault, R. J., and R. M. Fisher, 1983. "Microstructure of Fiber and Particulate SiC in 6061 Al Composites." Scripta metall., 17:67-68.

2. Miller, W. S., and F. J. Humphreys, 1991. "Strengthening Mechanisms in Particulate Metal Matrix Composites." Scripta metall., 25:33-38.

3. Arsenault, R. J., and S. B. Wu, 1987. "The Strength Differential and Bauschinger Effects in SiC-Al Composites." Mater. Sci. Engng., 96:77-88.

4. Snyder, M. D. and K. -J. Bathe, 1981. "A Solution Procedure for Thermo-Elastic-Plastic and Creep Problem." Nucl. Engng. Design, 64:49-80.

5. Arsenault, R. J., 1984. "The Strengthening of Aluminum Alloy 6061 by Fiber and Platelet Silicon Carbide." Mater. Sci. Engng., 64:171-181.

6. Papazian, J. M., and P. N. Adler, 1990. "Tensile Properties of Short Fiber-Reinforced SiC/Al Composites: Part I. Effects of Matrix Precipitates." Metall. Trans., 21A:401-410.

7. Shi, N., B. Wilner, and R. J. Arsenault. "A FEM Study of the Plastic Deformation Process of Whisker Reinforced SiC/Al Composites." Accepted for publication in Acta metall. mater.

8. Mahan, R. L., and J. A. Herzog, 1970. Whisker Technology, New York, NY: J. Wiley-Interscience.

9. ALCOA (Aluminum Company of America), 1967. Aluminum Handbook.

10. Arsenault, R. J., N. Shi, C. R. Feng, and L. Wang, 1991. "Localized Deformation of SiC-Al Composites." Mater. Sci. Engng., A131:55-68.

11. Hamann, R., P. F. Gobin, and R. Fougeres, 1990. "A Study of the Microplasticity of Some Discontinuously Reinforced Metal Matrix Composites." Scripta metall. mater., 24:1789-1794.

12. Levy, A., and J. M. Papazian, 1991. "Elastoplastic Finite Element Analysis of Short-Fiber-Reinforced SiC/Al Composites: Effects of Thermal Treatment." Acta metall. mater., 39(10):2255-2266.

13. Taya, M., K. E. Lulay, K. Wakashima, and D. J. Lloyd, 1990. "Baucshinger Effects in Particulate SiC-6061 Aluminum Composites." Mater. Sci. Engng., A124:103-111.